A Study of Adaptation Luminance for Mesopic Photometry

（薄明視測光のための順応輝度に関する研究）

January 2017

Doctor of Engineering

Tatsukiyo Uchida

Toyohashi University of Technology

Abstract

To measure light and lighting, current practice always uses the spectral luminous efficiency function, $V(\lambda)$, which represents the visual perception by light at equal power for each wavelength. However, the $V(\lambda)$ was developed only based on the sensitivity of the central field of view that adapts to higher light levels. It is known that the peripheral field of view shifts its spectral sensitivity to shorter wavelengths in darker light levels, called the mesopic range. Current lighting practice is not optimized for the light levels.

The recommended system for mesopic photometry published by the Commission Internationale de l'Éclairage (CIE) provides the spectral luminous efficiency function, $V_{\mathrm{mes};m}(\lambda)$, the shape of which changes depending on the adaptation luminance in the mesopic range. The system could open the door to more energy-efficient lighting. According to an estimate in this study, 10 % to 40 % energy saving could be possible. However, lack of methods to determine the adaptation luminance for particular lit scenes prevents the system being implemented.

This study aims to propose an adaptation field definition, where the average luminance sufficiently correlates to the adaptation luminance, for the mesopic photometry system implementation. The first question is whether the peripheral adaptation depends only on the local luminance or on the global average luminance in the field of view. A series of vision experiments revealed that the local luminance is the dominant factor even for the mesopic and peripheral adaptation. However, the surrounding luminance also slightly affects the adaptation and its impact may be significant when high-luminance sources exist in lit scenes.

Further vision experiments were conducted to characterize the surrounding luminance effect. According to the experiments, it can be considered as the veiling luminance caused by stray light in eyes. However, existing veiling luminance models do not agree with the experimental results. This study proposes a new model that is suitable to predict the peripheral veiling luminance in the mesopic range.

This study also proposes a method to simulate the adaptation luminance from the luminance distribution, by taking both the surrounding luminance effect and the eye movements into account. The simulation results show good agreement with the empirical data acquired in this study. By applying the simulation method to real road luminance distributions, adaptation field candidates were tested. According to the analysis, the adaptation field can be defined as the design area of the lighting (i.e. road surface) for typical road lighting. Limitations of this proposal are also discussed.

For rigorous field photometric measurements with the mesopic photometry system, special luminance meters that are not widely available at present are needed. To avoid use of such instruments, this study proposes simplified measurement methods. Since road surface spectral reflectance variations cause some errors with the proposed methods, the error was analyzed with real road surface spectral reflectance data. The analysis shows that a proposed method with a correction can measure the mesopic quantities accurately enough only with conventional instruments and source spectral power distribution data.

The proposed adaptation field definition and the field measurement method enable the mesopic photometry implementation to typical road lighting. These allow more energy-efficient lighting design for the applications. For more general adaptation field definitions, further field luminance distribution examples are needed. However, once such data is available, the methodology established in this study could give comprehensive solutions.

Acknowledgment

First and foremost I would like to thank Dr. Yoshi Ohno, a NIST Fellow. I had done most of the work as a NIST guest researcher hosted by him. I learned from him how I should analysis problems on a deeper scientific level. He also guided me through the CIE activities and taught me how fundamental researches are important for such activities. Without his advice, I would not have been able to overcome the numerous obstacles, which I had faced throughout my research.

I would like convey my deep appreciation to Prof. Shigeki Nakauchi for his sincere support for drafting and completing this dissertation. Ever since I openly aspired to a doctoral degree, he had consistently been a strong supporter. I am also grateful to the chair and a co-chair of my dissertation committee, Prof. Shigeru Kuriyama and Prof. Jun Miura, for their patience and beneficial discussions.

I would also like to express my gratitude to the members of the Japanese Solid-State Lighting Strategic Committee in 2010: Dr. Tetsuji Takeuchi, Mr. Masanori Doro, Dr. Takayoshi Fuchida, and Mr. Ken-ichi Suzuki. Not only was my research project at NIST a part of their grand plan, but also I would not have been able to start up and finish my project without their support. My experiments were designed based on Dr. Takeuchi's works. Dr. Fuchida introduced me to Dr. Ohno and recommended that I should take a doctorate degree. Mr. Suzuki's suggestion was the most significant factor when deciding on the subject of the project.

My sincere thanks also go to members of Optical Radiation Group at NIST, including Mr. Yuqin Zong, Dr. Cameron Miller, Dr. Maria Nadal, Dr. George Eppeldauer, and Dr. Vyacheslav Podobedov for their great support, advice, and friendship. I learned a plenitude of state-of-the-art photometry from them. They also assisted me to get accurate measurements, which underpinned the work.

Thank you as well to guest researchers that shared a NIST office room with me: Dr. Hideyoshi Horie, Dr. Arno Keppens, Dr. Kenji Godo, Dr. Christophe Martinsons, Dr. Irena Fryc, Mr. Tokihisa Kawabata, and Dr. Haiping Shen. Their

various expertise definitely offered fresh perspectives for this work. Furthermore, their friendship made my NIST research life delightful.

I am also grateful to the members of JCIE JTC-1 mirror committee: Prof. Miyoshi Ayama, Prof. Yukio Akashi, Prof. Naoya Hara, Mr. Toru Kitano, Mr. Yasuhiro Kodaira, Ms. Tomoko Kotani, Dr. Takako Kimura, Dr. Tomokazu Hagio, and Mr. Kazutoshi Sakai. The committee's constructive discussions were crucial to the completion of the simulation research in Chapter 5.

My sincere appreciation also goes to great scientists in the CIE, such as Dr. Teresa Goodman, Prof. Liisa Halonen, Dr. Marjukka Puolakka, Prof. Ronnier Luo, Dr. Ken Sagawa, Dr. Hiroshi Shitomi, and Prof. Janos Schanda. They inspired and encouraged me with their commentary. However, I am extremely saddened that Prof. Schanda passed away and we can no longer have our discussions anymore.

I am especially grateful to all Panasonic personnel that supported my work. The directors at the R&D Center of Panasonic's Lighting Business Unit, Mr. Kazuo Kamata, Mr. Katsumi Sato, Mr. Takayuki Imai, and Mr. Masaaki Isoda, approved me to pursue the project. Mr. Shinji Noguchi, Mr. Nobumichi Nishihama, Mr. Wataru Tanaka, Mr. Koji Noro, Dr. Ken-ichiro Tanaka, and Mr. Masato Ohnishi also generously allowed me to spend time for the work. If Mr. Toshihiko Sakaguchi had not recommended me for the project, I would not have had the opportunity to engage in such meaningful work. Without Mr. Atsunori Okada's logistic work, I would not have been able to finish my project successfully. Mr. Makoto Yamada accepted that I left his team for the project. Mr. Takashi Saito and Dr. Hiroki Noguchi also gave me both professional and personal advice.

Most of this work is a part of a project funded by the New Energy and Industrial Technology Development Organization (NEDO). I really appreciate NEDO and the Ministry of Economy, Trade and Industry for funding the project.

Lastly, I would like to thank my dearest family for all of their love and encouragement. When I decided to stay in the United States for the duration of the project, they agreed to come along with me even though they knew it would be challenging for them. I was relieved when my sons, Tamon and Ryojun, were able to overcome those challenges and adapt well to their new environment. Even after we returned to Japan, they allowed me to spend time in private to write. Most of all, I am thankful for my loving, supportive, encouraging, and patient wife, Asuka, whose faithful support kept me going. Thank you.

Contents

List of Figures

List of Tables

1 Introduction

1.1 Background

The role of lighting is facilitating human visual tasks and creating comfortable visual atmosphere. To design, specify, install, and maintain lighting, light needs to be dealt quantitatively so that the quantities can correspond to human visual sensations evoked by the light. The method to quantify light in such a way is photometry [1]. In current practice, a photometry system based on the spectral luminous efficiency function for the CIE (Commission Internationale de l'Éclairage) standard photometric observer, $V(\lambda)$ [2], is always used [3]. This function represents the visual perception by light at equal power for each wavelength, as shown in Figure 1.1.

The $V(\lambda)$ function is based on measurements of the spectral sensitivity at the center of the field of view by using small stimuli subtending angles of 2° or 3° [4,5]. An area in the retina corresponding to the small center field of view, which is called fovea, is almost occupied by a type of photoreceptor, named cones [6]. Thus, the $V(\lambda)$ function can roughly be considered as a model based on the spectral sensitivity of the cones.

In the periphery of the retina, the situation is completely different from that in the fovea. Almost all area except for the fovea, another type of photoreceptor that is more sensitive in short wavelengths than the cones, named rods, is dominant and the cones are minority [6]. The rods work principally in lower luminance levels while the cones work mainly in higher luminance levels. Thus, the peak spectral sensitivity of the peripheral retina shifts toward shorter wavelengths in lower light levels. This phenomenon is known as the Purkinje effect since the 19th century [7].

To deal this complex phenomenon of the human vision in photometry, three types of vision were identified [1] as:

- photopic vision, where the eyes adapt to higher luminance levels and the cones contribute visual perceptions mainly;
- scotopic vision, where the eyes adapt to extremely lower luminance levels and the rods contribute visual perceptions mainly; and
- mesopic vision, where the eyes adapt to intermediate luminance levels between the photopic vision and the scotopic vision, and where both the cones and the rods contribute visual perceptions.

As a consequence of the photometry system development in the first half of the 20th century, the $V(\lambda)$ function is applied to the photopic vision while another spectral luminous efficiency function, $V'(\lambda)$ as shown in Figure 1.1 [2], is applied to the scotopic vision [1]. The spectral luminous efficiency function for the mesopic vision had been left open for a long time because the spectral sensitivity changes depending on the adaptation state in the mesopic range and is difficult to be modeled simply enough for practical use.

From the view of lighting practice, there are no applications in the scotopic range since the adaptation luminance of the scotopic vision, which is considered below about $0.001\,\mathrm{cd\,m^{-2}}$ [3], is too low. For some applications, such as outdoor lighting, the recommended luminance levels are in the mesopic range [8]. However, as stated above, there had been no spectral luminous efficiency function for the mesopic vision. Because of these reasons, the $V(\lambda)$ function has been only option for the spectral luminous efficiency function for all lighting applications although there is a significant deviation from the spectral sensitivity of the human visual system in the mesopic range. Current light sources are optimized for photopic range applications (e.g. such as interior lighting), therefore, outdoor lighting has still room for energy saving.

However, such situation has been changed. After a long discussion in the CIE, a system for mesopic photometry has been recommended in CIE 191:2010 [3]. The system is based on peripheral visual task performance and defines a set of spectral luminous efficiency functions for the mesopic vision in simpler manner than other existing models. Almost coincidentally, light emitting diodes (LEDs) became available as a realistic option for artificial lighting sources [9]. Since LEDs' spectral power distributions (SPDs) can be designed more flexibly than conventional sources for outdoor lighting, e.g. high pressure sodium lamps (HPS) or metal

halide lamps (MH), the combination of these two novel technologies is expected to enable more visually and/or energy-efficient outdoor lighting.

Nevertheless, implementation of the mesopic photometry system to lighting applications is still impractical because some technical issues still remain. One of the critical issues is lack of methods to determine the adaptation state for specific lighting scenes [10]. Since CIE 191 defines the mesopic spectral luminous efficiency function as a set of functions to be chosen depending on the adaptation (see Figure 1.1), the adaptation state for a lighting scene need to be determined to identify which function should be applied to the scene. Unless this missing link is connected, the mesopic photometry system will never be implemented to real applications.

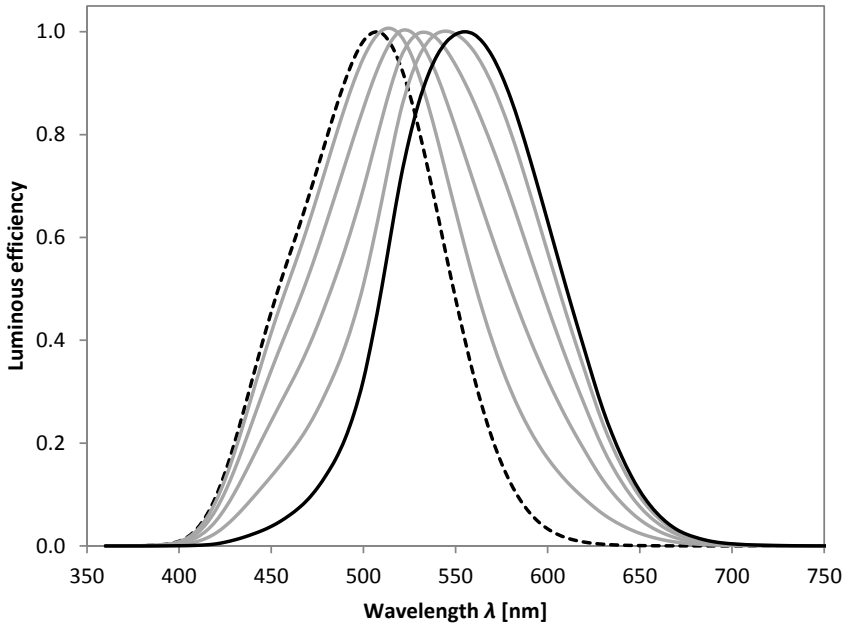

Figure 1.1: Spectral luminous efficiency functions. The black solid line and the black dash line show the photopic spectral luminous efficiency function $V(\lambda)$ and the scotopic spectral luminous efficiency function $V'(\lambda)$, respectively. The gray lines show some mesopic spectral luminous efficiency functions $V_{\mathrm{mes};m}(\lambda)$ with various adaptation coefficient, m

1.2 Objectives

The ultimate aim of the study is to enable implementing the mesopic photometry system to lighting design so that lighting installations are optimized in terms of

visual performance and energy efficiency by taking the Purkinje effect into account. For the purpose, this study addresses the remaining issue: the determination of the adaptation state for the mesopic photometry system. This approach consists of five specific objectives.

Firstly, evolution of photometry systems, especially the development of the system for mesopic photometry, will be reviewed in Chapter 2. Issues to be addressed for the mesopic photometry implementation are also identified.

The second objective is to investigate which is dominant for the adaptation state, the local luminance or the global luminance, to construct a framework for fundamental understanding of the peripheral adaptation mechanism in the mesopic range. The local luminance is the luminance at a peripheral visual task point and the global luminance means the average luminance of the entire field of view. This part will be described in Chapter 3.

The third objective is to characterize effects of a surrounding point source on the peripheral adaptation in terms of the luminous intensity and the geometrical position of the source. There are sometimes high-luminance point sources in real lit scenes. Since they may affect the adaptation state significantly, characterization of the effect is necessary for the adaptation state determination. This part will be explained in Chapter 4.

The fourth objective is to develop a method to simulate the adaptation luminance based on real luminance distributions and test possible adaptation field definitions with the simulation method. The simulation method is based on a comprehensive model that takes into account not only the surrounding luminance effect investigated in Chapters 3 and 4 but also knowledge of observers' eye movements by the other recent studies. The detail will be described in Chapter 5.

The fifth objective is to propose a simplified field measurement method for mesopic quantities. Photometric measurements are sometimes needed to verify whether the lighting installation conforms to the specifications or not. When the lighting is designed and specified with mesopic quantities, the measurement should also be done for the mesopic quantities. However, a straightforward solution for this mesopic measurement needs special instruments that are not widely available at present. Therefore, the aim is to propose a method to measure mesopic quantities with conventional photometric instruments. This method will be proposed and evaluated in Chapter 6.

Finally, the whole study will be reviewed and concluded in Chapter 7.

2 Evolution of Photometry Systems

2.1 The photopic and the scotopic photometry systems

The photometry system currently used was developed in conjunction with improvement of the physical photometry, which uses physical detectors to measure light. Originally, photometry was done visually: light sources were compared by human eyes with apparatuses, such as shown in Figure 2.1. With the advent of photothermal or photoelectric conversion elements (e.g. photocells, photodiodes, etc.), the basis of photometry was switched from human eyes to physical detectors of optical radiation. Figure 2.2 is such a physical detector used for photometric calibration at National Institute of Standards and Technology (NIST). Then photometry systems, especially the spectral luminous efficiency functions, became essential to design the detectors to measure light just as a human [11].

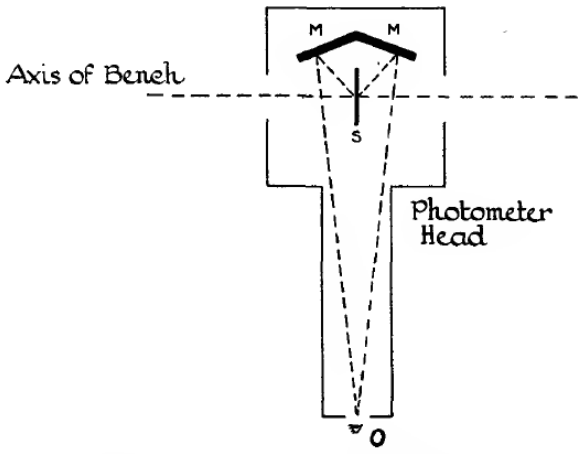

Figure 2.1: A photometer for visual photometry (Walsh, 1926 [12])

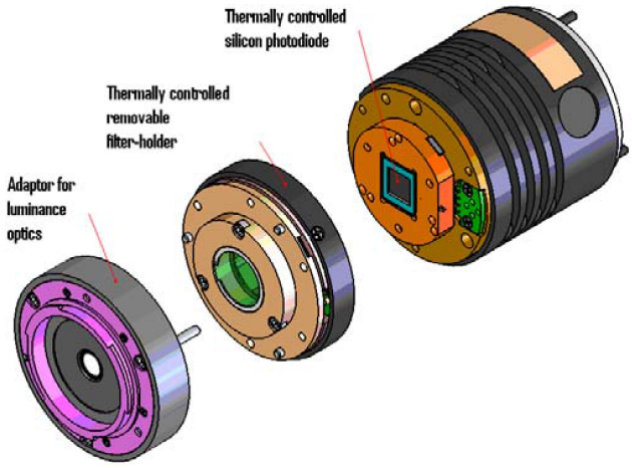

Figure 2.2: A physical detector of optical radiation, NIST working standard detector. (NIST Technical Note 1621 [13])

The most fundamental element of the photometry system is the definition of the candela, which is an SI (Système international d'unités) base unit for the luminous intensity. It was originally ratified in the ninth CGPM (Conference Générale des Poids et Mesuress) in 1948 [14] as:

> The candela is the luminous intensity, in the perpendicular direction, of a surface of 1/600 000 square meter of a black-body at the temperature of freezing platinum under a pressure of 101 325 newton per square meter.

The second element of the photometry system is the luminous efficiency functions. The $V(\lambda)$ and the $V'(\lambda)$ functions were agreed by the CIE in 1924 [5] and 1951 [15], respectively. As stated in Chapter 1, the $V(\lambda)$ is defined based on measurements of foveal spectral luminous efficiency in the photopic range [4]. For the measurements, a technique called "flicker photometry" was used. In this technique, a test and a reference stimuli alternating in a test field are presented and an observer controls the test stimulus to minimize the flicker sensation. On the other hand, the $V'(\lambda)$ is based on direct brightness matching for 20° bipartite field of view in the scotopic range [16].

The third element is an empirical law stating that the total luminance (or other luminous quantities) of a mixture of wavelengths is equal to the sum of the luminance of its monochromatic components. This is known as the Abney's law

of additivity [17]. Based on this law, the following equation can be established for the photometry system:

$$L_{\mathrm{v}} = K_{\mathrm{m}} \int L_{\mathrm{e},\lambda}(\lambda) V(\lambda) d\lambda \tag{2.1}$$

where $L_{\mathrm{e},\lambda}(\lambda)$ is the spectral radiance of a source in $\mathrm{W\,sr^{-1}\,m^{-2}\,nm^{-1}}$ and L_{v} is the luminance in $\mathrm{cd\,m^{-2}}$. K_{m} is a coefficient to convert a radiometric unit to the corresponding photometric unit, named the maximum luminous efficacy. The similar equations can be established for the other photometric quantities with different geometric concepts and also for the $V'(\lambda)$ function.

From these definitions, the K_{m} was derived as:

$$K_{\mathrm{m}} = \frac{L_{\mathrm{v}}(\mathrm{Pt})}{\int L_{\mathrm{e},\lambda}(\lambda, T_{\mathrm{Pt}}) V(\lambda) d\lambda} \tag{2.2}$$

where $L_{\mathrm{v}}(\mathrm{Pt})$ is the luminance of the black-body in the candela definition in 1948, the value of which is $600\,000\,\mathrm{cd\,m^{-2}}$; and $L_{\mathrm{e},\lambda}(\lambda, T_{\mathrm{Pt}})$ is the spectral radiance of the black-body, which can be determined with the Planck's law. Some values, from $670.8\,\mathrm{lm\,W^{-1}}$ to $686.7\,\mathrm{lm\,W^{-1}}$, were found for K_{m} [18]. The deviation was mainly due to uncertainties of the platinum freezing temperature T_{Pt}. Also, the values for the scotopic maximum luminous efficacy K'_{m}, determined in the same manner but with the $V'(\lambda)$ function, were from $1720\,\mathrm{lm\,W^{-1}}$ to $1765\,\mathrm{lm\,W^{-1}}$ in the same literature.

With improvement of the spectroradiometric technologies, the uncertainty of K_{m} became a problem for measurements of monochromatic radiation. Moreover, the realization of the candela according to the definition in 1948 was expensive, inconvenient, and less reproducible [19]. Because of these reasons, a new definition of the candela was adopted by the CGPM in 1979 [20] as:

> The candela is the luminous intensity, in a given direction, of a source that emits monochromatic radiation of frequency 540×10^{12} hertz and that has a radiant intensity in that direction of (1/683) watt per steradian.

The frequency of $540 \times 10^{12}\,\mathrm{Hz}$, corresponding to a wavelength of 555.016 nm, was chosen because it is the peak wavelength of the $V(\lambda)$ function; and, by chance, it is almost the intersection of two spectral luminous efficacy functions, $K(\lambda) =$

$K_{\mathrm{m}}V(\lambda)$ and $K'(\lambda) = K'_{\mathrm{m}}V'(\lambda)$ [18]. The $1/683\,\mathrm{W\,sr^{-1}}$, which means the $K_{\mathrm{m}} = 683.002\,\mathrm{lm\,W^{-1}}$, was adopted to keep consistency on the photopic photometric quantities with the old definition. It turned out that the values of K'_{m} became $1700\,\mathrm{lm\,W^{-1}}$, which is slightly smaller than that under the old definition. The luminous efficacy functions under the new definition are shown in Figure 2.3.

There are two key points that should be noted for mesopic photometry. The first point is that the new candela definition can be applied not only to the $V(\lambda)$ and the $V'(\lambda)$ but also to mesopic spectral luminous efficiency functions, which had not been agreed at the time [21]. In other words, all luminous efficacy functions would share the point of $683\,\mathrm{lm\,W^{-1}}$ at 555.016 nm. The another point is that there is no visual background for the proportion of the K'_{m} to the K_{m}. As shown above, it originally comes from the old candela definition based on the black-body radiation at the platinum freezing temperature. Thus, a scotopic luminance of $1\,\mathrm{cd\,m^{-2}}$ does not necessarily evoke the same visual sensation with a photopic luminance of $1\,\mathrm{cd\,m^{-2}}$. As evidence, although the proportion is just less than 2.5, the rods is more than 100 times sensitive than the cones [22] (See Figure 2.4).

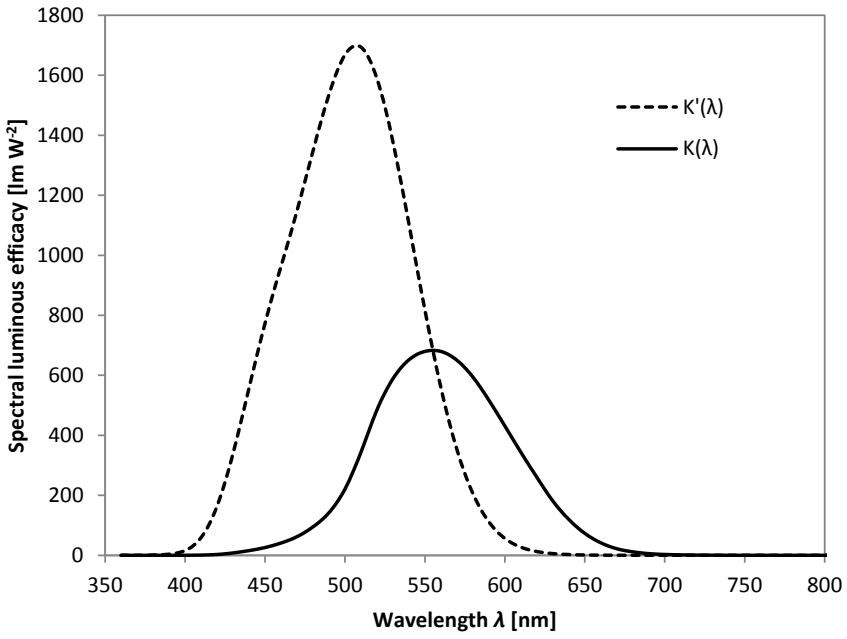

Figure 2.3: The photopic and scotopic spectral luminous efficacy functions, $K(\lambda)$ and $K'(\lambda)$. The intersection is coincident with the peak of $K(\lambda)$

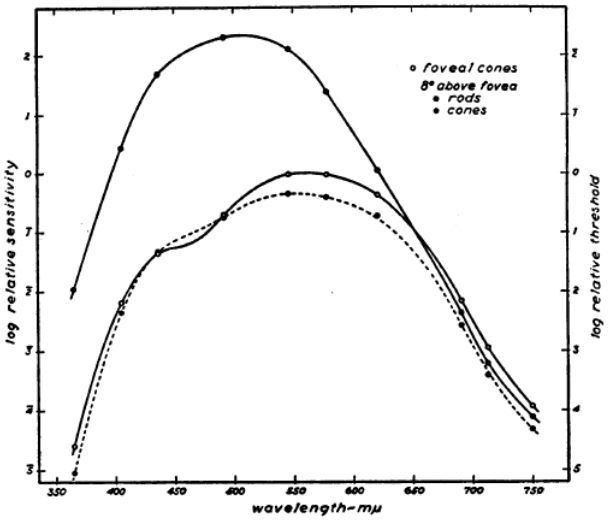

Figure 2.4: Spectral sensitivities of dark-adapted foveal cones, peripheral rods, and peripheral cones (broken line). All sensitivities are expressed relative to maximum sensitivity of the fovea (Wald, 1945 [22])

2.2 Development of mesopic photometry systems

2.2.1 Brightness based approach

The challenges to establish the mesopic spectral luminous efficiency functions have quite a long history, as reviewed in some literature [23–25]. Some investigations to measure the spectral luminous efficiency in low light level, which may include both the mesopic and the scotopic range, appeared in the beginning of the 20th century [26–32]. Figure 2.5 is one of such mesopic spectral luminous efficiency in the early studies [31].

Discussion for standardization of mesopic spectral luminous efficiency functions in the CIE was started in 1959 at the latest [33]. In 1963, a set of spectral luminous efficiency functions at luminance levels from $10 \times 10^{-5}\,\mathrm{cd\,m^{-2}}$ to $100\,\mathrm{cd\,m^{-2}}$ was tentatively recommended by the CIE [34]. However, it was not considered sufficiently accurate nor convenient [23]. An issue was that the brightness measured with the direct brightness matching technique definitely shows non-additivity, which is absent in the flicker photometry results and is not taken into account for the photopic photometry system. Obviously, the brightness sensation seems to depend on the chromatic channels: retinal mechanisms calculating the opponent color signals. To bridge this discrepancy between the brightness and the

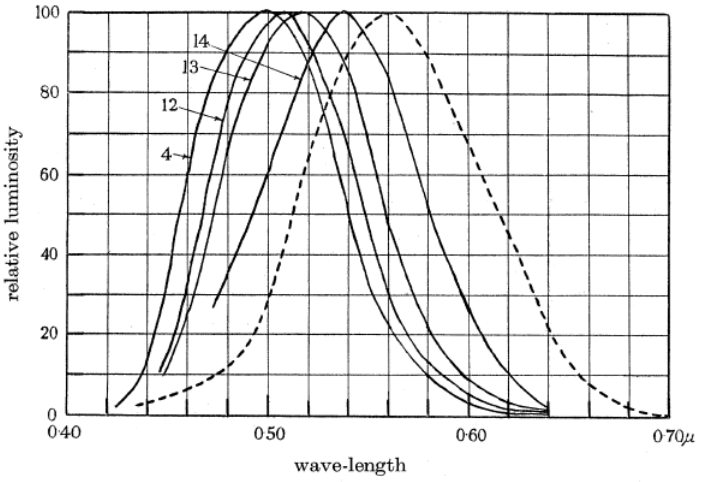

Figure 2.5: Mesopic spectral luminous efficiency at 10° eccentricity (Walters and Wright, 1942 [31])

luminance, an idea named "equivalent luminance" was introduced. At that time, the equivalent luminance of the field illuminated with an arbitrary source was defined as the luminance of black-body radiation with 2042 K that has the equal brightness with the test source [35]. In current definition, the reference radiation has been replaced with the monochromatic light at 555.016 nm [36].

Since then, several models to predict the brightness, or the equivalent luminance, by combining the photometric and the colorimetric quantities were proposed. Those can be classified into three groups. The first group includes models that do not take the chromatic channels into account. Palmer's first [37, 38] and second [23] models, which combine only the photopic luminance based on the $V_{10}(\lambda)$ function and the scotopic luminance, belong to this group. The $V_{10}(\lambda)$ function is the spectral luminous efficiency function where the eye is fully light adapted and the visual target has an angular subtense larger than 4° or is seen off-axis, which would be adopted as the spectral luminous efficiency function of the CIE 10° photopic photometric observer by the CIE in 2005 [39]. The second and the third groups take the chromatic channels into account, but in different ways. The second group models consider the chromatic channels and the cone luminance channel combine first, then the output combines with the rod luminance channel. Trezona model [40] and Sagawa-Takeichi model [41, 42] are in this group. In the third group models, the cone and the rod luminance channels combine first, then the output combines with the chromatic channels from

the cones. Kokoschka-Bodmann model [43], Ikeda-Ashizawa model [44, 45], and Nakano-Ikeda model [23] are the models in this third group.

As a result of the long discussion for the brightness models, the CIE published a supplementary system of photometry in 2011 [46]. The system, which belongs to the third group, determines the equivalent luminance for given light or an illuminated object in the mesopic and photopic range. It allows comparing the brightness of any light even if those light are in different luminance levels and/or have different SPDs. On the other hand, since the system takes the chromatic channels into account, and since the chromatic effects is more significant in higher adaptation luminance levels, the equivalent luminance may deviate from the photopic luminance even in the photopic range.

2.2.2 Visual task performance based approach

In the second half of 1990s, another stream of the mesopic photometry research appeared. A research group of the Lighting Research Center (LRC) at Rensselaer Polytechnic Institute employed reaction-time measurements to determine the mesopic spectral luminous efficiency [47, 48]. They considered that the reaction time is a suitable measure for the basis of mesopic photometry because only the luminance channels, where the additivity is valid, are involved. They also insisted that, from a practical perspective, the reaction time is more important than the brightness, as it is related to hazard-detection responses for drivers. In their experiments, subjects adapted to a uniform background. A small target, the diameter of which was 1.6° or 2.0°, was presented and the time until the subjects responded was measured. The eccentricity of the target in the field of view was 0° and 15° in the first experiment [47], and 12° in the second experiment [48]. Based on the results of the experiments with the peripheral stimuli, they proposed a preliminary mesopic spectral luminous efficiency model, which is a linear combination of the $V_{10}(\lambda)$ and the $V'(\lambda)$ functions. Later, Rea et al. [49, 50] modified the model to a linear combination of the $V(\lambda)$ and the $V'(\lambda)$ functions as:

$$V_{\mathrm{mes}}(\lambda) = XV(\lambda) + (1 - X)V'(\lambda) \tag{2.3}$$

where X is a parameter characterizing the relative proportions of the photopic and scotopic luminous efficiency at any luminance level. The new model was named as

the Unified System of Photometry (USP). The USP places priority on simplicity and compatibility with the conventional photometry system rather than accuracy of performance prediction.

In 2002, a research consortium was formed by six European institutes for comprehensive investigations of mesopic photometry [51]. The consortium, named project MOVE (Mesopic Optimization of Visual Efficiency), focused on night-time driving performance and identified three measures related to critical visual tasks for the application: detection threshold, reaction time, and recognition threshold. Totally eight experiments to measure these indices were conducted in the project [52–54]. Although the experimental methods were different among the experiments, the eccentricity of the targets was the same at 10°. The size of the targets was mostly 2° except for two experiments. As the same as the experiments by the LRC group, the subjects adapted to a large uniform background, sometimes fulfilled the entire field of view. As an outcome of the project, a model for the mesopic spectral luminous efficiency functions was proposed [55]. This is called the MOVE model. It is also a linear combination of the $V(\lambda)$ and the $V'(\lambda)$, but the coefficient for the functions behaves differently from that of the USP. Some their experiments that used quasi-monochromatic targets revealed the chromatic channels also influence the visual task performances and the MOVE model cannot fit perfectly to the results. However, the model shows reasonable prediction for experimental results with broadband stimuli, which are more likely in practical scenes than monochromatic stimuli.

Responding to the visual task performance approaches as shown above, the CIE established a technical committee TC1-58 to standardize a mesopic photometry system based on the visual task performance. Finally, TC1-58 decided to recommend an intermediate model between the USP and the MOVE model. This is the recommended system for mesopic photometry based on visual performance, reported in CIE 191:2010 [3]. In the following section, the system is reviewed closely.

2.3 Recommended system for mesopic photometry in CIE 191

2.3.1 Definition

According to CIE 191:2010 [3] and CIE TN004:2016 [56], the mesopic spectral luminous efficiency function $V_{\mathrm{mes};m}(\lambda)$ is given by:

$$M(m)V_{\mathrm{mes};m}(\lambda) = mV(\lambda) + (1-m)V'(\lambda) \tag{2.4}$$

where m is a coefficient that represents observers' adaptation state, and $M(m)$ is a normalizing function so that the maximum value of the $V_{\mathrm{mes};m}(\lambda)$ attains 1.

The adaptation coefficient m, the value of which ranges from 0 to 1, inclusive, is obtained by using an iterative approach with the following equations:

$$m_0 = 0.5 \tag{2.5}$$

$$L_{\mathrm{mes};m,\mathrm{a},n} = \frac{m_{(n-1)}L_{\mathrm{v,a}} + (1-m_{(n-1)})L'_{\mathrm{v,a}}V'(\lambda_{\mathrm{a}})}{m_{(n-1)} + (1-m_{(n-1)})V'(\lambda_{\mathrm{a}})} \tag{2.6}$$

$$m_n = a + b\log_{10}(L_{\mathrm{mes};m,\mathrm{a},n}) \tag{2.7}$$

where $L_{\mathrm{v,a}}$, $L'_{\mathrm{v,a}}$, and $L_{\mathrm{mes};m,\mathrm{a}}$ are the photopic, scotopic, and mesopic luminances of a visual adaptation field; a and b are parameters which have the value $a = 0.7670$ and $b = 0.3334$; and $V'(\lambda_{\mathrm{a}}) = 683/1700$ is the value of the scotopic spectral luminous efficiency function at $\lambda_{\mathrm{a}} = 555.016\,\mathrm{nm}$. This calculation converges in five or six iterations in most cases.

Then, the mesopic luminance of a test light $L_{\mathrm{mes};m,\mathrm{t}}$ is determined from $V_{\mathrm{mes};m}(\lambda)$ in Equation 2.4 and the spectral radiance of the test light $L_{\mathrm{e},\lambda,\mathrm{t}}(\lambda)$ as:

$$L_{\mathrm{mes};m,\mathrm{t}} = \frac{K_{\mathrm{cd}}}{V_{\mathrm{mes};m}(\lambda_{\mathrm{a}})}\int L_{\mathrm{e},\lambda,\mathrm{t}}(\lambda)V_{\mathrm{mes};m}(\lambda)d\lambda \tag{2.8}$$

where K_{cd} is the spectral luminous efficacy for monochromatic radiation at a wavelength of 555.016 nm, the value of which is $683\,\mathrm{lm\,W^{-1}}$, according to the SI candela definition.

Based on the definition, the mesopic spectral luminous efficacy function $K_{\mathrm{mes};m}(\lambda)$ is given by:

$$K_{\mathrm{mes};m}(\lambda) = K_{\mathrm{mes};m}V_{\mathrm{mes};m}(\lambda) = \frac{K_{\mathrm{cd}}}{V_{\mathrm{mes};m}(\lambda_{\mathrm{a}})}V_{\mathrm{mes};m}(\lambda) \tag{2.9}$$

where $K_{\mathrm{mes};m}$ is the mesopic maximum luminous efficacy. The mesopic spectral luminous efficacy functions for various adaptation coefficient m are shown in Figure 2.6. As is clear from Equation 2.8 and Figure 2.6, the $V_{\mathrm{mes};m}(\lambda)$ and $K_{\mathrm{mes};m}(\lambda)$ agree with the $V(\lambda)$ and $K(\lambda)$ at the upper end of the mesopic range ($m = 1$), and with the $V'(\lambda)$ and $K'(\lambda)$ at the lower end ($m = 0$), respectively.

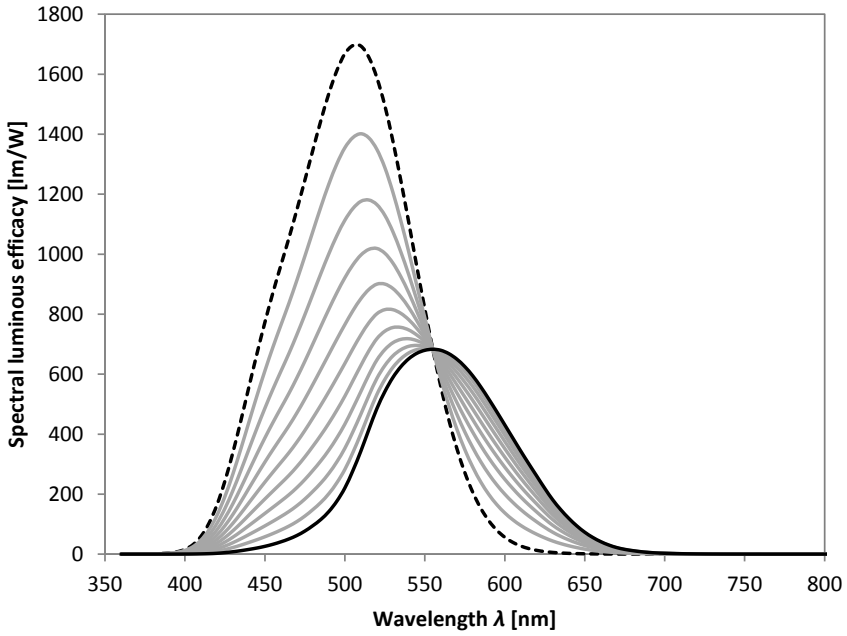

Figure 2.6: The mesopic spectral luminous efficacy functions. The function with $m = 1$ (black solid line) and with $m = 0$ (black dashed line) are the same as $K(\lambda)$ and $K'(\lambda)$, respectively

2.3.2 Impact on lighting design

As stated in Section 1.1, currently all lighting applications are designed with the photopic photometric quantities even if the lighting is in the mesopic range. However, such situation omits the luminous efficacy advantages of light sources that are rich in short wavelength components, such as LEDs, over conventional sources for outdoor lighting, such as HPS. The mesopic photometry system could solve this shortcoming of the conventional photometry system. Its impact can be estimated as the followings.

For the mesopic photometry system, light sources are characterized in terms of a ratio of the scotopic luminous flux to the photopic luminous flux. This is

referred to as S/P (Scotopic/Photopic) ratio, R_{SP}, and given by:

$$R_{\mathrm{SP}} = \frac{K'_{\mathrm{m}} \int \Phi_{\mathrm{e},\lambda}(\lambda) V'(\lambda) d\lambda}{K_{\mathrm{m}} \int \Phi_{\mathrm{e},\lambda}(\lambda) V(\lambda) d\lambda} \tag{2.10}$$

where $\Phi_{\mathrm{e},\lambda}(\lambda)$ is the spectral radiant flux of a source.

Assume that an area is illuminated by a source X with a S/P ratio of $R_{\mathrm{SP,X}}$ at a photopic luminance of $L_{\mathrm{v,X}}$ associated with a particular visual task performance. If the photopic adaptation luminance is coincident with $L_{\mathrm{v,X}}$ and if the reflectance of the illuminated area is spectrally neutral, the mesopic luminance of the area $L_{\mathrm{mes};m}$ and the adaptation coefficient m can be determined by substituting $L_{\mathrm{v,a}} = L_{\mathrm{v,X}}$ and $L'_{\mathrm{v,a}} = R_{\mathrm{SP,X}} L_{\mathrm{v,a}}$ to the iterative calculation with Equations 2.5 to 2.7. To ensure the same visual task performance at the same adaptation level with another source Y, the S/P ratio of which is $R_{\mathrm{SP,Y}}$, the area needs to be illuminated at a photopic luminance $L_{\mathrm{v,Y}}$ determined by:

$$L_{\mathrm{v,Y}} = L_{\mathrm{mes};m} \cdot \frac{m + (1-m) V'(\lambda_{\mathrm{a}})}{m + (1-m) R_{\mathrm{SP,Y}} V'(\lambda_{\mathrm{a}})}. \tag{2.11}$$

This is the photopic luminance for the source Y when the lighting is designed with the mesopic photometry system to keep the same level of the visual task performance with $L_{\mathrm{v,X}}$ with the source X. However, in current practice, the photopic luminance $L_{\mathrm{v,X}}$ is used as the design luminance for all sources, as stated in Section 1.1. Depending on the source S/P ratio, this may be too much (or too less) to ensure the same visual task performance.

From the photopic luminances, the energy-saving effect R_{ES} by lighting design with the mesopic photometry system over the conventional lighting design can roughly be calculated as:

$$R_{\mathrm{ES}} = \frac{L_{\mathrm{v,X}} - L_{\mathrm{v,Y}}}{L_{\mathrm{v,X}}}. \tag{2.12}$$

Figure 2.7 is the energy-saving effect for various S/P ratios and adaptation levels in a practical range. The reference source in this analysis is HPS with $R_{\mathrm{SP}} = 0.55$, which is one of the common light sources for outdoor lighting. As shown in Figure 2.7, roughly 10 % to 40 % energy consumption, depending on the source S/P ratio and the adaptation luminance, can be reduced by implementing the mesopic photometry system to lighting design. In other words, current practice wastes this advantages of high-S/P-ratio sources unintentionally.

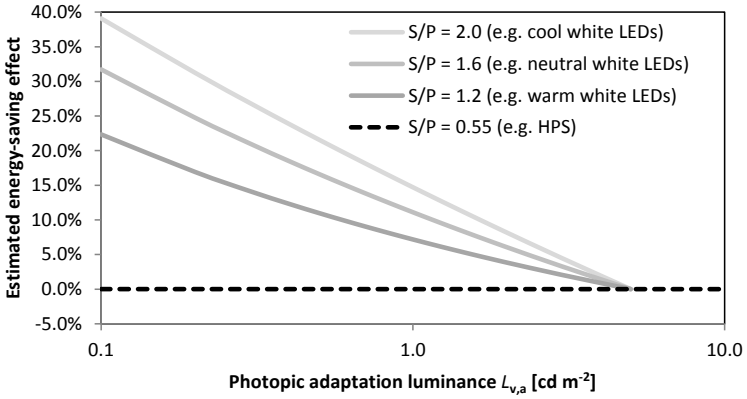

Figure 2.7: Estimated energy-saving effect by lighting design with the mesopic photometry system. An S/P ratio of 0.55, which represents HPS, was chosen as reference

2.3.3 Limitations

Although the mesopic photometry system is intended to predict visual task performance, it is not applicable to all tasks. There are some limitations due to simplification for modeling or limits of the underpinning visual evidences.

Firstly, the mesopic photometry system cannot be applied to tasks at all area on the retina. Since the density of the cones and the rods changes throughout the retina, and since the mesopic photometry system is based on visual tasks at 10° eccentricity and more or less, visual task performances at the other retinal area may be different from those predicted by the system. The MOVE project chose the 10° eccentricity because it is likely related to driving tasks. CIE 191 recommends to use the $V(\lambda)$ function for foveal task performance prediction at all adaptation levels because the fovea is occupied only by the cones [3].

Secondly, it is not known whether it can be used for situations where observers are adapted to high-saturated colors. This is because the experiments underpinning the CIE 191 system mainly used white light, which closes to the black-body locus on the chromaticity diagram, for adaptation and background of the tasks. Applying the mesopic photometry system to extremely high-S/P-ratio sources should be avoided.

Thirdly, although this is not clearly stated in CIE 191 and the other associated documents, comparison between mesopic quantities based on different adaptation coefficient m is meaningless. The value of the mesopic quantities depends on the mesopic maximum luminous efficacy $K_{\mathrm{mes};m}$, which obviously depends on the

values of the K_{m} and the K'_{m}. As shown in Section 2.1, the ratio of the K'_{m} to the K_{m} is an artifact originally from the old candela definition in 1948 and does not have any visual basis. Thus, even if a mesopic quantity is equal to the other mesopic quantity based on different m (e.g. $L_{\mathrm{mes};0.2} = L_{\mathrm{mes};0.8} = 1\,\mathrm{cd\,m^{-2}}$), it does not mean the two light evoke the same visual task performance, as well as a scotopic luminance of $1\,\mathrm{cd\,m^{-2}}$ does not mean the same visual sensation with a photopic luminance of $1\,\mathrm{cd\,m^{-2}}$. This is a critical difference between the CIE 191 performance based system and the CIE 200 brightness based system. Note that the calculation to estimate the energy-saving effect by the mesopic photometry system implementation in Section 2.3.2 compares only the mesopic luminances with the same adaptation coefficient m.

2.3.4 Remaining issues

Upon the publication of CIE 191, two significant technical issues for implementing the mesopic photometry system were recognized:

1. Lighting applications where the mesopic photometry system could be used; and

2. Adaptation field definitions.

Due to the limitations shown in Section 2.3.3, the mesopic photometry system is not valid for all lighting applications in the mesopic range. For example, some studies pointed out that the facial recognition by pedestrians has no correlation with the mesopic quantities or the S/P ratio [57–61].

The CIE published a technical report, CIE 206:2014 [62], that summarizes studies on the implications of source SPDs for tasks considered to be important for pedestrians. The report concluded that the mesopic photometry system can be used to predict brightness and peripheral obstacle detection in the mesopic range while facial recognition and color appearance should be cared for source selection for pedestrian lighting. In the United Kingdom, a road lighting recommendation allows reducing the design illuminance depending on the source S/P ratio for subsidiary streets only when the color rendering index (CRI) of the source is more than 60 [63].

For motorized traffic, the Federal Highway Administration (FHA) in the United States published a report that discusses the source SPD effect on drivers' visual tasks. One of the conclusions is that the mesopic photometry system cannot be applied to high-speed traffic, but applicable to lighting design for lower-speed traffic [64]. Since less evidences are available, new road lighting recommendation RP-8-14 published by the Illuminating Engineering Society of North America (IES) recommends to use the mesopic photometry system only to assess the luminance of off-road locations in street lighting applications where the posted speed limit is $40\,\mathrm{km\,h^{-1}}$ (25 miles per hour) or less for the meantime [65]. This issue is still under discussion at the international level.

Another issue is lack of adaptation field definitions for real lit scenes. As shown in Section 2.3.1, the mesopic calculation requires the adaptation luminance associated with the lit scene. For practice, a field in which the average luminance is well correlated with the adaptation luminance needs to be defined for real lit scenes. The field is referred to as "adaptation field". CIE 191:2010 does not mention any adaptation field definitions at all. The empirical studies underpinning CIE 191 do not give any suggestion for the adaptation field definitions because the backgrounds employed in those studies are basically uniform while those for real lit scenes are non-uniform. Additionally, methods for in-situ measurements of mesopic quantities had not been established.

After CIE 191 was published, the CIE established a new joint technical committee, CIE Joint Technical Committee 1 (JTC-1), to address these remaining issues. This study intends to address the second one, the adaptation field definitions.

3 Surrounding Luminance Effect on the Peripheral Adaptation

3.1 Introduction

As shown in Section 2.2.2, the mesopic photometry system recommended in CIE 191 is based on peripheral task performance measured in a number of experiments, primarily at 10° eccentricity [47, 48, 52–54]. For most of these experiments, determining the adaptation luminance is straightforward because the experiments employed uniform-luminance background in the whole field of view, and the adaptation luminance can be considered to be equal to the background luminance.

On the other hand, it is not easy to determine the adaptation luminance for real lit scenes, which have non-uniform and complicated luminance distributions. This is because adaptation state at a peripheral task point on the retina could be affected by the local luminance as well as by the surrounding luminance, which is the luminance distribution of the field outside the task point.

There are some existing studies to address this issue. Puolakka et al. suggested that studies regarding luminance distributions and observers' line of sight would be useful to the adaptation field definitions [10]. A report by the Netherlands Organisation for Applied Scientific Research (TNO; Dutch: Nederlandse Organisatie voor Toegepast Natuurwetenschappelijk Onderzoek) pointed out that the veiling luminance should be taken into account to determine the adaptation luminance and proposed that the adaptation luminance should be the average luminance of the entire field of view tentatively [59]. An IES technical memorandum, TM-12-12, recommends determining the mesopic luminance at each point by using only the local luminance at the point as the adaptation luminance [66]. Hereinafter, this is called the "point-by-point" method. This method is based on an experi-

mental study that shows task performance in night driving are more predictable with the local luminance at the task point than the road surface luminance. The local luminance was much lower than the road surface luminance [67]. Narisada reported that the fovea is adapted to the sum of the local luminance at the fovea and the veiling luminance caused by the surrounding luminance [68]. The veiling luminance can be calculated with a disability glare formula, such as the Stiles-Holladay disability glare formula [69].

The questions to be considered here are whether the surrounding luminance affects the peripheral adaptation state, and, if so, whether the surrounding luminance effect is significant in determining mesopic quantities. According to the studies above, there are two factors that make surrounding luminance affect the adaptation state. The first factor is hereinafter called the "surrounding luminance effect", which makes the surrounding luminance influence the adaptation state even when the line of sight is fixed. The veiling luminance, which is caused by stray light inside the eyes, or lateral neural interactions in the visual system are candidate mechanisms for the surrounding luminance effect. The second factor is eye movements, which depends on the lighting application [70–73]. This factor broadens the area that affects the adaptation state determined by the first factor. Thus, the surrounding luminance effect should be considered to define adaptation fields for all lighting applications.

As seen above, Narisada's studies pointed out that the surrounding luminance effect can be described with the veiling luminance model. However, empirical evidences employed or corrected for this notion and the glare formula are based on the foveal task performance [68,74–77]. It is not clear whether those are applicable to peripheral tasks, for which the mesopic photometry system is designed [78–80].

Therefore, a series of visual experiments were conducted to measure surrounding luminance effect on the adaptation state at a peripheral task point.

3.2 Method

The experiments were designed to estimate the adaptation state of subjects by measuring the luminance contrast detection threshold for a visual target. Generally, the luminance contrast detection threshold varies depending on the target size, the duration of the target, the target position, the background luminance,

and the adaptation state. Therefore, when a subject adapts to a luminance distribution, while factors other than the adaptation are fixed, the threshold can represent the adaptation state corresponding to the luminance distribution [69].

3.2.1 Adaptation pattern experiment

Set-up

The experimental set-up is shown in Figure 3.1. A computer-controlled liquid crystal display (LCD) was employed to present stimuli consisting of the target to be detected and surrounding patterns, which were the luminance distributions on the entire LCD screen. Neutral density (ND) filters were put in front of the LCD to lower the luminance to the mesopic range while maintaining the LCD's ability to control luminance with high resolution. Prior to every experimental session, the LCD was warmed up to ensure that stabilization was reached. The luminance of the LCD was automatically monitored and it was judged that stability was reached when the variation of the luminance over 20 minutes, taken five minutes apart, was less than 0.5 %. Then, before the experiment, the luminance at the target position on the LCD screen was measured by using a calibrated luminance meter placed at the subject's eye position. The uniformity of the LCD was checked at nine points on the screen, and the one standard deviation of the luminance was 6.5 %, which was not considered significant for the experiments. The experiments were done using three different color stimuli on the display. These were white, red, and blue. The target and the surrounding patterns of the same color were presented in each experiment. The SPD of each color stimulus is shown in Figure 3.2. The S/P ratios of the light stimuli were 1.57, 0.26, and 10.9, for the white, red, and blue stimuli, respectively.

Subjects were positioned at a viewing distance of 55 cm and fixed their head on a chin rest during adaptation and experimental trials. At this distance, the LCD screen subtended $60^\circ \times 40^\circ$ of visual angles. Subjects responded whether they saw a target on the LCD by clicking a mouse. The response data was automatically collected by the computer, which also controlled the LCD. All experiments were conducted in a darkroom.

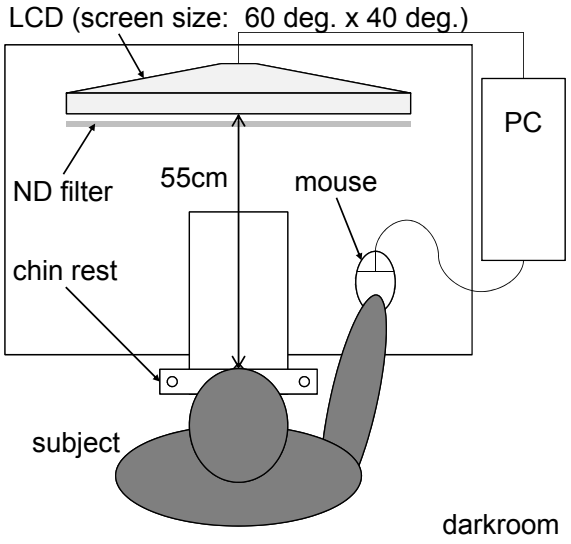

Figure 3.1: Depiction of the experimental set-up for the adaptation pattern experiment and the adaptation background luminance experiment

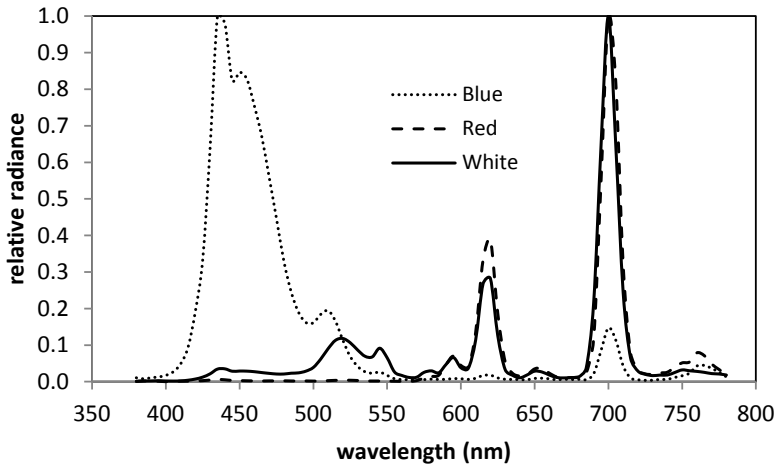

Figure 3.2: Spectral power distributions for white (solid line), red (dashed line) and blue (dotted line) stimuli presented on the display

Stimuli

The first experiment was conducted in order to measure the surrounding luminance effect by comparing three adaptation patterns depicted in the top row of Conditions A, B, and C in Figure 3.3. Additionally, Condition D was conducted to verify whether this experiment can show the Purkinje effect. The bottom row of Figure 3.3 shows task patterns, which were presented for only a short time while subjects conducted the detection tasks. Each adaptation pattern and task pattern for a condition were presented sequentially as described detail later. The presentation of the task patterns was brief enough so that it did not affect the adaptation state. The luminance of the illuminated field on the task pattern is referred to as the "task background luminance", while that of the adaptation pattern is referred to as the "adaptation background luminance". All conditions were conducted for the three light stimuli of different colors (white, red, and blue).

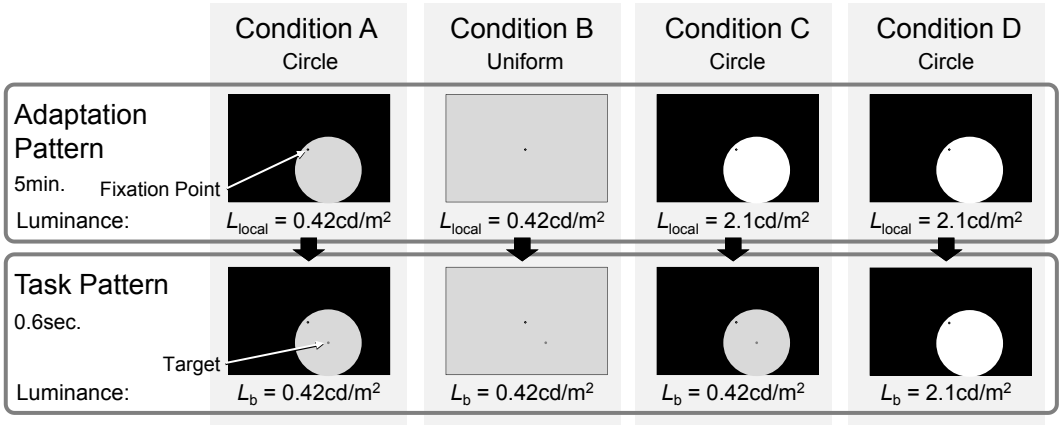

Figure 3.3: Adaptation patterns and task patterns used for the adaptation pattern experiment. The top row shows the adaptation patterns, and the bottom row shows the task patterns, for each Condition A to D. The circular illuminated area of the adaptation pattern for Condition C is 20 % of the entire screen illuminated for Condition B, and the luminance is five times higher than that for Condition B. Thus, the mean luminances of the adaptation pattern for Conditions B and C are nearly equal

A fixation point was presented at the center of the screen during the adaptation and the task pattern presentations. The target to be detected by subjects was a circular dark spot, the diameter of which was a visual angle of 1°. It always appeared in the same position, which was at the lower right of the fixation point. The visual angle between the fixation point and the target was 10°.

The adaptation pattern for Conditions A, C, and D had a circular illuminated area, the radius of which was a visual angle of 12.4°. The circle was centered at the target position. The radius of the circle was set so that the area of the circle was equal to 20 % of the entire screen. On the other hand, the entire screen was illuminated uniformly for the adaptation pattern of Condition B. The levels of the adaptation background luminance were $0.42\,\mathrm{cd\,m^{-2}}$ for Conditions A and B, $2.1\,\mathrm{cd\,m^{-2}}$ for Conditions C and D. These luminance levels were chosen after considering the CIE luminance recommendation for road lighting [8].

Note that the target size, the position, the duration, and the task background luminance were the same for Conditions A, B, and C. Thus, if detection thresholds are different among conditions, it is because of the adaptation pattern differences. In principle, the luminance distribution of the task pattern for Condition B should also have been the same circular pattern as for the other conditions. However, change of subjects' view from the uniform adaptation pattern to the circular task pattern tended to cause significant disturbance in the attention of subjects, and this caused large variations in experimental results with naive subjects. On the other hand, the veiling luminance caused by the uniform task pattern affects the detection threshold, but this effect is considered insignificant based on previous studies. It was also verified with repeated experiments with a well-trained subject. Thus, the task pattern for Condition B was set to the same uniform pattern as the adaptation pattern for that condition.

The assumptions about how the experiment can estimate the surrounding luminance effect are below. If the adaptation state is not at all affected by surrounding luminance, such as for the difference between Conditions A and B, the luminance contrast detection threshold depends only on the local luminance, which is the adaptation background luminance. Thus, the threshold for Condition B should be equal to that for Condition A, and very different for Condition C. This will be referred to as the "local adaptation hypothesis".

On the other hand, if the adaptation state is strongly affected by the surrounding luminance and correlates to the average luminance of the whole field of view (that is the entire screen), the threshold for Condition B should be equal to that for Condition C, because the adaptation pattern for Condition B was set so that the average luminance of the entire screen was equal to that for Condition C. This is referred to as the "global adaptation hypothesis". Note that the illuminated area

of the adaptation pattern for Condition C is one fifth of that for Condition B, and the luminance is five times that for Condition B.

In other words, which hypothesis is true can be checked by comparing luminance contrast detection thresholds for Conditions A, B, and C.

Procedure

The measurements for the four conditions depicted in Figure 3.3 were conducted in one session on a given day. The order of the conditions was randomized. The procedure for a measurement is described below. During all procedures, subjects were asked to fix their line of sight on the fixation point.

1. A subject was asked to adapt the adaptation pattern for five minutes.
2. After the adaptation, the pattern was changed to the task pattern at the same condition for 0.6 s.
3. The target was presented for 0.2 s in the middle of the task pattern duration.
4. After the task pattern duration of 0.6 s, the adaptation pattern returned to the screen.
5. The subject responded whether he/she could/could not see the target.
6. The adaptation pattern was maintained for five seconds after the subject's response to preserve the adaptation state.
7. Steps 2 to 6 were repeated with different values of target luminance (contrast ratio) until enough response data were collected according to the random-staircase method.

To maintain the adaptation state at the level where subjects fully adapt to the adaptation pattern, the duration of the task pattern should be as short as possible. In addition, the repeatability of the target duration should also be ensured. The target duration, 0.2 s, was chosen considering these requirements. The time lags between the adaptation pattern and the target presentation were provided to avoid possible forward/backward effects due to delays in neural response [68, 81]. The

time length of 0.2 s was chosen based on these previous studies and for the same reasons for the target duration.

Before an experimental session, subjects adapted to a uniform pattern that had the same luminance as the adaptation pattern of the first condition for at least five minutes.

Subjects

Eleven subjects with normal vision participated in the adaptation pattern experiment with each color stimulus. Their ages were 29 years to 68 years, but most of them were between 30 years and 50 years. Five out of 11 subjects participated in experiments with all color stimuli, and the other six subjects were different between white and blue/red stimuli.

3.2.2 Adaptation background luminance experiment

Set-up, procedure and stimuli

The second experiment was conducted to determine the relationship between the detection threshold and the adaptation background luminance of the circular pattern.

When the surrounding luminance affects the adaptation state partially, the threshold for Condition B could fall into between those for Conditions A and C. If the detection threshold increases monotonically with respect to the adaptation background luminance, then the detection threshold can be considered a bijective function of the adaptation background luminance. In this case, the threshold for Condition B can be converted to an adaptation background luminance by this function, and the surrounding luminance effect of the uniform pattern can be described as the adaptation background luminance of the circular pattern that increases the adaptation state equivalently with the uniform pattern.

For the measurements, the set-up was exactly the same as the adaptation pattern experiment. The stimuli and the procedures were also the same as for Conditions A and C in the adaptation pattern experiment, except for the adaptation background luminance. To determine the magnitude of the surrounding luminance effect, the thresholds at additional two adaptation background luminance

levels between Conditions A and C on circular adaptation patterns were measured. The luminances were $0.72\,\mathrm{cd\,m^{-2}}$ and $1.23\,\mathrm{cd\,m^{-2}}$. For white stimuli, this experiment was conducted in the same experimental session as the adaptation pattern experiment.

Subjects

All subjects who participated in the adaptation pattern experiment with white stimuli took part in the adaptation background luminance experiment with white stimuli. One of them was employed for the adaptation background luminance experiment with red/blue stimuli.

3.3 Results

3.3.1 Adaptation pattern experiment

The mean luminance contrast detection thresholds of all subjects are shown in Figure 3.4. The thresholds represented by A, B, C and D in Figure 3.4 correspond to the conditions represented by the same letters in Figure 3.3. For clarity, depicted adaptation background luminance levels are slightly shifted from actual luminance levels to avoid the symbols overlapping with each other. For example, all symbols for Conditions A and B in the figure are at the same $0.42\,\mathrm{cd\,m^{-2}}$. The luminance levels for Conditions C and D are also equal. Figure 3.4 shows the luminance contrast detection threshold C_{th} as the ordinate. The threshold C_{th} was calculated from the equation:

$$C_{\mathrm{th}} = \frac{L_{\mathrm{v,b}} - L_{\mathrm{v,t}}}{L_{\mathrm{v,b}}} \tag{3.1}$$

where $L_{\mathrm{v,b}}$ is the task background luminance and $L_{\mathrm{v,t}}$ is the target luminance at the threshold. Thus, higher C_{th} means a lower task performance.

For all three color stimuli, it is observed that Condition B threshold levels are much closer to those for Condition A than to those for Condition C, which favors the local adaptation hypothesis. The error bars in Figure 3.4 show the standard deviation of the mean, which is considered to include the inter-subject variations in contrast sensitivity. To possibly remove these inter-subject variations, the individual results are normalized to the value for Condition A, as shown in

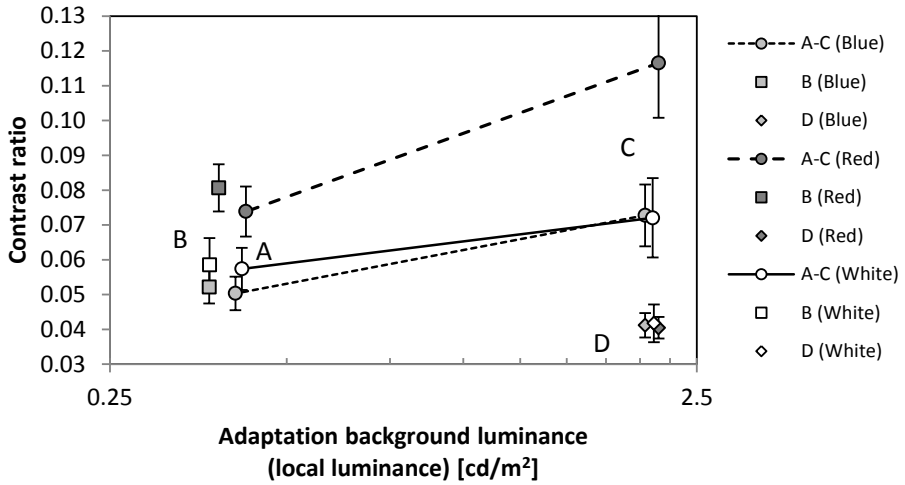

Figure 3.4: The mean luminance contrast detection thresholds for all subjects in the adaptation pattern experiment. The circle symbols show the thresholds for Conditions A and C, which have the same task background luminance and the circular adaptation patterns of different luminance levels. The square symbols show thresholds for Condition B, which has the uniform adaptation patterns. The diamond symbols show thresholds for Condition D. The white, light grey and dark grey symbols show thresholds for white, blue and red stimuli, respectively

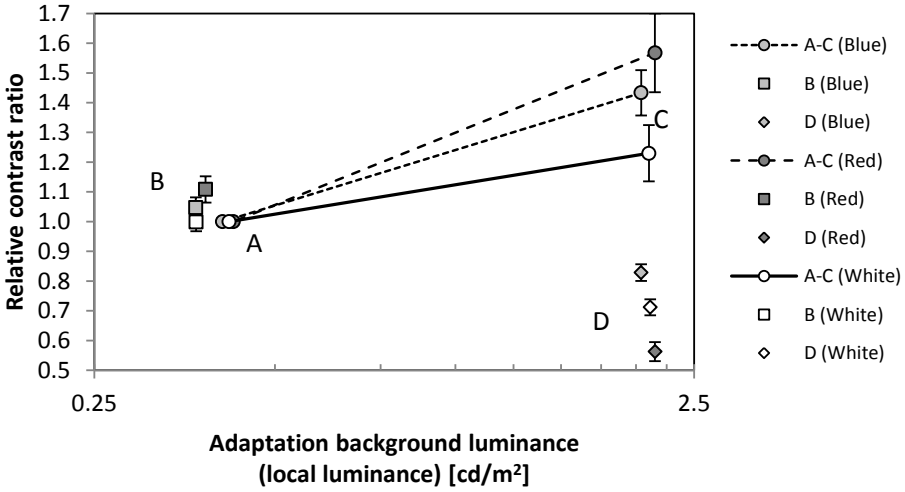

Figure 3.5: The mean luminance contrast detection thresholds normalized for the Condition A thresholds in adaptation pattern experiment. Each symbol shows the same type of data as in Figure 3.4

Figure 3.5. The normalization in Figure 3.5 removed the inter-subject variations and served to examine only the relative positions for Condition A versus Condition B or C. As a result, the error bars, which indicate one standard deviation of the mean for each point after normalization, are much smaller in Figure 3.5. This graph shows the tendency of the detection thresholds, which supports the local adaptation hypothesis, more clearly. Additionally, there are also small differences between the results for Conditions A and B. These seem to demonstrate a small effect of the surrounding luminance distribution.

To assess such observations on Figures 3.4 and 3.5, a two-way analysis of variance (ANOVA) was conducted using all of detection thresholds for Conditions A, B and C in Figure 3.4. The number of data was 99 (11 subjects $\times$ three color stimuli $\times$ three adaptation conditions). Table 3.1 shows the results of the ANOVA. Both the adaptation condition and the color of the stimuli affect the detection threshold significantly, but there is no interaction between them. Then, a multiple comparison test between Conditions A, B and C was conducted on all data for the three color stimuli by using the Bonferroni's method. The detection thresholds are significantly different between A and C ($p < 0.01$), as well as between B and C ($p < 0.01$), but there are no significant differences between A and B. The statistical analysis also supports the local adaptation hypothesis clearly.

For Conditions A and D, the levels of the adaptation background luminance and the task background luminance were the same. Thus, subjects adapted to a luminance and performed the detection task at the same luminance. This situation is similar to an experiment by Freiding et al. [52], which provided some of the fundamental data for the mesopic photometry system. Focusing on Conditions A and D in Figure 3.4, the relative positions of the thresholds shows some consistency with their experimental results. For example, a lower luminance of the adaptation pattern causes a higher luminance contrast detection threshold. It is also consistent in that a lower S/P ratio condition implies a higher threshold at a low adaptation background luminance. These consistencies suggest that the experiment shows the Purkinje effect. However, another ANOVA for Conditions A and D does not detect both the color effect and an interaction between the color and the luminance, as shown in Table 3.2. This is probably because the luminance difference between Conditions A and D is too small for the Purkinje effect to be shown significantly by this experiment.

An inexplicable observation on the statistical analyses is that the color effect is significant on the first ANOVA while it is not significant on the second ANOVA. This is mainly caused by the difference between the detection thresholds for red stimuli and the others under Condition C. According to the mesopic photometry system, both conditions have the same adaptation pattern, which induces a mesopic luminous efficiency function that is relatively close to the $V(\lambda)$. Thus, all detection thresholds for Condition C should be nearly equal to each other, as should those for Condition D. This inconsistency seems to be due to some visual mechanisms that are not taken into account by the mesopic photometry system, such as chromatic channels. Further research is needed for this phenomenon.

Table 3.1: Two-way ANOVA for Conditions A, B and C in the adaptation pattern experiment

Source of variation	*SS*	*df*	*MS*	*F*	*p*	
Color of the stimulus	0.0198562483	2	0.009928	11.689	0.000	**
Adaptation pattern	0.0138909207	2	0.006945	8.177	0.001	**
Interaction	0.0025550319	4	0.000639	0.752	0.559	

**significance criterion: $p < 0.01$

Table 3.2: Two-way ANOVA for Conditions A and D in the adaptation pattern experiment

Source of variation	*SS*	*df*	*MS*	*F*	*p*	
Color of the stimulus	0.0014826117	2	0.000741	2.480	0.092	
Adaptation background luminance	0.0061986158	1	0.006199	20.736	0.000	**
Interaction	0.0017332315	2	0.000867	2.899	0.063	

**significance criterion: $p < 0.01$

3.3.2 Adaptation background luminance experiment

The results of the adaptation background luminance experiment are shown in Figure 3.6. The white square symbols with error bars show the mean luminance contrast detection thresholds for 11 subjects for white stimuli. Both ends of the data are the same as Conditions A and C in Figure 3.4. The other symbols without error bars show the detection thresholds for red, blue and white stimuli for one subject.

The thresholds for white and red stimuli monotonically increase while those for blue stimuli show a different curve with a local minimum around $0.72\,\mathrm{cd\,m^{-2}}$. This means that the surrounding luminance effect can be easily quantified for white and red stimuli with regression lines determined from the thresholds. However, the quantification is not applicable to blue stimuli, because the linear regression is not appropriate for the blue results.

The relationship of the detection threshold level between color stimuli for one subject is not consistent with that in Figure 3.4, which shows results for 11 subjects. This is probably due to the day-to-day intra-subject variation, which can be canceled by repetition of the experiment. Each experiment for a color of the stimuli was conducted on a different day.

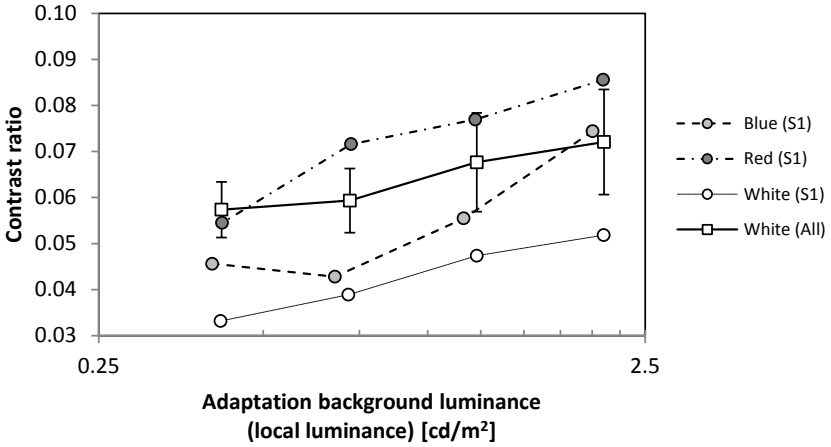

Figure 3.6: The contrast detection thresholds in the adaptation background luminance experiment. The square symbols show thresholds by 11 subjects for white stimuli. The circle symbols colored white, light-grey and dark-grey symbols show thresholds by the same one subject for white, blue and red stimuli, respectively

3.4 Discussion

3.4.1 Magnitude of the surrounding luminance effect

The thresholds for Condition B in Figure 3.5, which have the uniform adaptation pattern, are close to the thresholds for Condition A and far from those for Condition C. This strongly supports the local adaptation hypothesis. The adaptation state at the peripheral task point depends mostly on the local luminance in the

circle.

The small differences between results for Conditions A and C are not statistically significant. Nevertheless, the systematic differences seem to imply a small effect of the surrounding luminance distribution outside of the circle. To evaluate these effects, those for the white and red stimuli were quantified by converting to the adaptation background luminance of the circular pattern, which would cause an equivalent adaptation state (without surrounding luminance distribution). This adjusted luminance is referred to as the "effective adaptation luminance".

The steps to determine the effective adaptation luminance for the white stimuli are given below (see also Figure 3.7). First, a logarithmic regression line was determined from the thresholds in Figure 3.6. Second, the threshold level for Condition B was projected onto the regression line. Finally, the luminance at the intersection was read as the effective adaptation luminance for Condition B.

The steps for the red stimuli are almost the same; except for the fact that the regression line was determined only from the thresholds at $0.42\,\mathrm{cd\,m^{-2}}$ and $2.1\,\mathrm{cd\,m^{-2}}$ in Figure 3.4. A regression line based on the red data in Figure 3.6 is not applicable to that in Figure 3.4 for the determination of the effective adaptation luminance. This is because the data in Figure 3.6 are the result for one subject, while the data in Figure 3.4 are the mean threshold for 11 subjects.

The calculated effective adaptation luminance levels for Condition B were $0.47\,\mathrm{cd\,m^{-2}}$ for white stimuli and $0.58\,\mathrm{cd\,m^{-2}}$ for red stimuli. Because the adaptation background luminance for Condition B was $0.42\,\mathrm{cd\,m^{-2}}$, the surrounding luminance outside of the circle increases the effective adaptation luminance by $0.05\,\mathrm{cd\,m^{-2}}$ and $0.13\,\mathrm{cd\,m^{-2}}$, respectively.

There are two questions regarding the effective adaptation luminance. The first question is how significant the surrounding luminance effect is on the calculated mesopic luminance. Another question is whether the effective adaptation luminance can be predicted by the sum of the local luminance and the veiling luminance calculated by a foveal glare equation. To consider these questions, the photopic effective adaptation luminance and the mesopic luminance of a test target, the photopic luminance of which is $1\,\mathrm{cd\,m^{-2}}$, were calculated with the experimental results and two models. The models to calculate the effective adaptation luminance are as follows:

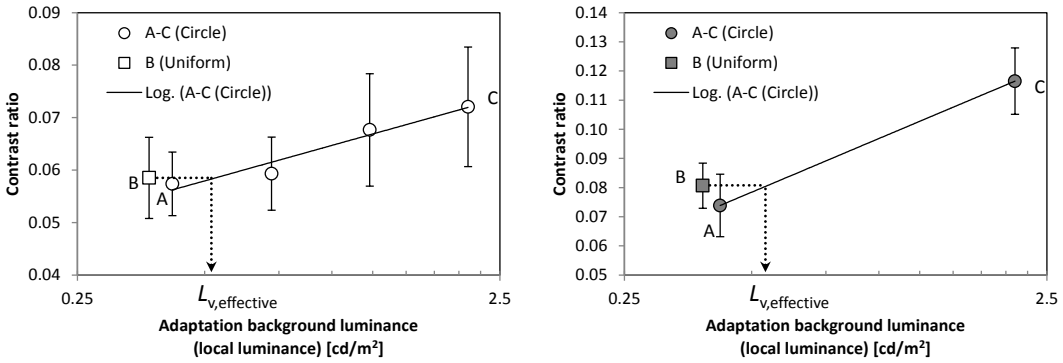

(a) White stimuli (b) Red stimuli

Figure 3.7: Conceptual diagrams for how to determine the effective adaptation luminance for (a) white and (b) red stimuli. Logarithmic regression lines (solid lines) were determined from thresholds for the circular adaptation pattern (circular symbols). Using these regression lines, the threshold levels for the uniform adaptation pattern (square symbols) were converted to the effective adaptation luminance $L_{\mathrm{v,effective}}$ (arrowed dot line). The regression line for red stimuli was determined only from the detection thresholds for Conditions A and C

1. the sum of the photopic local luminance and the veiling luminance calculated with the Stiles-Holladay formula [82]; and

2. only the photopic local luminance.

Note that the local luminance is equal to the adaptation background luminance in the experiments.

In Model 1, the veiling luminance that was caused by the difference image between the uniform adaptation pattern and the circular adaptation pattern was calculated. The difference image was divided into pixels, 0.2505 mm on a side, and then the veiling luminance caused by each pixel was calculated and integrated. The pixels were assumed to be Lambertian sources. In the definition of the Stiles-Holladay formula, angle θ means the angle between the line of sight (fixation point) and a glare source. But, for this analysis, θ was interpreted as the angle between the peripheral task point and a glare source (pixel). The uniform adaptation pattern was assumed to have ideally uniform luminance distribution of $0.42\,\mathrm{cd\,m^{-2}}$. The luminance of the surrounding dark part of the circular adaptation pattern was assumed to be $0\,\mathrm{cd\,m^{-2}}$.

The calculated photopic effective adaptation luminance and mesopic test luminance are shown in Table 3.3. The model predictions for the effective adaptation

luminance are still lower than the effective adaptation luminance derived from the experimental results. The uncertainty of the effective adaptation luminance is too large to make a firm conclusion, yet this result suggests that the surrounding luminance effect at a peripheral task point is larger than the effect at the fovea based on the Stiles-Holladay formula. Additionally, it is still not clear whether the veiling luminance is the main cause of the surrounding luminance effect.

However, for uniform luminance distributions such as the uniform adaptation pattern, the errors related to the models do not prevent us from predicting the mesopic luminance of a test. The errors of the mesopic luminance are at most 0.5 % for the white stimuli and 2.8 % for the red stimuli. The calculation of the mesopic luminance is not sensitive to the error in the effective adaptation luminance.

When a lighting scene has high-luminance sources such as luminaires or headlamps of oncoming cars, their effects on the adaptation state may significantly affect the mesopic luminance. Some studies also pointed out that the glare models for fovea cannot give sufficient prediction for peripheral tasks [78–80]. Such high-luminance source effects will be discussed in the next chapter.

Table 3.3: The photopic effective adaptation luminance and the mesopic test luminance calculated from the experimental data and models

Model	Photopic effective adaptation luminance				Mesopic test luminance for $L_{\mathrm{v,t}} = 1.0\,\mathrm{cd\,m^{-2}}$			
	Red		White		Red		White	
	$L_{\mathrm{v,effective}}$ $\mathrm{cd\,m^{-2}}$	Error	$L_{\mathrm{v,effective}}$ $\mathrm{cd\,m^{-2}}$	Error	$L_{\mathrm{mes,t}}$ $\mathrm{cd\,m^{-2}}$	Error	$L_{\mathrm{mes,t}}$ $\mathrm{cd\,m^{-2}}$	Error
Experiment	0.58	-	0.47	-	0.88	-	1.09	-
1. $L_{\mathrm{v,local}}+L_{\mathrm{v,veil}}$	0.43	25.5 %	0.43	8.2 %	0.86	2.5 %	1.10	0.4 %
2. L_{local}	0.42	27.4 %	0.42	10.9 %	0.85	2.8 %	1.10	0.5 %

3.4.2 Suggestions for adaptation field definitions

Based on the experimental results, how should adaptation fields be defined? It is already suggested that the adaptation field for a lighting scene should take into account: the surrounding luminance effect, which was investigated by the experiments; and eye movements. The local adaptation hypothesis means that

the size and the shape of the adaptation field depend on eye movements and the task area. Since those depend on the lighting application, the adaptation field definition is also application dependent.

The point-by-point method, which is adopted in IES TM-12-12 [66], seems to be appropriate considering the local adaptation hypothesis. However, it neglects eye movements, which is probably significant in most lit scenes. And, for road lighting, the luminance distribution on the road surface moves in the driver's field of view as the car goes forward. Thus, even when the driver's eye movements can be neglected, the projected luminance onto peripheral points on the retina varies temporally. If the adaptation speed is slower than such luminance temporal changes, the adaptation luminance can deviate from the luminance at each point. These need to be verified for the point-by-point method.

4 Effect of a Surrounding Point Source on the Peripheral Adaptation

4.1 Introduction

As shown in Chapter 3, the adaptation state for a peripheral detection task in the mesopic range depends primarily on the local luminance of the task point, but could also be slightly affected by the surrounding luminance. The experimental results in Chapter 3 also suggest that the surrounding luminance effect may be larger than the effect predicted by a foveal veiling luminance model. However, the veiling luminance levels in the experiments were too low to evaluate the magnitude of the surrounding luminance effect accurately. Furthermore, the experimental results do not give any information regarding the relationship between the surrounding luminance effect and the position nor the luminous intensity of the surrounding source, because the experiments investigated only the effect caused by an area light source that had a given luminance level.

To define adaptation fields for the mesopic photometry system, it is further necessary to determine the effects of high-luminance point sources (glare sources) on the adaptation state in the mesopic range. Even though the previous experiments suggest that the surrounding luminance can be nearly neglected for uniform surrounding luminance distributions, it is still important to characterize the effect for the case of point sources. This is because outdoor lighting scenes often have high-luminance point-like sources, such as direct light from luminaires and headlamps of oncoming cars. Their luminous intensity is sometimes very high and may affect the adaptation state significantly. Although there are some existing

veiling luminance models for fovea or periphery, it is not clear that the models can predict the surrounding luminance effect on the peripheral adaptation state in the mesopic range.

Therefore, vision experiments were conducted to characterize the surrounding luminance effect from a high-luminance point source on the adaptation state for a peripheral task point. In the experiments, two aspects regarding the point source were investigated: the luminous intensity and the visual angle between the point source and a task point. These aspects have been considered critical in the existing veiling luminance models.

4.2 Veiling luminance models

For the foveal adaptation, it is shown that the surrounding luminance effect on the adaptation state when the line of sight is fixed can be described by the formula of the veiling luminance in the studies by Narisada [68,69]. These studies focused on the effects of glare sources on the foveal adaptation state rather than the luminance contrast reduction effect by glare sources. According to these studies, the effective adaptation luminance $L_{\mathrm{v,effective}}$ can be predicted by the equation:

$$L_{\mathrm{v,effective}} = L_{\mathrm{v,local}} + L_{\mathrm{v,veil}} \tag{4.1}$$

where $L_{\mathrm{v,local}}$ is the local luminance at which the fovea looks and $L_{\mathrm{v,veil}}$ is the veiling luminance caused by the surrounding luminance distribution. $L_{\mathrm{v,veil}}$ can be calculated by using models for the veiling luminance.

The Stiles-Holladay disability glare formula [75–77, 82, 83] is the most widely used for disability glare evaluation in current lighting practice [84, 85]. According to the formula, $L_{\mathrm{v,veil}}$ is obtained by:

$$L_{\mathrm{v,veil}} = \frac{10}{\theta^2} E_{\mathrm{v,vertical}} \tag{4.2}$$

where $E_{\mathrm{v,vertical}}$ is the vertical illuminance at the observer's eye due to a glare source, and θ is the visual angle (in degrees) between the glare source and the line of sight.

According to studies taking into account age, eye pigment, and the data for ranges of angle near fovea [74, 86, 87], the CIE has developed and recommended

the general disability glare equation as:

$$L_{\mathrm{v,veil}} = \left\{ \frac{10}{\theta^3} + \left[\frac{5}{\theta^2} + \frac{0.1p}{\theta} \right] \cdot \left[1 + \left(\frac{A}{62.5} \right)^4 \right] + 0.0025p \right\} E_{\mathrm{v,vertical}} \tag{4.3}$$

where A is the age of the observer in years, p is the eye pigment factor, which ranges from 0 for black eyes to 1.2 for very light-blue eyes. The experimental data for these models are also for fovea.

Stiles and Crawford [88] proposed a model for the veiling luminance on the peripheral task, based on a number of vision experiments, as:

$$L_{\mathrm{v,veil}} = \frac{16}{\theta^2} E_{\mathrm{v,n}} \tag{4.4}$$

where $E_{\mathrm{v,n}}$ is the normal illuminance (on a plane perpendicular to the direction from the source) at the observer's eye due to a glare source and θ is the visual angle (in degrees) between the glare source and a task point where the veiling luminance is caused. The value of the veiling luminance predicted by the model is more than 1.6 times of the value predicted by the Stiles-Holladay equation for the same condition. Since this formula is based on data in both photopic and mesopic ranges, it is not clear whether this model can predict the surrounding luminance effect on the adaptation state particularly in the mesopic range.

It should be noted that the three models for the veiling luminance are based on experiments in which subjects adapted to a stimulus with a glare source and performed detection tasks with the same stimulus, thus mixing the effects of the adaptation state changes and the masking effect caused by the luminance increment on the task point during the detection tasks. Narisada showed that the adaptation state changes alone can be modeled using the Stiles-Holladay formula for the fovea [68, 69], but it has not been shown that the Stiles-Crawford formula applies for periphery.

4.3 Method

The bases of the experiments in this chapter are the same as those in the experiments in Chapter 3. The adaptation state of subjects is estimated by measuring the luminance contrast detection threshold.

Three experiments were conducted. The first and second experiments measured detection thresholds when subjects were adapted to a uniform background with

a high-luminance point source, with its luminance and the position varied. The first experiment in this chapter focused on the luminous intensity of the point source rather than the point-source position, while the second one focused on the position. The first and second experiments are hereinafter referred to as the "point-source intensity experiment" and the "point-source position experiment", respectively. The third experiment is a control experiment. It characterized the effect of the uniform adaptation background, of varied luminances, on luminance contrast detection threshold. This is referred to as the "uniform experiment". The uniform experiment was conducted to verify the linear relationship between the detection threshold and the effective adaptation luminance, which was suggested by the adaptation background luminance experiment in Chapter 3.

4.3.1 Point-source intensity experiment

Set-up

The experimental set-up is analogous with that in Chapter 3, but modified as shown in Figure 4.1. A computer-controlled LCD, the screen of which was covered with neutral density filter panels, was employed to present the target and its background. For more precise detection threshold measurements than in previous experiments, the LCD has 10-bit control (1024 levels) of the pixel luminance. Calibration and warming-up of the LCD were done as in Chapter 3. The target and background presented by the LCD were white. The correlated color temperature (CCT) and the S/P ratio of these were 4690 K and 2.21, respectively. A white circular LED unit was used as a high-luminance point source. It consists of a LED module with a diameter of 20 mm and a diffuser, placed in front of the LCD screen, producing fairly uniform luminance distribution over the light emitting surface and near-Lambertian angular luminous intensity distribution. The LED unit was placed in front of the LCD at 4 cm from the LCD screen. Care was taken so that no light from the LED fell on the LCD screen. The LED was driven with a direct current (DC) power supply controlled by the computer and dimmed by changing the current level. This dimming method caused small chromaticity changes depending on the current level. However, through the current range employed in the experiment, the change of chromaticity, when changing the luminance level, was less than 0.002 in the CIE (u', v') diagram, which was

not considered significant. The temporal luminance change, which is caused by the change of temperature of the LED, was less than 1 % in three minutes. To calibrate the luminous intensity of the LED, the vertical illuminance from the LED at the subject's eye position was measured by using an illuminance meter, which was calibrated with a spectroradiometer (calibrated against NIST spectral irradiance scale) measuring the particular LED used in the experiment. In the later part of this chapter, the luminous output of the LED is described in terms of the vertical illuminance at observer's eye position. The CCT and the S/P ratio of the LED, measured with the spectroradiometer, were 6120 K and 2.28. This LED was chosen because its S/P ratio was nearly equal to that of the LCD.

Each subject was positioned at a viewing distance of 65 cm and fixed his/her head on a chin rest during adaptation and experimental trials. At this distance, the LCD screen subtended a visual angle of 49° × 29°, and the diameter of the LED was a visual angle of 1.8°. Subjects responded whether they saw a target on the LCD by clicking a mouse (left or right click). The response data were automatically corrected with the computer. All experiments were conducted in a darkroom.

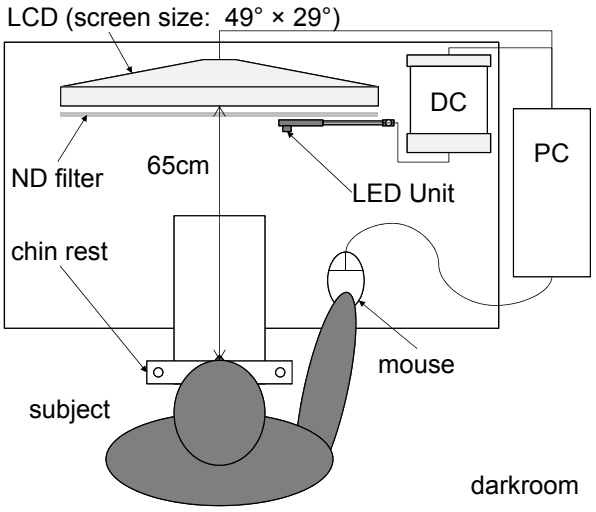

Figure 4.1: Depiction of the set-up for the point-source intensity experiment

Stimuli

The patterns employed in the point-source intensity experiment are shown in Figure 4.2. In this chapter, "pattern" means luminance distribution consisting of

the LCD and the LED, to which subjects adapted or on which subjects performed the detection tasks. In Figure 4.2, the top row shows the adaptation patterns, to which subjects adapted; and the bottom row shows the task patterns, on which subjects performed the tasks. For each pattern, the bottom half of the LCD screen was uniformly set at a background luminance shown in the figure. The luminance of the top half part of the LCD was set as low as possible, which was less than $0.001\,\mathrm{cd\,m^{-2}}$. Magnifications of these patterns are shown in Figure 4.3. These patterns represented rough simulations of road lighting scenes at night, which has the dark sky and a lit road surface. The luminance of the illuminated area for the adaptation pattern is referred to as the adaptation background luminance and that for the task pattern will be referred to as the task background luminance. Each adaptation pattern and task pattern at a condition was presented sequentially so that the LED source was turned off during the task to remove the masking effect by the LED source on the detection thresholds during the tasks. This is analogous with the adaptation pattern experiment in Chapter 3. The conditions in Figure 4.2 can be separated into point-source conditions (three conditions on left side) and reference conditions (two conditions on right side).

A fixation point was shown as a small cross on the screen and was positioned at the center of the screen during the time the task pattern was presented. The target to be detected by the subject always appeared in the same position, which was to the lower right of the fixation point. The visual angle between the fixation point and the target was 10°. The diameter of the target was a visual angle of 1°. The target luminance was varied between trials but was always lower than the task background luminance. While the adaptation pattern was presented (i.e. during the time the subject was adapted to it), the fixation point was moved around in a $2° \times 5°$ oval area centered at the center of the screen every two seconds so that the point source did not excessively stimulate a fixed point on subjects' retina. This procedure was taken for consideration of photobiological safety of subjects, but also it simulates eye movements in real applications.

The position of the point source (the visual angle from the task point to the point source) θ and the vertical illuminance from the source $E_{\mathrm{v,vertical}}$ for the adaptation pattern varied between the point source conditions. Positions of the point source θ were at 7°, 15°, and 30° above the target. The vertical illuminances measured at the subject's eye position $E_{\mathrm{v,vertical}}$ were 0.3 lx, 0.7 lx, 2.2 lx, and 5.4 lx. Thus, the

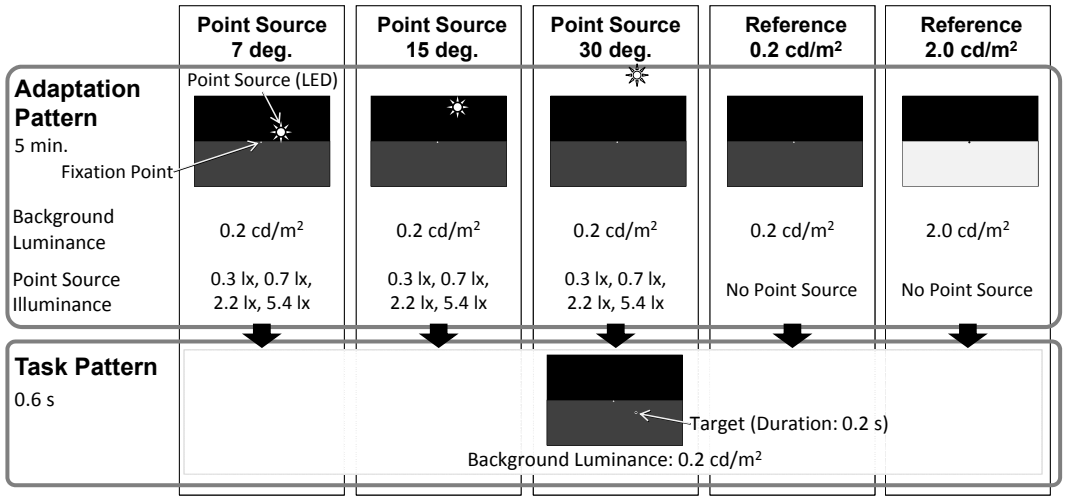

Figure 4.2: Adaptation patterns and a task pattern used for the point-source intensity experiment. The top row shows the adaptation patterns, and the bottom row shows the task pattern, for each condition

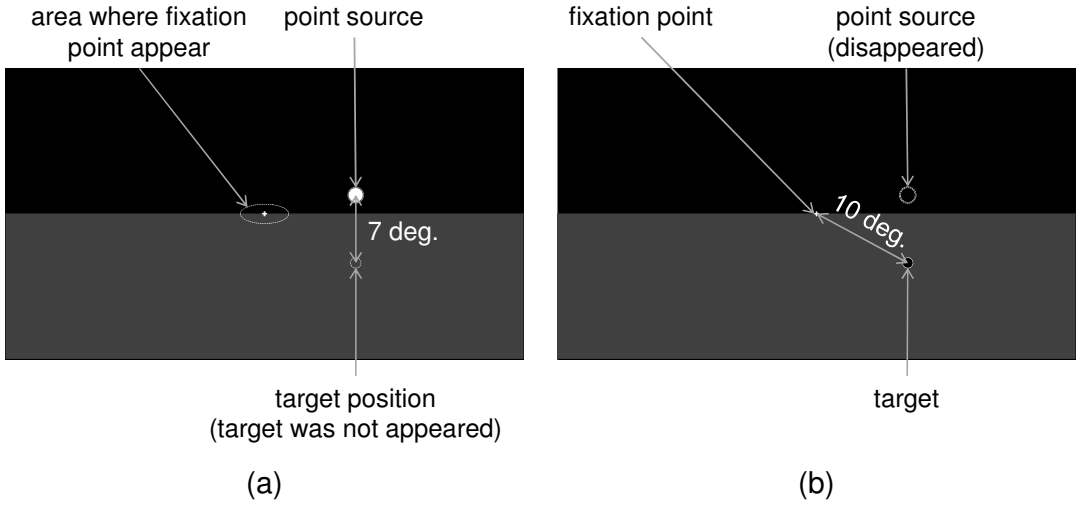

Figure 4.3: Magnification of an adaptation (a) and the task pattern (b) for one of the near-point-source condition in Figure 4.2. The position of the fixation point in the adaptation pattern (a) was changed inside the oval area dynamically. The point source was turned off during the task pattern (b) presentation

total number of the point-source conditions was 12. The adaptation background luminance was constant at $0.2\,\mathrm{cd\,m^{-2}}$ for all the point-source conditions. For the reference conditions, there was no point source and the adaptation background luminances were $0.2\,\mathrm{cd\,m^{-2}}$ and $2.0\,\mathrm{cd\,m^{-2}}$. The task background luminance was $0.2\,\mathrm{cd\,m^{-2}}$ for all the conditions, including the point-source conditions and the reference conditions. These luminance levels were chosen considering the CIE road lighting recommendations [8].

Procedure

The task for subjects was to indicate whether or not the target was seen on each experimental trial. At the beginning of every experimental condition, subjects adapted to an adaptation pattern for five minutes. The task pattern was then presented for 0.6 s. In the middle of the task pattern presentation, the target appeared for 0.2 s. Following the task pattern presentation, the adaptation pattern was presented again to maintain a constant adaptation state. Five seconds after the subject completed each trial, the task pattern was presented again and the next trial began with a different target luminance. The tasks were repeated until the number of the tasks reached enough to determine a luminance contrast detection threshold, according to the random-staircase method.

For this point-source intensity experiment, an experimental session consisted of the two reference conditions and four point-source conditions of different source intensities at the same point-source position. Each subject performed three such sessions for the three point-source positions. The reference conditions were included in each of three sessions, thus, repeated three times per subject. The sequence of the conditions was randomized, except for the reference condition with an adaptation background luminance of $2.0\,\mathrm{cd\,m^{-2}}$, which was always conducted third. The order of the $2.0\,\mathrm{cd\,m^{-2}}$ reference condition was fixed at the middle of the session so that the effect of subjects' fatigue can be removed from the comparison of the reference condition results between experimental sessions to cancel any inter-session deviations of results. Before an experimental session, subjects adapted to a uniform LCD screen, the luminance of which was $0.2\,\mathrm{cd\,m^{-2}}$, for more than five minutes.

Subjects

Seven subjects with normal vision participated in the point-source intensity experiment. To estimate the surrounding luminance effect for the entire age group, subjects were chosen from various age groups. Their ages were 32-68 years. Four of them were younger than 40 years, one was younger than 50 years, and the others were older than 60 years. Three of them had dark brown eyes, another three had brown eyes, and one of them had light-brown eyes.

4.3.2 Point-source position experiment

Set-up

For the point-source position experiment, the experimental set-up is the same as the point-source intensity experiment, described in Section 4.3.1, except for the point-source LED and its driver.

Eight white LED modules were used as point sources and were placed in front of the LCD at 4 cm from the LCD screen. Only one of the LEDs was turned on for an experimental condition. Each LED module was a chip-on-board (CoB) LED module with a diameter of emission surface of 15 mm. Those were fixed on an aluminum jig with screws and heat conductive paste so that the heat from the LEDs was released effectively. A schematic elevation of the CoB LEDs, the jig, and the LCD is shown in Figure 4.4. Instead of the DC power supply used in the point-source intensity experiment, the LEDs were driven by a multichannel DC current source controlled by the computer. The luminous intensity of LEDs was varied by changing the current level over a range from 2 mA to 95 mA. For the current of 40 mA, the average CCT and the average S/P ratio of the LEDs were 6090 K and 1.99. The chromaticity change caused by the current change was less than 0.003 in the CIE (u', v') diagram, which can be considered insignificant for the experiment. It was also checked that the temporal change of the luminous intensity and the chromaticity of LEDs during an experimental session were negligible.

Stimuli

Adaptation patterns and a task pattern employed in the experiment are shown in Figure 4.5. Almost all conditions, such as the task background luminance, the

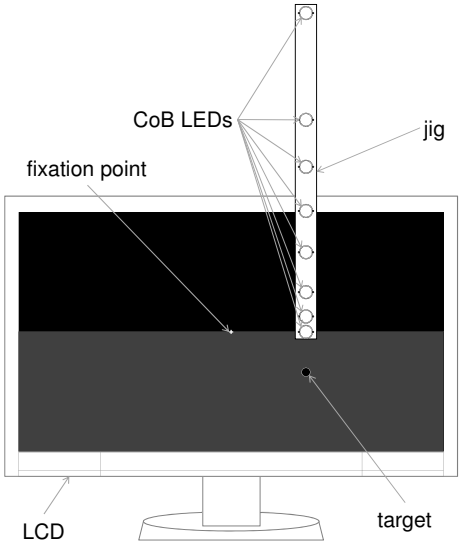

Figure 4.4: Schematic elevation of the LEDs, the jig and the LCD for the point-source position experiment

adaptation background luminance, the target size, etc., were the same as those for the point-source intensity experiment. Exceptions were only the position and the luminous intensity of the point source.

Depending on the existence or the position of the point source in the adaptation pattern, the experimental conditions were sorted into three groups: near-point-source conditions (four conditions), far-point-source conditions (four conditions) and reference conditions (two conditions). The near- and far-point-source conditions had a point source right above the task point in the adaptation pattern, but the visual angle from the task point to the point source, θ, and the vertical illuminance at the subject's eye position from the point source, $E_{\mathrm{v,vertical}}$, were different for each condition. The visual angles θ were: 5°, 7°, 10° and 15° for the near-point-source conditions; 20°, 25°, 30° and 40° for the far-point-source conditions. The vertical illuminances $E_{\mathrm{v,vertical}}$ for the near- and far-point-source conditions were 3 lx and 45 lx, respectively.

Procedure

An experimental session consisted of six conditions out of the ten conditions in Figure 4.5: Four point-source conditions (near or far) and the two reference conditions. Each subject was asked to complete two experimental sessions. Thus, each

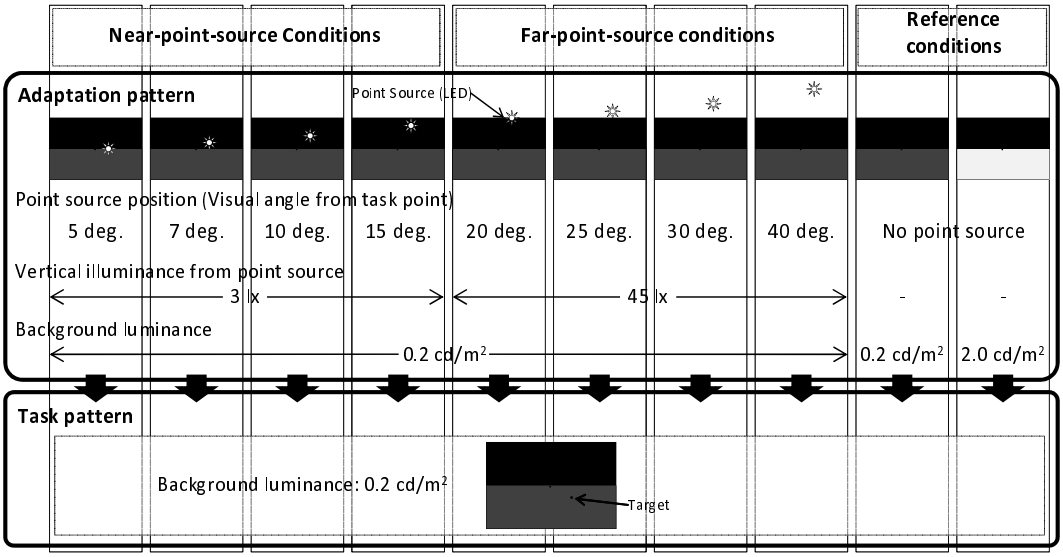

Figure 4.5: Adaptation patterns and a task pattern used for the point-source position experiment

subject performed each point-source condition once, and each reference condition twice. The sequence of the condition was basically random, but the reference conditions were always conducted third or fourth to remove the effect of subjects' fatigue from the comparison of the reference condition results between experimental sessions.

Other procedures are the same as the point-source intensity experiment, described in Section 4.3.1.

Subjects

Nine subjects with normal vision participated in the experiments. Their ages were 27 to 70 years. Two of them were younger than 30 years, three of them were younger than 40 years, another three of them were younger than 50 years and the other one was 70 years. Four of them had dark-brown eyes, other four had brown eyes.

4.3.3 Uniform experiment

Set-up

The third experiment was conducted to determine the relationship between the detection threshold and the adaptation background luminance for the reference

conditions (with no point source) in greater detail. The same set-up as the point-source intensity experiment without the LED point source was used.

Stimuli

The patterns used in the uniform experiment are illustrated in Figure 4.6. As with Figure 4.2, the top row shows the adaptation patterns and bottom row shows the task pattern. In this experiment, no conditions had the point source, and the adaptation background luminance was varied gradually between conditions. Nine levels of the adaptation background luminance from $0.2\,\mathrm{cd\,m^{-2}}$ to $2.5\,\mathrm{cd\,m^{-2}}$ were used. The task patterns, the target, and the fixation point were the same as those for the point-source experiment. The fixation point during adaptation was moved around though there was no LED source, to conform the experimental conditions to those in the point-source intensity/position experiments.

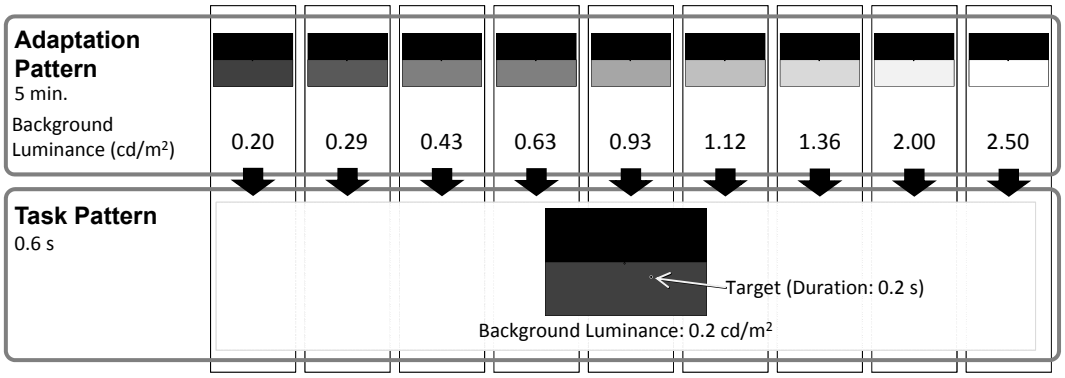

Figure 4.6: Adaptation patterns and a task pattern used for the uniform experiment

Procedure

The procedure of the uniform experiment was also the analogous of the point-source experiments. Since there were many conditions, and since each condition was repeated four to six times, the experiments were conducted for four conditions as a session, and the whole experiment was conducted in 13 separate sessions.

Subject

The uniform experiment was conducted with a well-trained subject, one of the subjects used for the point-source experiments.

4.4 Results

4.4.1 Point-source intensity experiment

The mean luminance contrast detection thresholds of all subjects are shown in Figures 4.7 to 4.9, for point-source positions of 7°, 15° and 30°, respectively. These figures show luminance contrast detection threshold C_{th} (ordinate) as a function of the point-source illuminance (abscissa). The luminance contrast detection threshold C_{th} was calculated as Equation 3.1. For descriptive purposes, results of the reference conditions without the point source were plotted at the left end of the graph, which is noted as "Ref." on the abscissa, with square and triangle symbols. The error bars are one standard deviations of the mean.

The results show that higher point-source illuminances basically cause higher detection thresholds, which means lower visual performance. The steeper gradient for the closer point source (Figure 4.7) shows that the effect of the luminous intensity of the source is higher than at larger angles.

Additionally, the relationship between the results of two reference conditions suggests that higher effective adaptation luminances cause higher detection thresholds. Because the point source is absent in both conditions, the difference between them is only the adaptation background luminance, which indubitably correlates with the effective adaptation luminance at the task point. Assuming that the surrounding luminance effect can be neglected for the reference conditions, the effective adaptation luminances for the reference conditions are nearly equal to the adaptation background luminance.

These results clearly suggest that the presence of the point source increases the effective adaptation luminance at the task point. For example, in Figure 4.7, the detection threshold at the point-source illuminance of 5.4 lx (at an adaptation background luminance of $0.2\,\mathrm{cd\,m^{-2}}$) is very close to that for the reference condition at an adaptation background luminance of $2.0\,\mathrm{cd\,m^{-2}}$, shown as the square symbol plotted at the left end of the graph. In this case, the effective adaptation luminance of the 5.4 lx point-source condition can be estimated to be close to $2.0\,\mathrm{cd\,m^{-2}}$. Further analysis of this point is discussed in Section 4.5.1.

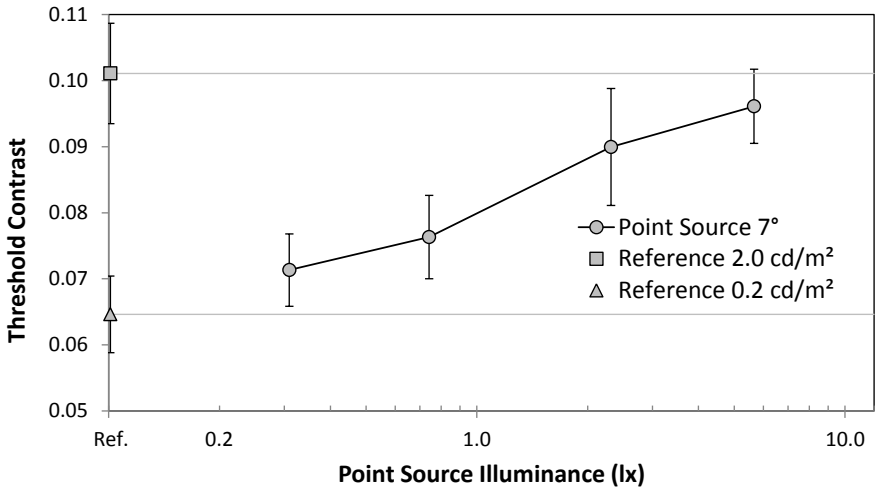

Figure 4.7: The mean luminance contrast detection thresholds for all subjects for a point-source position of 7° in the point-source intensity experiment

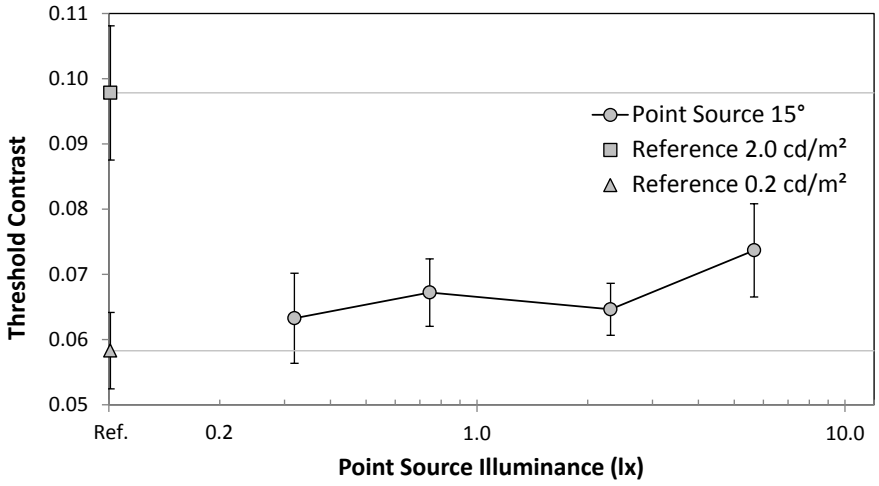

Figure 4.8: The mean luminance contrast detection thresholds for all subjects for a point-source position of 15° in the point-source intensity experiment

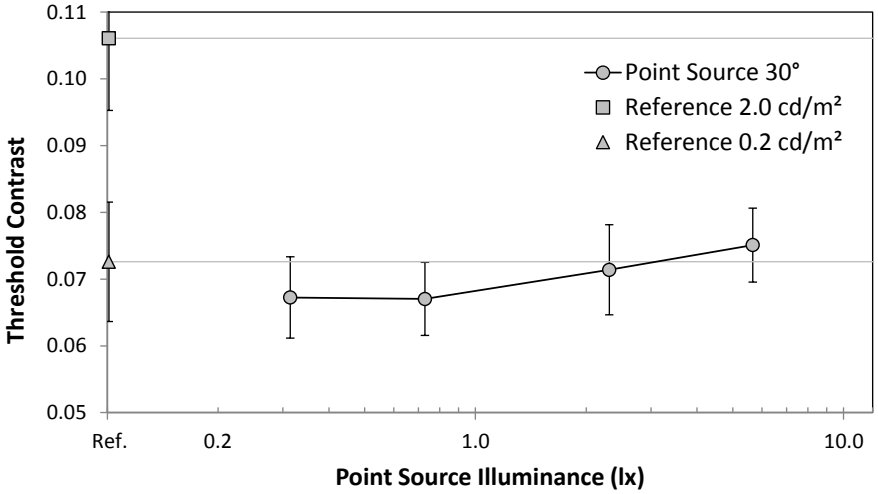

Figure 4.9: The mean luminance contrast detection thresholds for all subjects for a point-source position of 30° in the point-source intensity experiment

4.4.2 Point-source position experiment

The mean luminance contrast detection thresholds of all subjects are shown in Figures 4.10 and 4.11 for the near-point-source conditions and the far-point-source conditions, respectively. All conditions in each figure were conducted in one experimental session for each subject. For comparison purposes, results of the reference conditions in the same experimental session were plotted in the same figures, at the left end of each graph.

The experimental results are basically consistent with those of the point-source intensity experiment. The point-source condition results suggest that a nearer point source increases the effective adaptation luminance more. Note that the illuminance from the near-point-sources is only 3 lx while that from the far-point-source is 45 lx, which is 15 times higher. If the illuminance of the far-point-sources had been the same as that of the near-point-sources, the thresholds would have been much lower than those shown in Figure 4.11 and the effect would have been too small to measure by the experiment. By contrast, the detection threshold for 5° is much higher than others, even though the point source has only 3 lx of vertical illuminance at the subject's eye position. It is reasonable that the difference in the detection threshold, which implies a difference in the effective adaptation luminance, was caused by changes of the surrounding luminance effect due to the positions and the illuminances of the point source.

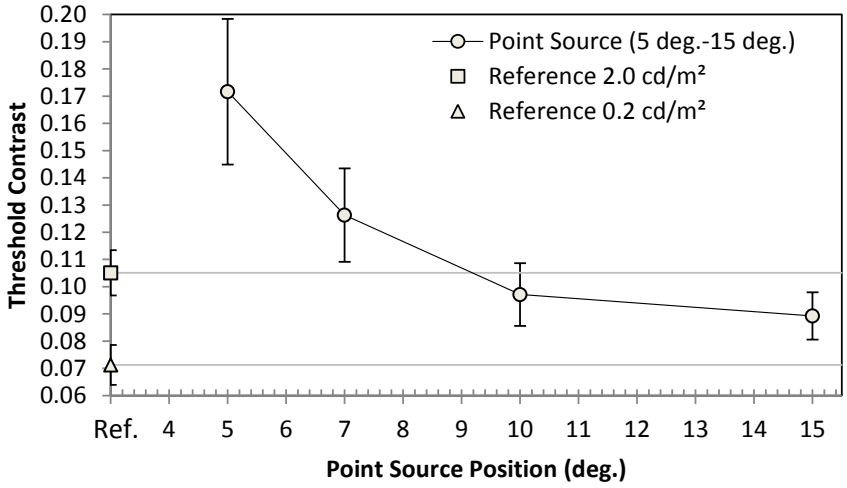

Figure 4.10: The mean luminance contrast detection thresholds for all subjects for the near-point-source conditions and associated reference conditions in the point-source position experiment

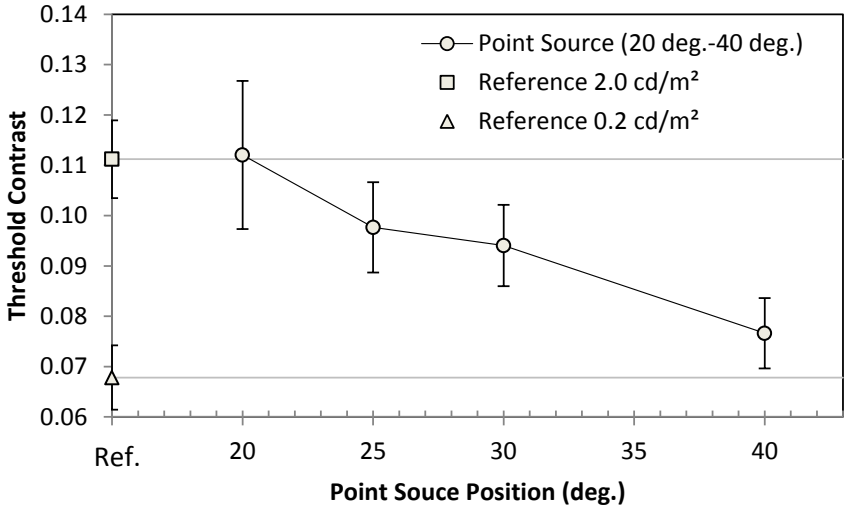

Figure 4.11: The mean luminance contrast detection thresholds for all subjects for the far-point-source conditions and associated reference conditions in the point-source position experiment

Detection thresholds for the reference conditions with an adaptation background luminance of $2.0\,\mathrm{cd\,m^{-2}}$ are 0.105 and 0.111 in Figures 4.10 and 4.11, respectively. Those with an adaptation background luminance of $0.2\,\mathrm{cd\,m^{-2}}$ are 0.071 and 0.068. The differences between the experimental sessions, which are smaller than the differences between the results of the conditions in an experimental session, mean that the experiment has sufficient repeatability to compare the results between the sessions.

4.4.3 Uniform experiment

The results of the uniform experiment are shown in Figure 4.12. This figure shows luminance contrast detection threshold (ordinate) as a function of the adaptation background luminance (abscissa). Each point represents the mean of repeated trials with one subject. The numbers of trials are nine for the adaptation background luminance of $0.2\,\mathrm{cd\,m^{-2}}$ and four to six for the other luminance levels. The error bars show one standard deviation of the mean.

Even though the data have some variation, the trend clearly shows that the detection threshold is linear to the logarithm of the adaptation background luminance. The solid line in Figure 4.12 is a regression line with an equation:

$$C_{\mathrm{th}} = a \log_{10} L_{\mathrm{v,effective}} + b \tag{4.5}$$

where $L_{\mathrm{v,effective}}$ is the effective adaptation luminance and a and b are regression coefficients. For the uniform experiment, the effective adaptation luminance can be considered equal to the adaptation background luminance because there is no point sources affecting the effective adaptation luminance. The regression line shows good agreement with the experimental results. This tendency is also consistent with results of the adaptation background luminance experiment by 11 subjects, shown in Figure 3.6.

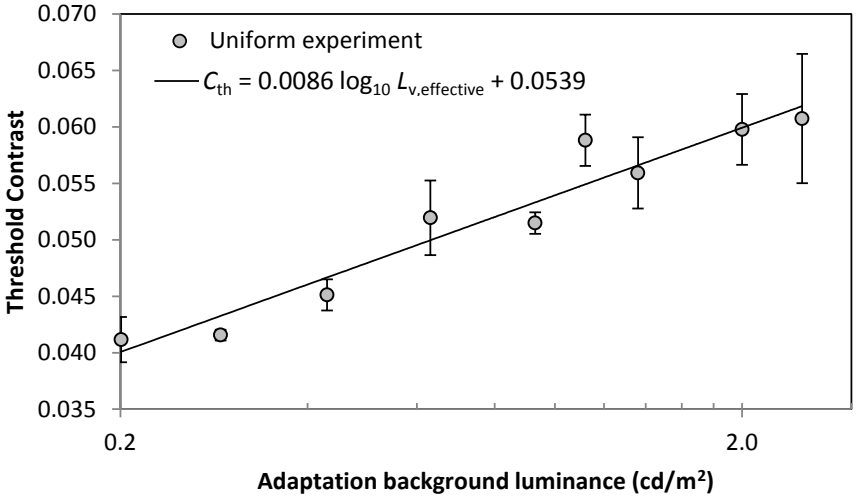

Figure 4.12: The mean luminance contrast detection thresholds for repeated trials with one subject in the uniform experiment

4.5 Discussion

4.5.1 Surrounding luminance effect with respect to the point-source luminous intensity

Even though the point-source intensity experiment results show a tendency for the point source to increase the effective adaptation luminance, the results give only detection thresholds and do not indicate the effective adaptation luminance for each condition directly. However, by using Equation 4.5, the effective adaptation luminance for the point-source intensity experiment results can be determined from the detection thresholds in Figures 4.7 to 4.9. The steps are: first, determine the coefficients a and b in Equation 4.5 by substituting the reference condition results (two sets of the adaptation background luminance and the detection threshold); then, calculate the effective adaptation luminance for each condition, by substituting the detection threshold to the equation determined in previous step. This calculation removes the inter-session deviation, which appears in the variation of the reference condition results among Figures 4.7 to 4.9.

To compare with the results of the experiment, the effective adaptation luminance $L_{\mathrm{v,effective}}$ were also calculated by using three models:

1. $L_{\mathrm{v,effective}} = L_{\mathrm{v,local}} + L_{\mathrm{v,veil}}$, $L_{\mathrm{v,veil}}$ is calculated by the Stiles-Holladay formula (Equation 4.2);

2. $L_{\mathrm{v,effective}} = L_{\mathrm{v,local}} + L_{\mathrm{v,veil}}$, $L_{\mathrm{v,veil}}$ is calculated by the CIE general disability glare equation (Equation 4.3); and

3. $L_{\mathrm{v,effective}} = L_{\mathrm{v,local}} + L_{\mathrm{v,veil}}$, $L_{\mathrm{v,veil}}$ is calculated by the Stile-Crawford formula (Equation 4.4).

For the model calculations, $L_{\mathrm{v,local}}$ was assumed to be equal to the adaptation background luminance, which was $0.2\,\mathrm{cd\,m^{-2}}$. In Models 1 and 2, θ was interpreted as the visual angle between the target and the point source. For Model 2, the average age of subjects (46 years) and an eye pigment factor of 0.5 (brown) were employed to calculate the CIE general disability glare equation.

The calculated effective adaptation luminances $L_{\mathrm{v,effective}}$ as functions of the point-source illuminance are shown in Figure 4.13. For the point-source positions of 7° and 15°, Model 3 shows the best prediction, especially for 7°. The results of these conditions support that the surrounding luminance effect on the peripheral adaptation state can also be described as the veiling luminance. Evidence for non-linear factors, such as the lateral neural interaction, is not observed. Additionally, the magnitude is more consistent with the Stiles-Crawford formula, which is for the peripheral vision, rather than the foveal models.

However, all models overestimate the effective adaptation luminance for the point-source position of 30°. This is probably due to the deviation between Equation 4.5 and the real function for the detection threshold of the effective adaptation luminance. The real effective adaptation luminances for 30° should be slightly more than $0.2\,\mathrm{cd\,m^{-2}}$ (adaptation background luminance) and less than $0.3\,\mathrm{cd\,m^{-2}}$. The uniform experiment results do not demonstrate that Equation 4.5 applies accurately in this low-level range. The real function may have a local minimum in this range. If this is true, the deviation between the models and experimental data for the point-source position of 30° can be explained. Whether or not, in terms of the uncertainty of the experimental method and analysis, the results of conditions with closer/brighter point sources are more reliable for estimating the surrounding luminance effect on the adaptation state.

How significant is the surrounding luminance effect of glare from road lighting luminaires, assuming that the surrounding luminance effect can be predicted with the Stiles-Crawford formula? To evaluate this impact, the mesopic luminance of a test object was calculated for each lighting class in the CIE road lighting

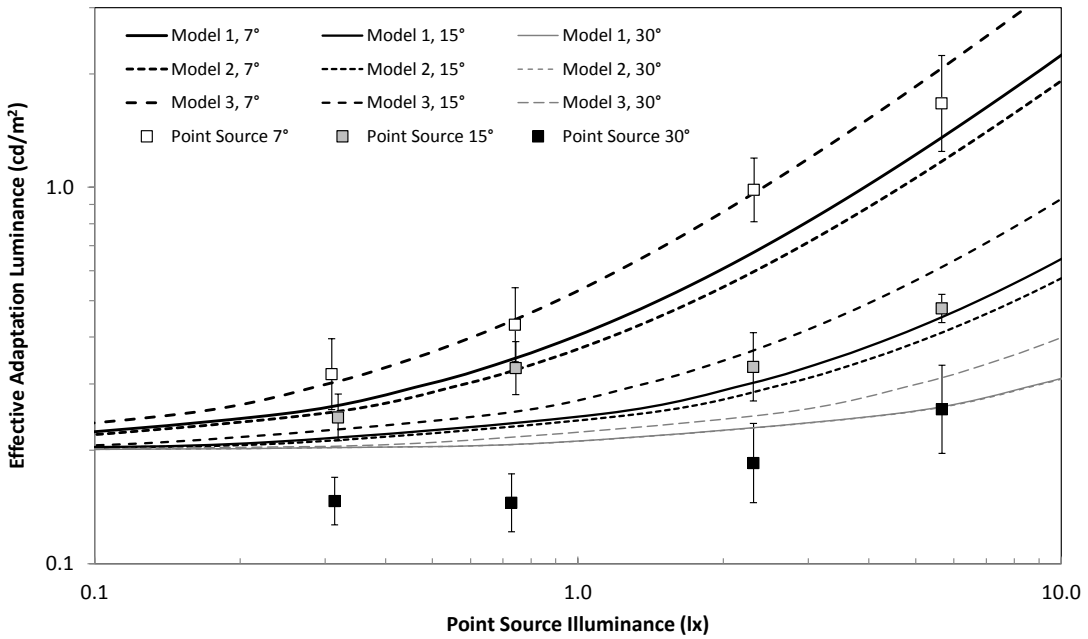

Figure 4.13: The effective adaptation luminances determined from the experimental results and the models, as functions of the vertical illuminance from the point source. Square symbols show the experimental results; white, grey, and black correspond to $7°$, $15°$, and $30°$, respectively. Lines show the effective adaptation luminance from the models; solid, short dashed, and long dashed lines correspond to the Models 1, 2, and 3, respectively

recommendations in CIE 115:2010 [8]. The CIE recommendations, based on the road surface luminance, have requirements for an upper limit of the threshold increment (TI). TI is determined from the average luminance of the road surface and the veiling luminance (from direct light from the luminaires) calculated with the Stiles-Holladay formula [84]. Thus, when assuming a road lighting installation that has the average luminance of the road surface and the TI listed in the recommendations, the surrounding luminance effect on the adaptation state and the mesopic luminance of a test object can be calculated. In this calculation, the S/P ratio is assumed to be 2.4, which is the highest among those of commercially available sources listed in IES TM-12-12 [66]. It was also assumed that the difference between the vertical illuminance and the normal illuminance from glare sources can be neglected. This assumption allowed determining the surrounding luminance effect just by multiplying 1.6 to the veiling luminance based on the Stiles-Holladay formula.

Table 4.1 shows the calculation comparing two mesopic luminances of a test object, the photopic luminance of which is $1\,\mathrm{cd\,m^{-2}}$. One (in the eighth column) is calculated using Model 3 for the effective adaptation luminance calculation; another (in the 11th column) is calculated assuming that the effective adaptation luminance is equal to the average luminance of the road surface, neglecting the surrounding luminance effect. The right-end column shows the difference of the two mesopic luminances in per cent. Based on this analysis, the surrounding luminance effect decreases the mesopic luminance of a test object by at most 4.67 %.

Note that these calculated differences in the mesopic luminance can be considered close to the largest estimations, when assuming the observers' eye movement is fixed. Lower S/P ratios or lower TI would make the differences smaller. However, when taking observers' eye movements into account, and when the surrounding field of view is darker than the road surface as is usual in road lighting scenes, the surrounding luminance effect may be more significant. This is because the local luminance $L_{\mathrm{v,local}}$ in the models can be considered the average luminance on where a peripheral task point on the retina is focused, and the average luminance is lower than the average luminance of the road surface when the peripheral point scans the surrounding darker area. For this point, further study with real luminance distribution data will be described in Chapter 5.

Table 4.1: The impact of the surrounding luminance effect on the mesopic luminance of a test object for the CIE road lighting classes

CIE Recommendation			Veiling luminance		$L_{v,effective} = L_{v,ave} + L_{v,veil}$ (Stiles-Crawford)			$L_{v,effective} = L_{v,ave}$			Diff.
Lighting Class	Average luminance of the road surface	Threshold increment	Stiles-Holladay	Stiles-Crawford[a]	Effective adaptation luminance		Mesopic test luminance[b]	Effective adaptation luminance		Mesopic test luminance[b]	
	$L_{v,ave}$ [cd m^{-2}]	TI [%]	$L_{v,veil}$ [cd m^{-2}]	$L_{v,veil}$ [cd m^{-2}]	$L_{v,effective}$ [cd m^{-2}]	$L_{mes,effective}$ [cd m^{-2}]	$L_{mes,t}$ [cd m^{-2}]	$L_{v,effective}$ [cd m^{-2}]	$L_{mes,effective}$ [cd m^{-2}]	$L_{mes,t}$ [cd m^{-2}]	[%]
M1	2.00	10	0.27	0.43	2.43	2.57	**1.06**	2.00	2.15	**1.07**	**1.57**
M2	1.50	10	0.21	0.34	1.84	1.99	**1.08**	1.50	1.65	**1.10**	**1.70**
M3	1.00	15	0.23	0.37	1.37	1.52	**1.11**	1.00	1.14	**1.14**	**2.70**
M4	0.75	15	0.18	0.29	1.04	1.18	**1.13**	0.75	0.88	**1.17**	**2.91**
M5	0.50	15	0.13	0.21	0.71	0.83	**1.17**	0.50	0.61	**1.21**	**3.24**
M6	0.30	20	0.12	0.19	0.49	0.59	**1.21**	0.30	0.38	**1.27**	**4.67**

[a]Assuming that the vertical illuminance is equal to the normal illuminance.

[b]Mesopic target luminance for a photopic target luminance of 1 cd m^{-2}.

The bold type numbers are referred in Section 4.5.1.

4.5.2 Surrounding luminance effect with respect to the point-source position

To compare the results of both point-source experiments with the veiling luminance models in Section 4.2 with respect to the point-source position, the surrounding luminance effect per one lux was estimated for the experimental results. The steps are:

1. Determine an effective adaptation luminance for each detection threshold in the same manner stated in Section 4.5.1;

2. Calculate the surrounding luminance effect, $L_{\mathrm{v,veil}}$ in Equation 4.1, by substituting the effective adaptation luminance determined in the first step and the local luminance. For this calculation, the adaptation background luminance, which was always $0.2\,\mathrm{cd\,m^{-2}}$ for all point-source conditions, was used as the local luminance; and

3. Divide the surrounding luminance effect by the vertical illuminance $E_{\mathrm{v,vertical}}$ or the normal illumiance $E_{\mathrm{v,n}}$ for each condition to cancel the difference of the illuminances between the conditions.

The determined surrounding luminance effects per one lux of the vertical illuminance or the normal illuminance for each condition are shown in Figure 4.14. Both results for the point-source intensity and position experiments are plotted in the same figure with different symbols. As shown in this figure, the difference between the vertical illuminance and the normal illuminance is not significant when evaluating the angular characteristics of the surrounding luminance effect.

Three existing veiling luminance models are plotted as thin lines in Figure 4.14. Those are the Stiles-Holladay equation [82] (Equation 4.2), the CIE general disability glare formula [89] (Equation 4.3), and the Stiles-Crawford equation [88] (Equation 4.4). As shown in Figure 4.14, none of them seems to predict the experimental results well over the whole range of the visual angle. The trend of the experimental results seems steeper than those of the existing models.

Thus, a new model was developed to provide a more accurate prediction of the experimental results. Unfortunately, it was decided that the results for 5° should not be taken into account for the new model. Although the process to

determine the effective adaptation luminance relies on the linear relation between the detection threshold and the logarithm of the effective adaptation luminance, it has been verified only over a range between and around the two levels of the adaptation background luminances for the reference conditions, as shown in the uniform experiment results in Figure 4.12. However, the result for 5° is outside the range over which the linear relation has been shown. The new model, which is based on a regression line for the surrounding luminance effect per one lux for all experimental results, is:

$$L_{\mathrm{v,veil}} = \frac{260}{\theta^3} E_{\mathrm{v,vertical}}. \tag{4.6}$$

It is plotted as a thick line in Figure 4.14. The graph shows that the new model can predict the experimental results better than the existing models.

The experimental results do not give any suggestion as to why the new model is different from the existing models. However, hypotheses can be deduced from existing knowledge. Possible causes of the difference are the difference of the receptive field size between fovea and the peripheral field, or a difference in the amount of stray light inside the eyes. For example, larger receptive fields for retinal ganglion cells in the peripheral field than in the fovea [90] can be considered as a reason for the larger surrounding luminance effect than is expected from the Stiles-Holladay equation, which predicts foveal veiling luminance.

The deviation between the Stiles-Crawford equation and the results may be due to the difference in the positions of the target and the point sources. While the experiments in this chapter employed only one target position, the eccentricity of which is 10°, their experiments employed a number of target eccentricities from 5° to 50°. The azimuthal angle of the target in their experiments also varied from 0° to 270° depending on the eccentricity [88].

There are some limitations to the model. First, the model represents only the task performance at the particular task point. Also, the angular characteristic was measured in a particular direction, which was right above the task point. When the locations of task point or the direction of the source is different, the angular characteristic may also be different from the model. A lower limit of the visual angle that the model can be applied is also unclear. Further research is needed to overcome those limitations.

However, when the luminaires on streets or roads are the main sources of the

surrounding luminance effect, it is reasonable to apply the new model. This is because the adaptation patterns for the point-source conditions are analogous to typical street or road lighting scenes: The bright bottom part of the screen corresponds to a lit road surface and the point source corresponds to a luminaire.

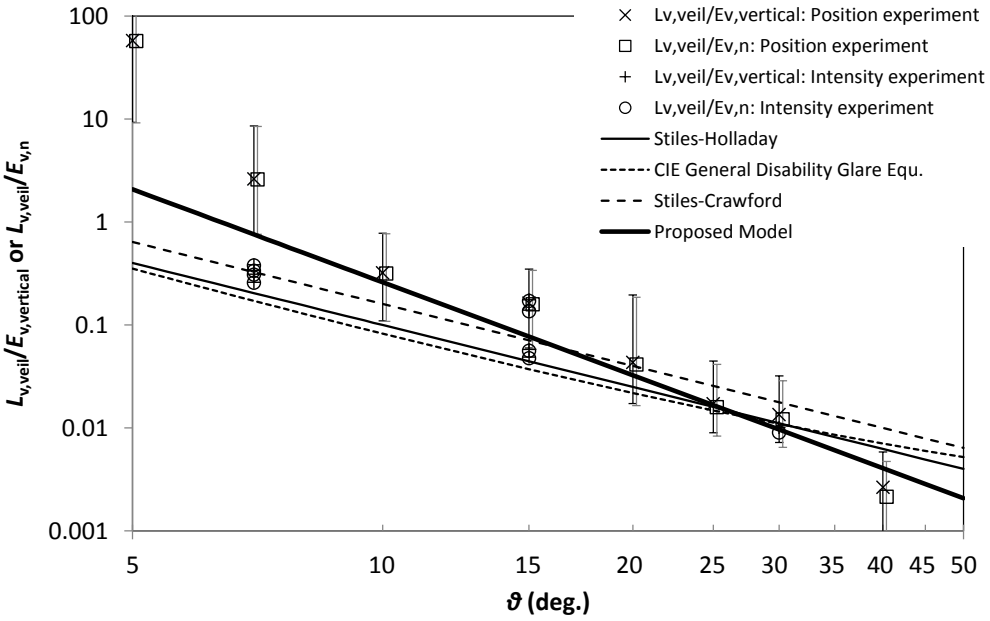

Figure 4.14: The surrounding luminance effects from the experiments (symbols) and the veiling luminance predicted with the models (lines), per one lux of vertical or normal illuminance from the point source

5 Adaptation Luminance Simulation for Mesopic Photometry

5.1 Introduction

The experiments in Chapter 3 suggest that the adaptation field definitions for the mesopic photometry system should take the surrounding luminance effect (abbreviated as SLE in this chapter) and the eye movement (EM, likewise) of observers into account. Moreover, in Chapter 4, the SLE has been investigated and characterized. On the other hand, some researches using eye tracking techniques studied EMs of drivers and pedestrians, and give some data for various situations [10, 70–73, 91].

However, there is still difficulty to define the adaptation fields for real lit scenes because it is unknown how those factors interact with the luminance distribution (LD) of lit scenes and each other. Although some studies have taken both EMs and LDs into account to investigate the adaptation luminance [70–72], no study has taken all three factors into consideration. Moreover, the studies that considered both EMs and LDs mainly discussed luminance falling on the fovea, whereas the mesopic photometry system implementation needs to determine the peripheral adaptation luminance.

Therefore, this chapter proposes and verifies a numerical simulation method for the peripheral adaptation luminance for mesopic outdoor lit scenes, thereby taking into account all three factors: LD, EM, and SLE. Also, the simulation method was applied to real outdoor LDs to test two possible simple predictors for the adaptation luminance.

5.2 Factors affecting the adaptation luminance

5.2.1 Coordinate systems for the simulation

Earlier studies have pointed out some factors that influence the adaptation state of observers. In this chapter, those factors are categorized into three types: LD, EM, and SLE. Additionally, this study introduces an idea named "area of measurement", which will be described in a later section.

To model the four factors and derivatives from them as distribution functions in the field of view, two coordinate systems are introduced (Figure 5.1). One coordinate system is a spherical coordinate system (α, β), where α is the horizontal angle and β is the vertical angle, to basically present the position on the retina. This will be referred to as the "retinal coordinate system". Another coordinate system is also a spherical coordinate system that has the same structure with different symbols (α', β') but fixed to the world outside the observer, not to the observer's visual system. This will be referred to as the "object coordinate system". Both coordinate systems share the origin at the observer's eye position as shown in Figure 5.1. When discussing the adaptation state of an arbitrary peripheral point in the field of view, the point $(\alpha, \beta) = (0, 0)$ in the retinal coordinate system corresponds to a peripheral point, not the fovea. The point $(\alpha', \beta') = (0, 0)$ in the object coordinate system is a point corresponding to the point $(\alpha, \beta) = (0, 0)$ in the retinal coordinate system when the observer looks at an "original point" in the object coordinate system. Since the position of the original point does not matter for the simulation process, it is not given specifically. When the observer moves his/her line of sight, the retinal coordinate system follows the movement while the object coordinate system does not.

5.2.2 Luminance distributions

The LD of a lit scene is a fundamental factor for the adaptation luminance. Usually, the luminance range for outdoor lighting at night is much wider than that for indoor lighting. According to the CIE road lighting recommendations, CIE 115:2010, average luminances of $0.3\,\mathrm{cd\,m^{-2}}$ to $2.0\,\mathrm{cd\,m^{-2}}$ are recommended [8]. Since a certain level of non-uniformity is allowed in the recommendation, the minimum luminance, usually at the end of lit areas, may be $0.1\,\mathrm{cd\,m^{-2}}$. On the other

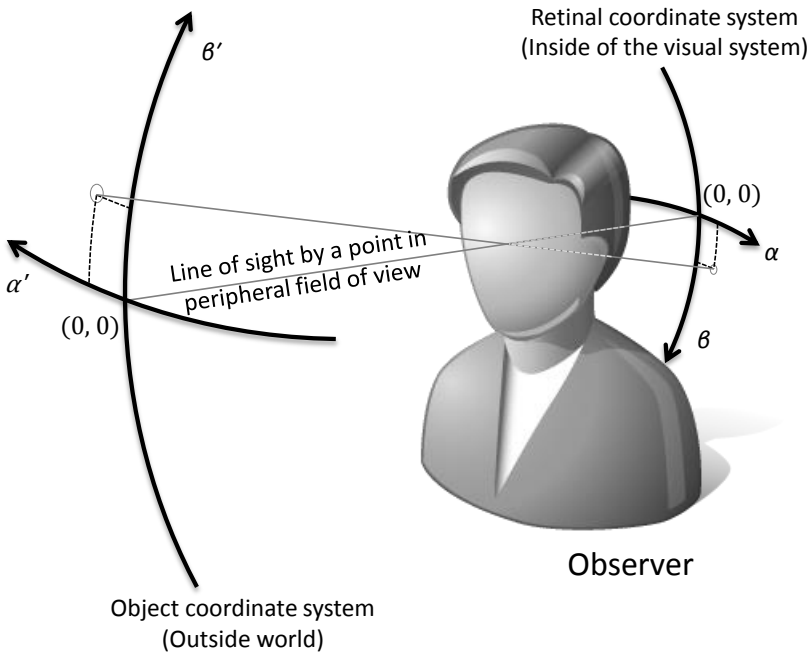

Figure 5.1: The object coordinate system and the retinal coordinate system. Both coordinate systems share a pivot at the observer's eye position

hand, there may be various bright light sources, such as luminaires, headlamps of oncoming cars or luminous signs, in the same scene. For example, some luminaires have a luminance of more than $10\,000\,\mathrm{cd\,m^{-2}}$. In this chapter, a LD is expressed as a photopic luminance level function $L_\mathrm{v}(\alpha', \beta')$ with respect to the object coordinate system (α', β').

5.2.3 Eye movements

In this study, the EM is modeled as a two-dimensional (2D) Gaussian probability density distribution $f_\mathrm{EM}(\alpha', \beta')$ with no correlation expressed as:

$$f_\mathrm{EM}(\alpha', \beta') = \frac{1}{2\pi\sigma_{\alpha'}\sigma_{\beta'}} \exp\left[-\frac{1}{2}\left\{\left(\frac{\alpha'}{\sigma_{\alpha'}}\right)^2 + \left(\frac{\beta'}{\sigma_{\beta'}}\right)^2\right\}\right] d\alpha' d\beta' \qquad (5.1)$$

where $\sigma_{\alpha'}$ and $\sigma_{\beta'}$ are standard deviations (SD) for the horizontal and vertical directions. This function is defined with respect to the object coordinate system. It should be noted that the EM function is centered at the origin of the object coordinate system so that it just expresses relative movements of the line of sight.

Table 5.1: Extent of the eye movements in existing studies

Extent of eye movements in existing studies				SD when assuming 2D Gaussian distribution (°) $\sigma_{\alpha'}$	$\sigma_{\beta'}$
Cengiz et al. [72] (Drivers on rural road)	Range of 50 % contour (°)				
	Conditions	Vertical	Horizontal		
	Lit	2.9	3.6	1.1	1.2
	Unlit	3.3	3.3	1.2	1.2
Winter and Völker [71] (Drivers)	Range most[a] of fixation are located within (°)				
	Conditions	Vertical	Horizontal		
	Main road	10	10	1.6	1.6
	Residential street	10	20	1.5	2.2
Foulsham et al. [91] (Pedestrians)		SD of gaze frequency distribution (°)			
		Vertical	Horizontal		
		5.2	7.6	5.2	7.6

[a]Probability that the fixation are located within the area is 84 % for main road and 89 % for residential street.

Table 5.1 is a summary of existing studies regarding the extent of EMs for drivers and pedestrians. Assuming a 2D Gaussian distribution, the SD for the vertical and horizontal directions can be determined from each study. The EM distribution is the narrowest in the rural driving sequence [72]. For drivers on a main road and a residential street, the extent is marginally wider than that on the rural road [71, 73]. Especially, the horizontal SD on the residential street is nearly 1.8 times wider than that for the rural road. The study with pedestrians shows the widest EM distribution. Pedestrians move their line of sight much wider than drivers [91]. Note that the horizontal SD for pedestrians determined by Foulsham et al. [91] is based on the EM in a "head-centered" frame. The real SD, which is in a "world-centered" frame, may be different.

5.2.4 Surrounding luminance effect

As shown in Chapters 3 and 4, the SLE is an increment of the adaptation luminance at a point in the field of view caused by the surrounding luminance and can be characterized with the veiling luminance model in Equation 4.6. The model is used to predict the SLE at a task point from a surrounding source, but it also can be converted to a function to predict the SLE due to a point source for its surrounding area. The SLE function f_{SLE} due to a small square source causing a luminance of $1\,\mathrm{cd\,m^{-2}}$, the size of which is $d_\alpha \times d_\beta$ in visual angle, can be derived from Equation 4.1 as:

$$f_{\mathrm{SLE}}(\alpha, \beta) = \frac{260}{\theta^3} d\omega \tag{5.2}$$

where

$$\theta = \tan^{-1} \sqrt{\tan^2 \alpha + \tan^2 \beta} \tag{5.3}$$

$$d\omega = 4 \sin^{-1} \left(\sin \frac{d\alpha}{2} \sin \frac{d\beta}{2} \right). \tag{5.4}$$

The $d\omega$ is the solid angle of the image of a small source in the retinal coordinate system. The SLE function $f_{\mathrm{SLE}}(\alpha, \beta)$ is a function in the retinal coordinate system, with the source causing the SLE at the coordinate origin.

Note that the range of (α, β) over which Equation 5.2 is applied should be limited because Equation 4.6 is modeled based on experiments with a limited angle range. Specifically, the model may overestimate the SLE in an area just

adjacent to the source. Thus, in this study, Equation 5.2 is just applied to a range outside a threshold angle θ_{th} for θ. For inside θ_{th}, f_{SLE} is defined as:

$$f_{\mathrm{SLE}}(\alpha,\beta) = \frac{1 - \iint_{D_{\mathrm{out}}} f_{\mathrm{SLE}}(\alpha,\beta)d\alpha d\beta}{\iint_{D_{\mathrm{in}}} d\alpha d\beta} \tag{5.5}$$

where

$$D_{\mathrm{out}} = \{(\alpha,\beta)|\theta \geq \theta_{\mathrm{th}}\} \tag{5.6}$$

$$D_{\mathrm{in}} = \{(\alpha,\beta)|\theta < \theta_{\mathrm{th}}\} \tag{5.7}$$

which is uniform inside θ_{th}. The second term of the numerator, which is the integration of the function outside of θ_{th}, means the subtraction of the light scattered outside of θ_{th} from the light coming from the direction $(\alpha,\beta) = (0,0)$. It adjusts the global integration of $f_{\mathrm{SLE}}(\alpha,\beta)$ to one.

5.2.5 Area of measurement

This study takes an approach to determine an average adaptation luminance for an area of measurement (AOM). The AOM is an area that is illuminated by a lighting installation to be tested and is measured photometrically to verify the installation. For example, a road surface that the lighting design intends to illuminate is the AOM. The road surface is usually seen as a trapezoidal area from drivers' view point.

For the adaptation luminance simulation, AOM is modeled as a 2D function $f_{\mathrm{AOM}}(\alpha',\beta')$ with respect to the object coordinate system (α',β'). This function takes a value of one for inside the AOM and zero for outside the AOM.

5.3 Simulation method

The simulation method in this study integrates the four factors, the LD, the EM, the SLE, and the AOM, into an adaptation luminance of the AOM.

To simplify the simulation process, some assumptions are introduced. The first assumption is that the four factors are independent each other. The simulation method neglects possible correlations between the EMs and the LDs due to observers' aversive behavior to glare sources. In most cases, this simplification is

considered to increase simulated adaptation luminances. When the S/P ratio of the light source is more than one, a higher adaptation luminance corresponds to lower mesopic quantities, which means underestimation of the lighting effect. Therefore, the error caused by the assumption can be considered on the safe side.

The second assumption is that the observers never rotate their head around an axis of the line of sight. Observers sometimes tilt their head to a side, but this was considered negligible in the simulation.

The third assumption is that the SLE, modeled as Equation 5.2, is the same for each point in the field of view and forms a complete solid of revolution centered at a source (a point at $\theta = 0$). As shown in the difference between the Stiles-Holladay formula [82] for the fovea and the Stiles-Crawford formula [88] for the peripheral field of view, coefficients in Equation 5.2 may depend on the position in the field of view. Additionally, even for a point in the field of view, the veiling luminance caused by a source may vary depending on the azimuthal angle from the source. This non-uniformity of the SLE has been studied for the fovea [92]; however, enough data is not available for the peripheral SLE at present.

The simulation method consists of the following four steps:

1. Effective luminance distribution calculation;
2. Adaptation luminance distribution calculation;
3. AOM hit probability distribution calculation; and
4. Adaptation luminance calculation.

Each step will be explained in the following sections. All distributions (functions) derived in the simulation steps are with respect to the retinal coordinate system.

5.3.1 Effective luminance distribution

The effective luminance is the luminance after taking the SLE into account. It is the adaptation LD when the observer's line of sight is fixed. In this case, if there were no SLE, then each point of the retina would adapt to a nominal luminance from each direction. However, light from each direction slightly scatters to an area surrounding the corresponding point in the retinal coordinate system, as characterized as the SLE function. As a result, SLEs due to the light from each

direction overlap each other and slightly diffuse the LD projected on the retinal coordinate system.

In this step, since the observer's line of sight is assumed to be fixed at the original point for the effective LD, the LD projected to the retinal coordinate system $L_{\mathrm{v}}(\alpha, \beta)$ is determined from $L_{\mathrm{v}}(\alpha', \beta')$ by substituting as $(\alpha, \beta) = (\alpha', \beta')$. Then the effective LD $L_{\mathrm{v,effective}}(\alpha, \beta)$ can be calculated by convolution of the projected LD and the SLE as:

$$L_{\mathrm{v,effective}}(\alpha, \beta) = (L_{\mathrm{v}} * f_{\mathrm{SLE}})(\alpha, \beta). \tag{5.8}$$

5.3.2 Adaptation luminance distribution

Although the effective LD is the adaptation LD when the line of sight is fixed, actually observers' line of sight moves as expressed by the EM function. If a point in the retinal coordinate system looks at two points with 50-50 probability due to the EM, the adaptation luminance can be considered the average of the effective luminances for the two points. Generalizing this concept, each point of the retinal coordinate system adapts to an average effective luminance weighted by the EM. This process can be expressed as:

$$L_{\mathrm{v,a}}(\alpha, \beta) = (L_{\mathrm{v,effective}} * f_{\mathrm{EM}})(\alpha, \beta) \tag{5.9}$$

where $L_{\mathrm{v,a}}(\alpha, \beta)$ is the adaptation LD. The $f_{\mathrm{EM}}(\alpha, \beta)$ is derived from $f_{\mathrm{EM}}(\alpha', \beta')$ just by substituting as $(\alpha, \beta) = (\alpha', \beta')$.

5.3.3 AOM hit probability distribution

Each point on the retinal coordinate system has different probability to look inside the AOM, depending on the EM. For instance, a pedestrian's lower parts of the retinal coordinate system more probably look at a street surface (AOM) than upper parts of the retinal coordinate system. The probability for each point on the retinal coordinate system to look inside AOM, $P_{\mathrm{AOM}}(\alpha, \beta)$, can be calculated as:

$$P_{\mathrm{AOM}}(\alpha, \beta) = (f_{\mathrm{AOM}} * f_{\mathrm{EM}})(\alpha, \beta). \tag{5.10}$$

This function is referred to as "AOM hit probability distribution".

In other words, this equation expresses that the EM spreads the retinal image of the AOM over a large area. In the next step, an adaptation luminance is determined for the spread AOM projection in the retinal coordinate system.

5.3.4 Adaptation luminance

Finally, the adaptation luminance of the AOM, which is the average adaptation luminance weighted with the AOM hit probability distribution, is derived as:

$$L_{\mathrm{v,a,AOM}} = \frac{\iint L_{\mathrm{v,a}}(\alpha,\beta) P_{\mathrm{AOM}}(\alpha,\beta) d\alpha d\beta}{\iint P_{\mathrm{AOM}}(\alpha,\beta) d\alpha d\beta} \tag{5.11}$$

where $L_{\mathrm{v,a,AOM}}$ is the adaptation luminance of AOM.

5.4 Verification of the simulation method

5.4.1 Method

To verify whether the adaptation luminance simulation method can predict the real adaptation luminance accurately, the simulation method was applied to the adaptation patterns used in the point-source intensity experiment in Chapter 4.

Totally 12 LDs for the adaptation patterns (three point source positions × four point source luminous intensities) in Figure 4.2 were generated from the design of the patterns. The resolution of the LDs was set at 0.2 °/pixel. The size, the location, and the luminance of the illuminated area in the adaptation patterns were simulated in the LDs as stated in Section 4.3.1. The luminance of other area was deemed to be $0\,\mathrm{cd\,m^{-2}}$. The point source was assumed a Lambertian, circular, and uniform source, the diameter of which is a visual angle of 1.8°. The luminance was calculated from the vertical illuminance at the eye position, by using the Lambert's cosine law and the photometric distance law (the inverse square law).

The EM was assumed uniform in the 2° × 5° oval area in which the fixation point moved in the adaptation phase. The function $f_{\mathrm{SLE}}(\alpha,\beta)$ in Section 5.2.4 was employed as the SLE without any changes. The AOM was set as an isosceles trapezoidal area horizontally centered in the patterns. The upper side and the lower side were positioned at 2.5° and 7.5° below the center of the fixation area.

The length of the upper and the lower side of the trapezoidal area were set at 9.8° and 29.4° visual angle, respectively, which corresponding a six meter width road so that the task point is inside the AOM.

From these functions, the adaptation luminance of the AOM was calculated according to the simulation method in Section 5.3. Then, the results were compared with the empirical effective adaptation luminance calculated in Section 4.5.1.

5.4.2 Results

The comparison of the simulated and the empirical adaptation luminance is shown in Figure 5.2.

The graph clearly shows that the simulation results behavior agrees with that of the empirical adaptation luminance quite well. The trend that the adaptation luminance increases with the luminous intensity of the point source is well reproduced by the simulation. In both the simulation and the experimental results, the closer point source affects the adaptation luminance more significantly.

The simulation error is also acceptable. The error of the adaptation luminance is

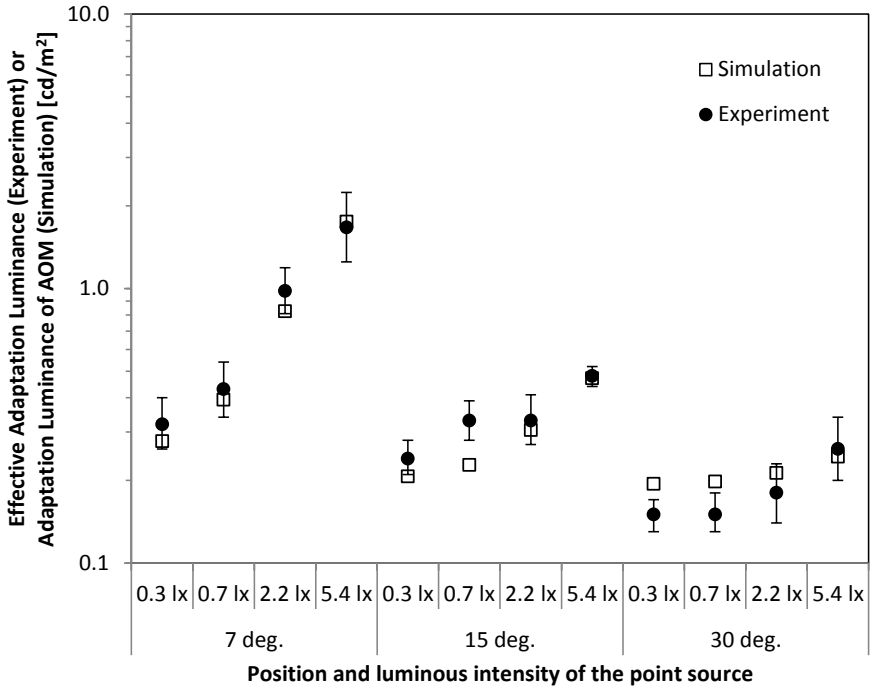

Figure 5.2: Comparisons of the simulated adaptation luminance and the effective adaptation luminance in the point-source intensity experiment

15.2 % on the average and 32.1 % on the maximum. Assuming a worst case, which takes a real photopic adaptation luminance of 0.3 cd m^{-2} and an S/P ratio of 2.4, errors of a mesopic test luminance associated with the average and the maximum adaptation luminance errors are 1.61 % and 3.86 %, respectively. From a practical perspective, these values are sufficiently small comparing the uncertainty of road lighting measurements.

5.5 Testing simple predictors with the adaptation luminance simulation

5.5.1 Method

Even though the simulation method shows good performance to estimate the adaptation luminance, applying the method to each lighting design is burdensome for lighting designers, which design a number of lighting installations. They usually need simple predictors that can be calculated and verified easily. For example, the average luminance of a specific area is preferable. This is the idea of the adaptation field.

Thus, in this section, two possible adaptation luminance predictors are proposed and tested with the simulation method. The predictors are the average luminance of whole scene (LD) and the average luminance of the AOM. To test them, the simulation method described in Section 5.3 was applied to real LD examples.

Totally 16 LDs of real lit scenes were employed for the simulation. They consist of nine scenes of sidewalks in an urban area and seven scenes of walkways in a park (see Figures 5.3 and 5.4). The luminance levels of the urban area scenes are basically higher than those of the park scenes because those scenes contain more bright sources such as signs, luminaires, headlamps of cars, etc. All LDs were measured with a calibrated imaging luminance meter developed in Panasonic corporation, which can measure from 0.1 cd m^{-2} to 10 000 cd m^{-2} of luminance with a high dynamic range (HDR) technique. The visual angles covered by the LDs were 42.5° × 32.4°. Although each LD is actually a LD of a plane, in this simulation, it was assumed to be a LD in the object coordinate system. Note that this assumption causes distortion of the LDs and some error in the simulation

Figure 5.3: Luminance distribution examples: Sidewalks in urban area. Areas delineated with dashed lines are AOMs

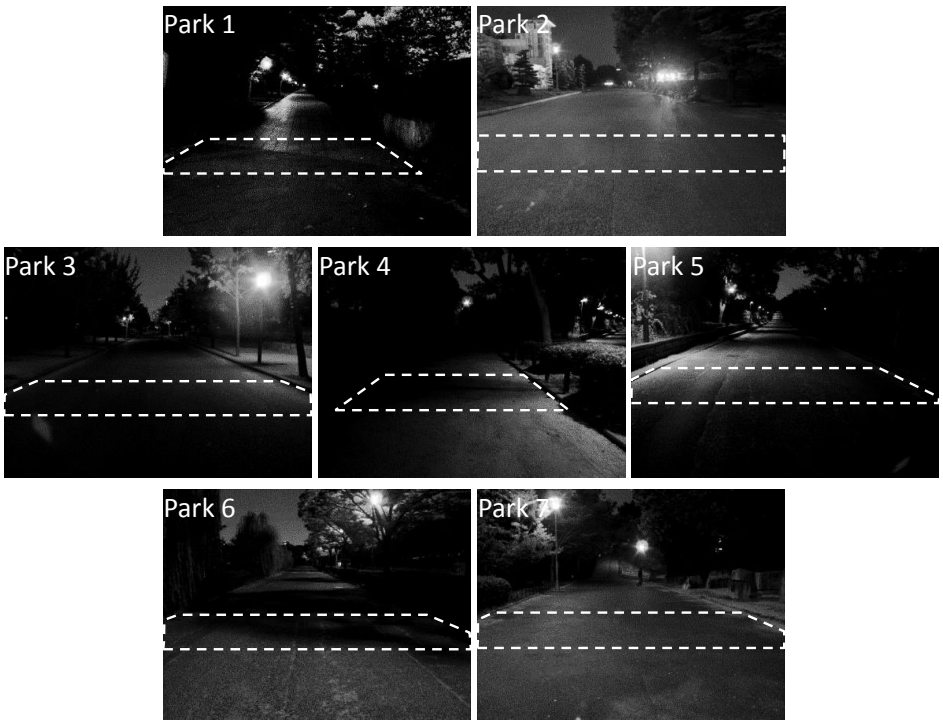

Figure 5.4: Luminance distribution examples: Walkways in a park. Areas delineated with dashed lines are AOMs

results. The solid angle of a pixel at a corner of the LDs under this assumption is 36.7 % larger than the real solid angle of the pixel. However, the distortion is smaller for pixels closer to the center of the LD. The number of pixels of the LDs was originally 1392×1040, but the resolution was reduced to 139×104 to reduce the amount of calculation. The error on the average luminance of the whole scene caused by the resolution reduction is 0.36 % at most, which is not significant. At the reduced resolution, one pixel covered nearly $0.38^\circ \times 0.38^\circ$ of visual angle.

Three types of EMs were employed for the simulation. All EMs were modeled as 2D Gaussian functions, as Equation 5.1, with various SDs. The SDs were $\sigma_{\alpha'} = 1.2^\circ/\sigma_{\beta'} = 1.2^\circ$ (small EM), $\sigma_{\alpha'} = 2.2^\circ/\sigma_{\beta'} = 1.5^\circ$ (midsize EM) and $\sigma_{\alpha'} = 10^\circ/\sigma_{\beta'} = 5^\circ$ (large EM), which correspond to drivers on rural road, drivers on a residential street and pedestrians, respectively (see Table 5.1). Tentatively, θ_{th} took a value of 1°.

Since the sidewalks and the walkways have various geometric dimensions, the AOM is not the same for all LDs. In the simulation, the AOM was defined as an area that is delimited with horizontal lines 2.5° and 7.5° below the vanishing point of the LD image, and the two side edges of the sidewalk or the walkway. The AOMs are shown in Figures 5.3 and 5.4 as delineated areas.

The resolutions of all functions involved in the simulation are adjusted to be the same as the LDs.

5.5.2 Results

The simulated adaptation luminance and the two predictors for each LD are plotted in Figures 5.5 to 5.7. Figures 5.5, 5.6, and 5.7 are based on the small EM, the midsize EM and the large EM, respectively. For all of the figures, open squares show the simulated adaptation luminances; filled diamonds are the average luminances of whole scene, and the filled circles are the average luminances of the AOM.

For the small EM and the midsize EM, the simulated adaptation luminances are very close to the average luminances of the AOM and far from the average luminances of the whole scene. This means that the adaptation luminance could be simply predicted with the average luminance of the AOM.

For the large EM in Figure 5.7, the tendency is slightly different from that of

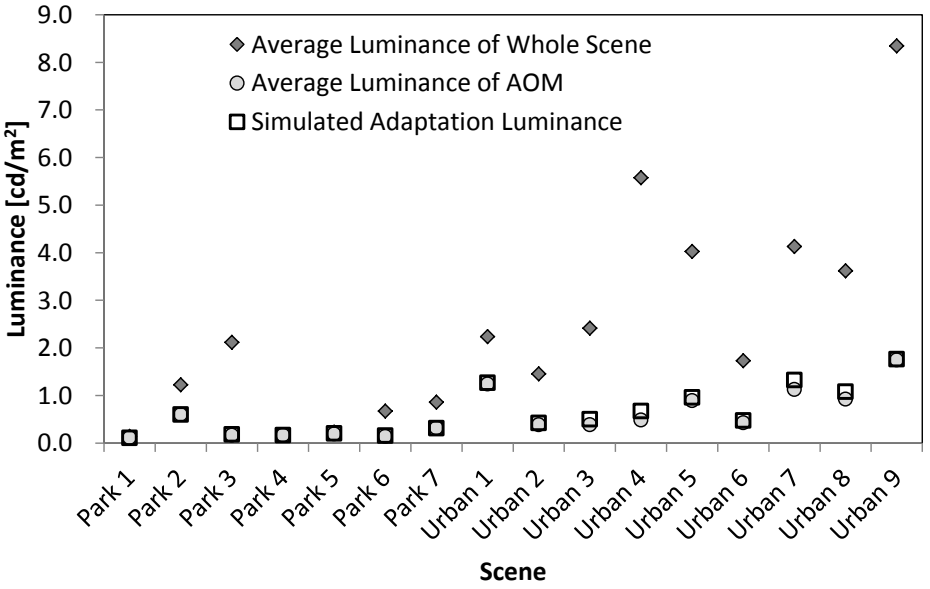

Figure 5.5: Simulated adaptation luminance with small EM

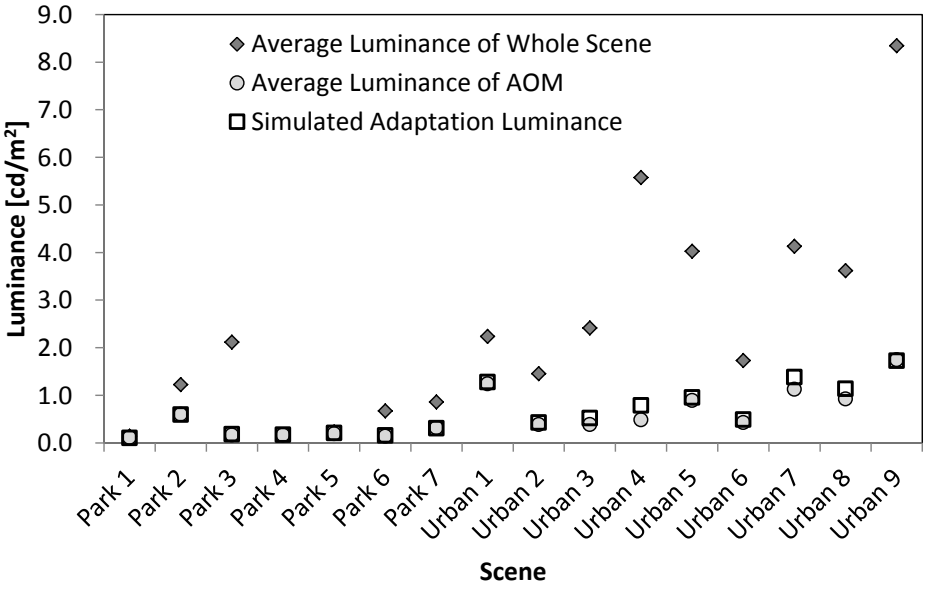

Figure 5.6: Simulated adaptation luminance with midsize EM

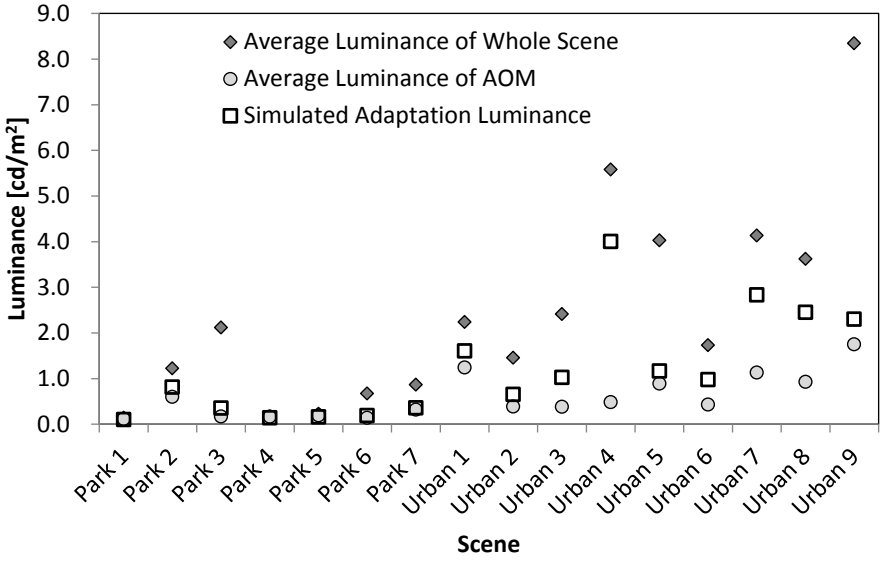

Figure 5.7: Simulated adaptation luminance with large EM

the other EMs. For the Urban 4, Urban 7 and Urban 8 scenes, the simulated adaptation luminances are closer to the average luminances of whole scene than those of the AOM. Also, for other scenes, the simulated adaptation luminances tend to be higher than those for the small or the midsize EM in Figure 5.5 or 5.6. However, those simulation results are still closer to the average luminance of the AOM.

Unexpectedly, the average luminance of whole scene is always higher than the average luminance of the AOM. This is because the LDs include very high-luminance light sources, such as luminaires or headlamps of cars.

5.6 Discussion

5.6.1 Applicability of the simulation method

As shown in Section 5.4, the simulation method shows accurate adaptation luminance estimations for the LDs used in the point-source intensity experiment in Chapter 4. These results do not verify the SLE model since the model was established based on the same experiment. However, the results support that the simulation method combine the EM, the AOM, and the SLE appropriately. Because the LDs roughly mimic typical nighttime road lighting scenes, the simulation

method can be considered applicable to such scenes.

The correlation between the simulation result and the adaptation luminance may depend on the relative size of the AOM with respect to the other factors, the position of the AOM, and the LDs. To verify whether the simulation method is generally applicable or not, adaptation luminances for various LDs are necessary. Although such data sets can be found in a recent study [93], the data variation is still not enough. Understanding limits of the simulation method application unfortunately remains an issue.

Another remaining issue is that it can be applied only to static LDs at present. To apply the simulation for sequential LDs representing dynamic luminance distribution changes, e.g. LDs along a driving course, a time constant of the peripheral adaptation state needs to be determined. Then, the dynamic change of adaptation luminance can be simulated from the sequential LDs.

5.6.2 Are HDR LDs necessary for the simulation?

To verify if the HDR technique is critical for the simulation, the same simulation method was applied to non-HDR LDs corresponding to three different exposure levels. Each non-HDR LD was obtained by applying only one optics-electronic conversion function, corresponding to one exposure level, to the original HDR LDs. The maximum measurable luminance for each exposure level is $20.54\,\mathrm{cd\,m^{-2}}$, $10.27\,\mathrm{cd\,m^{-2}}$, and $5.14\,\mathrm{cd\,m^{-2}}$. Thus, luminances in each original LD more than the maximum value are saturated at the maximum luminance in each non-HDR LD. The luminance resolution for each exposure level, which slightly depends on the luminance, is at most $0.090\,\mathrm{cd\,m^{-2}}$, $0.045\,\mathrm{cd\,m^{-2}}$, and $0.025\,\mathrm{cd\,m^{-2}}$, respectively.

The average ratio of the simulated adaptation luminances for non-HDR LDs to those for the original HDR LDs are shown in Figure 5.8. It is suggested that the simulated adaptation luminance significantly decreases without HDR LDs. This is because of LDs that have high-luminance parts cannot be measured correctly unless the HDR technique is used, and, especially for the large EM, such high-luminance parts affect the adaptation luminance.

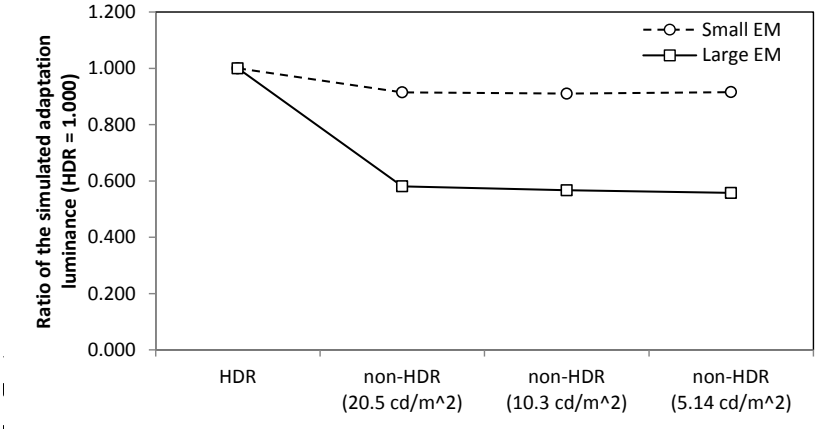

Figure 5.8: Ratio of the simulated adaptation luminance for non-HDR LD to that for the HDR LD. The simulations were done with the large EM and the small EM

5.6.3 An adaptation field definition based on the simulation results

The simulation results for small and midsize EMs suggest that AOM could be considered as the adaptation field for those conditions. Since both EMs are based on drivers' EM, this result provides a basis for treating the average luminance of the road surface as the adaptation luminance for motor traffic lighting applications.

For pedestrian traffic lighting, the result shows that the average luminance of the AOM underestimates the simulated adaptation luminance for the Urban 4, Urban 7 and Urban 8 scenes. These scenes have luminaires near the AOM or many light sources, such as signs and headlamps, above the AOM. Because the SLE is constant for all simulations, these differences are mainly due to the EM. An idea to predict the adaptation luminance for such scenes is to establish a total SLE function that includes both EM and the veiling luminance, and to apply it to bright sources. Since the new SLE depends not only on visual angle between sources and task point but also on the size of the AOM, further research with various lit scenes are necessary to establish a general function.

For other scenes that do not have so many sources around the AOM, the average luminance of the AOM can predict the simulated adaptation luminance reasonably well even for pedestrians. The average error of the mesopic test luminance based on the average luminance of the AOM for those scenes is 2.6 %, which can be considered acceptable.

It should be noted that these observations and suggestions are based on the simulation results. The simulation employs some assumptions as stated in Section 5.3. Also, the models of adaptation factors involved in the simulation have accuracy limitations. Furthermore, the number of the LD examples is limited. Especially, the LDs do not include lit scenes from drivers' view point. For a more confident conclusion, more LD examples are needed for the simulation as well as experimental approaches to measuring real adaptation luminances in real lit scenes.

6 Simplified Measurement Methods for the Mesopic Photometry System

6.1 Introduction

In many cases, after road lighting is installed, photometric field measurements are conducted to verify whether the installation conforms to specifications and achieves the objective of the lighting. These measurements are simple with the photopic photometry system, which is currently used for lighting design; because the luminous efficiency function is always the $V(\lambda)$. All instruments, such as illuminance meters or luminance meters, need to realize a relative spectral responsivity that matches only the $V(\lambda)$. On the other hand, for the mesopic photometry system, the field measurement is more complicated. This is because the mesopic luminous efficiency function $V_{\mathrm{mes};m}(\lambda)$ changes depending on observers' adaptation state, which is caused by the lighting installation itself. As shown in Chapter 2, since the mesopic spectral luminous efficiency function is a combination of that for photopic vision, $V(\lambda)$, and that for scotopic vision, $V'(\lambda)$, the instruments for mesopic photometry need to realize both $V(\lambda)$ and $V'(\lambda)$ detectors [94]. Such instruments will be referred to as "S/P luminance meters" or "S/P illuminance meters".

However, S/P luminance/illuminance meters are not widely available at present. Currently, there is also no field measurement method that is agreed nor approved in any lighting community. This chapter is going to discuss some options for mesopic field measurement methods without S/P luminance/illuminance meters and the error of the methods due to the spectral reflectance of road surfaces.

6.2 Field measurement methods

6.2.1 Rigorous method adhering to CIE 191

In conventional field measurements for road lighting, the luminances (or the illuminances) at grid points on the road surface are measured and utilized as a basis of lighting calculations. The points to be measured are referred to as "test points".

As shown in Section 2.3.1, the measurement of the mesopic luminance of a test point needs two steps: The adaptation luminance measurement (Equations 2.5 to 2.7) and the test luminance measurement (Equation 2.8). The second step, Equation 2.8, can be transformed into

$$L_{\mathrm{mes};m,\mathrm{t}} = \frac{mL_{\mathrm{v,t}} + (1-m)L'_{\mathrm{v,t}}V'(\lambda_{\mathrm{a}})}{m + (1-m)V'(\lambda_{\mathrm{a}})} \tag{6.1}$$

where $L_{\mathrm{v,t}}$ and $L'_{\mathrm{v,t}}$ are the photopic and scotopic luminances of the test point. Thus, both measurements need a S/P luminance meter, because the photopic and the scotopic luminances are necessary as inputs for Equations 2.6 and 6.1.

However, this type of luminance meter has not penetrated the market yet. Moreover, the scotopic channel of the S/P luminance meters is supposed to have lower signal/noise (S/N) ratio than conventional luminance meters in the mesopic range. This is because photodiodes have lower sensitivity at shorter wavelengths, which is needed for the $V'(\lambda)$. Spectral radiance meters, which are another option to realize S/P luminance meters, also have a lower S/N ratio for each spectral channel than filter-type photometers since the incident light is divided into a number of channels. Overall, the accuracy of S/P luminance meters would be expected to be lower than that of photopic luminance meters. This may be critical to measure the mesopic luminance of test points per road lighting measurement standards. Those standards require luminance meters having a field of view less than 20 min of arc [95–97]. Luminance meters with a small field of view have lower S/N ratios. At present, a S/P luminance meter with 2° field of view for laboratory use has been reported [94]. It can measure the luminance level of $0.005\,\mathrm{cd\,m^{-2}}$ with 1 % standard deviation of the mean by integration within two seconds.

The adaptation luminance measurement is easier than the test luminance measurement in terms of accuracy. According to the investigation in the previous chapters, the adaptation fields should cover a significant area, i.e. AOM.

6.2.2 Adaptation SPD method

To avoid using an S/P luminance meter that has a pinpoint field of view, a simplified field measurement method can be considered by assuming that all test points in the adaptation field have the same SPD as the adaptation field.

In this method, the parameter m is determined from the photopic and the scotopic luminance of the adaptation field in the same manner as the rigorous method by Equations 2.5 to 2.7. By assuming that the SPD of the test point is approximately equal to that of the adaptation field, the scotopic luminance of the test point can be approximated from the photopic luminance of the test point and the S/P ratio of the adaptation field, $R_{\mathrm{SP,a}}$. Then, the mesopic luminance of the test point can also be estimated as:

$$L_{\mathrm{mes};m,\mathrm{t}} \simeq \tilde{L}_{\mathrm{mes};m,\mathrm{t}} = \frac{mL_{\mathrm{v,t}} + (1-m)L_{\mathrm{v,t}}R_{\mathrm{SP,a}}V'(\lambda_{\mathrm{a}})}{m + (1-m)V'(\lambda_{\mathrm{a}})} \tag{6.2}$$

as derived from Equation 6.1.

The mesopic enhancement factor, $F_{\mathrm{mes}}(L_{\mathrm{v,a}}; R_{\mathrm{SP,a}})$, is the ratio of the mesopic adaptation luminance to the photopic adaptation luminance [98] as defined as:

$$\begin{aligned} F_{\mathrm{mes}}(L_{\mathrm{v,a}}; R_{\mathrm{SP,a}}) &= \frac{L_{\mathrm{mes};m,\mathrm{a}}}{L_{\mathrm{v,a}}} \\ &= \frac{m + (1-m)R_{\mathrm{SP,a}}V'(\lambda_{\mathrm{a}})}{m + (1-m)V'(\lambda_{\mathrm{a}})}. \end{aligned} \tag{6.3}$$

By substituting Equation 6.3 into Equation 6.2, the mesopic luminance of the test point can simply be estimated by:

$$\tilde{L}_{\mathrm{mes};m,\mathrm{t}} = F_{\mathrm{mes}}(L_{\mathrm{v,a}}; R_{\mathrm{SP,a}})L_{\mathrm{v,t}} \tag{6.4}$$

where the scotopic luminance of the test point is no longer required.

Since this method assumes that the relative SPD of every test point is the same as that of the adaptation field, it could have some error when the SPDs are different. Such differences can be caused by:

- non-uniformity of the spectral reflectance among test points in the field;
- the variation of SPD of the installed lighting in different directions; and
- existence of other types of light sources that have different SPDs from that of the installed lighting, etc.

On the other hand, an S/P luminance meter with a pinpoint field of view is no longer required; because Equation 6.4 just needs the photopic luminance of the test point, and does not need the scotopic luminance. An S/P luminance meter to measure the adaptation luminances is still necessary. However, the S/N ratio of the scotopic detector output can be larger than that of the S/P luminance meter used to measure the test points. This is because the adaptation field probably has a larger field of view than that of the test points, which allows the S/P luminance meter for measuring the adaptation luminances to have a larger field of view and more incident light.

6.2.3 Source SPD method

Another approximation method assumes that all SPDs for the adaptation field and the test points are the same as the known SPD of the light source employed in the lighting installation. This method requires the light source SPD to be known or measured separately.

In this method, the scotopic adaptation luminance $L'_{\mathrm{v,a}}$ is approximated from the photopic adaptation luminance $L_{\mathrm{v,a}}$ and the light source S/P ratio $R_{\mathrm{SP,s}}$ as

$$L'_{\mathrm{v,a}} \simeq R_{\mathrm{SP,s}} L_{\mathrm{v,a}}. \tag{6.5}$$

Then, parameter m and the mesopic adaptation luminance $L_{\mathrm{mes};m,\mathrm{a}}$ are calculated with the iterative calculation using Equations 2.5 to 2.7. The mesopic enhancement factor and the mesopic luminance of the test point are calculated in the same manner as in the Adaptation SPD method, but also with the source S/P ratio $R_{\mathrm{SP,s}}$ instead of the adaptation field S/P ratio $R_{\mathrm{SP,a}}$.

Although the light reaching observers' eyes is usually reflected from the road surface or other objects in the field [99], this method does not take into account the spectral reflectance of the objects reflecting the light. Therefore, when the spectral reflectance is not neutral, this method could cause some error. Additionally, this method could also cause the same type of error as the Adaptation SPD method, which comes from the non-uniformity of the SPDs in the adaptation field.

However, this method has a unique merit that S/P luminance meters are no longer necessary provided that the source SPD is known in advance. As with existing field measurement methods, the measurement can be taken with conventional luminance meters, the spectral responsivity of which matches the $V(\lambda)$.

6.3 Method of error simulation

As described in Section 6.2, the two simplified methods could have errors caused by discrepancies between their assumptions and the real SPDs in the field. An error source that is usually observed in road/street lighting scene is the spectral reflectance of road surfaces and its variation. Thus, an error simulation was conducted using a road surface spectral reflectance library, named the Santa Barbara Asphalt Road Spectral Library [100, 101].

The library has data on 57 spectral reflectances of road surfaces, mainly from asphalt on roads in Santa Barbara in the United States. It also includes some other types of spectral reflectance, such as paint on asphalt, concrete, gravel, green vegetation, etc. The measurement geometry for these data is not the same as the geometry of drivers or pedestrians observing road surfaces in outdoor lit scenes. However, the variation of the spectral reflectance is still useful to evaluate the error of the simplified methods. According to pictures in the database, the road surfaces were measured in dry conditions. The data of the wavelength range from 360 nm to 830 nm, at 1 nm intervals, were used for the error simulation.

In the simulation, 42 of them, which are the data for asphalt and paint on asphalt, were used to calculate the adaptation luminance. Sixteen out of the 42 spectra (38 %) were for road surfaces in good conditions, and 24 out of the 42 (57 %) were for damaged road surfaces, which included cracked road surfaces, slurry patches and oil spots. Two of them (5 %) were for fresh paint on asphalt, the colors of which were yellow and white. These spectral reflectance data are shown in Figures 6.1 to 6.3. This data selection was done under an assumption that the adaptation field is almost entirely filled with the road surface, which is implied in Chapter 5. The adaptation field was assumed to consist of the same proportion as the 42 data. Forty data, except for the road paints, were assigned to the test points where the errors for the simplified methods were calculated because the field luminance measurements are not conducted for paints usually.

For convenience in the simulation, it was assumed that the photopic luminance of every point in the adaptation field, corresponding to each spectral reflectance datum, was the same. Eleven adaptation luminances were used ranging from $0.1\,\mathrm{cd\,m^{-2}}$ to $2.0\,\mathrm{cd\,m^{-2}}$. Three light sources, which were a MH, a HPS, and an LED, were chosen to calculate the errors. Their SPDs are shown in Figure 6.4.

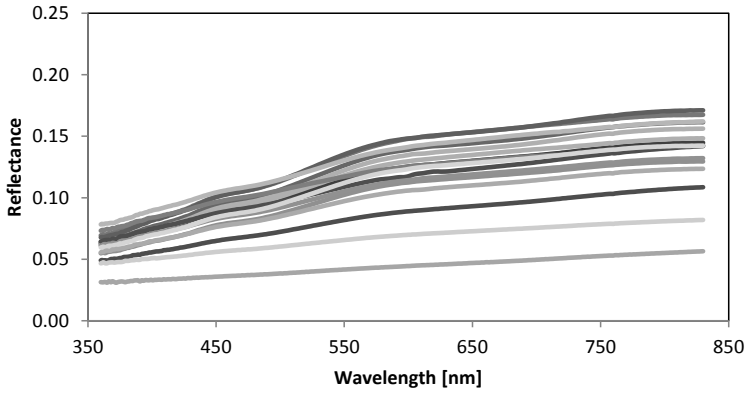

Figure 6.1: The spectral reflectance of road surfaces in good condition

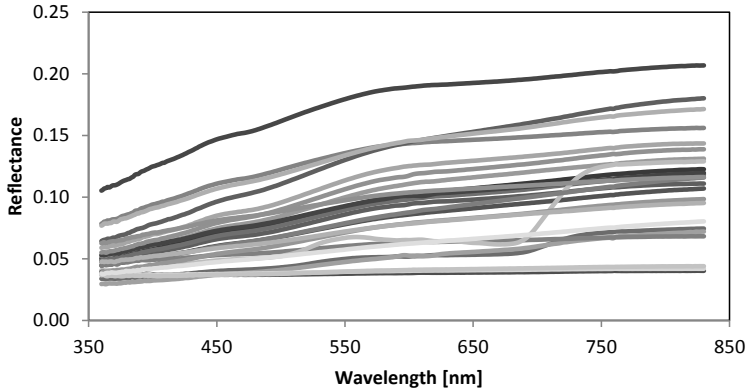

Figure 6.2: The spectral reflectance of damaged road surfaces

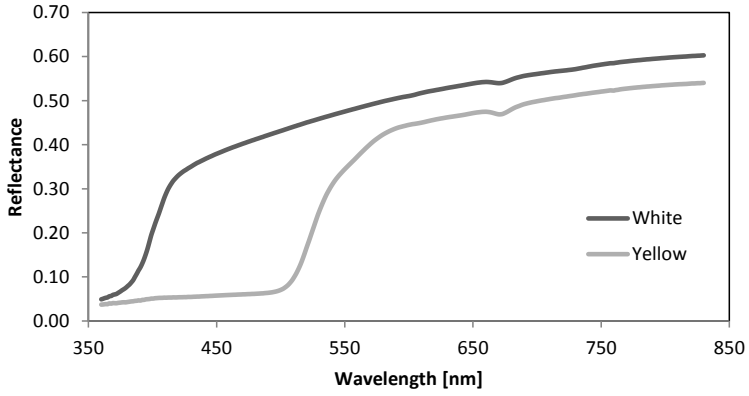

Figure 6.3: The spectral reflectance of fresh yellow and white paint on a road

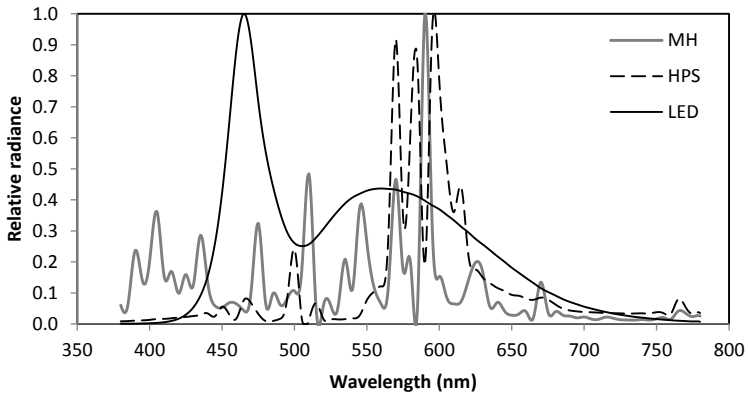

Figure 6.4: The SPDs of the light sources used in the error simulation

The S/P ratios were 1.69, 0.65, and 2.49 for MH, HPS, and LED, respectively. These values were used as the S/P ratio of the adaptation field in the two simplified methods and the test points in the Source SPD method.

The simulation was conducted as follows for each photopic adaptation luminance level. First, the real S/P ratio and the scotopic luminance of each test point and the adaptation field were determined from the spectral reflectance data, the SPD of the light sources, and the given photopic adaptation luminance. The S/P ratio $R_{\mathrm{SP,t},i}$ of a test point i was calculated from the source SPD $S(\lambda)$ and the spectral reflectance $R_i(\lambda)$ as:

$$R_{\mathrm{SP,t},i} = \frac{K'_{\mathrm{m}} \int S(\lambda) R_i(\lambda) V'(\lambda) d\lambda}{K_{\mathrm{m}} \int S(\lambda) R_i(\lambda) V(\lambda) d\lambda}. \tag{6.6}$$

Since the photopic luminance $L_{\mathrm{v,t},i}$ in this simulation is equal for all i, the S/P ratio of the adaptation field $R_{\mathrm{SP,a}}$ is given by

$$R_{\mathrm{SP,a}} = \frac{1}{n} \sum_{i=1}^{n} R_{\mathrm{SP,t},i} \tag{6.7}$$

where n is the number of the test points. The scotopic adaptation luminance $L'_{\mathrm{v,a}}$ and the scotopic luminance $L'_{\mathrm{v,t},i}$ of a test point i were determined from their respective photopic luminances using their respective S/P ratios. Since percentage error is independent of the luminance of the test point, an arbitrary value was used for $L_{\mathrm{v,t}}$.

Second, the real mesopic luminance of a test point $L_{\mathrm{mes};m,\mathrm{t},i}$ was determined from $L_{\mathrm{v,a}}$, $L'_{\mathrm{v,a}}$, $L_{\mathrm{v,t},i}$, and $L'_{\mathrm{v,t},i}$ by the rigorous method.

Third, the approximate mesopic luminances of test points $\tilde{L}_{\mathrm{mes};m,\mathrm{t},i}$ were calculated by each simplified method. The photopic and scotopic adaptation luminances for the Adaptation SPD method were the same as the respective values in the rigorous method. On the other hand, $L'_{\mathrm{v,a}}$ was re-calculated for the Source SPD method by Equation 6.5.

Finally, errors of the mesopic luminance of test points determined by each simplified method, $e_{\mathrm{method},i}$, were calculated as

$$e_{\mathrm{method},i} = \frac{\tilde{L}_{\mathrm{mes};m,\mathrm{t},i} - L_{\mathrm{mes};m,\mathrm{t},i}}{L_{\mathrm{mes};m,\mathrm{t},i}} \tag{6.8}$$

These errors were calculated for each simplified method.

6.4 Results of error simulation

6.4.1 Adaptation SPD method

The error distribution for the Adaptation SPD method for each photopic adaptation luminance, for each source, is shown in Figures 6.5 to 6.7. Figures 6.5 to 6.7 show the simulation results with MH, HPS, and LED, respectively.

A common observation among all light sources is that the errors are distributed in wider range for darker adaptation luminance levels. Furthermore, the extent of the errors varies between light sources. LED has the largest error distribution, that of MH is the second largest, and that of HPS is the smallest. The error distribution range depends on the absolute difference of the S/P ratio of the light source to one. The error range is larger when the absolute difference is larger.

For all light sources, there are a few spectral reflectance data that have much larger error than the others. For instance, while the errors of the mesopic luminance at $0.1\,\mathrm{cd\,m^{-2}}$ of the photopic adaptation luminance for almost all test points are within $+1.2\,\%$ to $-3\,\%$, only three exceptions are out of this range. These exceptions are the spectral reflectance data of slurry seals, which are used to repair cracks on road surfaces. For the same condition, the errors of the mesopic luminance for good road surfaces are distributed within $+1.2\,\%$ to $-2.5\,\%$.

Average errors, which are shown as filled diamond symbols in the figures, slightly deviate from zero for lower adaptation levels. This deviation is mainly caused by the colored paints (yellow paints, specifically) in the adaptation field, the spectral

reflectance of which differs much from that of the test points (asphalt). The existence of such points with a different color shifts the S/P ratio of the adaptation field $R_{\mathrm{SP,a}}$ from the average S/P ratio of the test points to that of the points with different color. This shift can be an error source for the Adaptation SPD method, which assumes that the SPDs of test points are equal to that of the adaptation field. This will be discussed in Section 6.5.3.

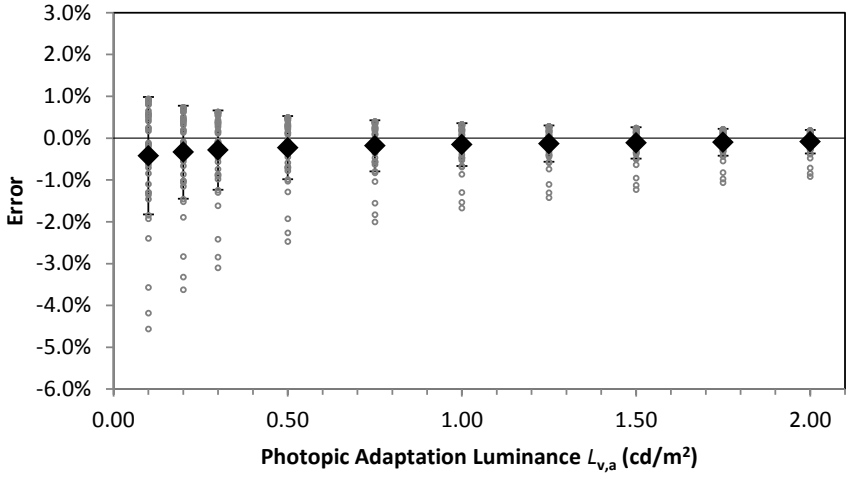

Figure 6.5: Simulated error distribution for the Adaptation SPD method with MH lighting. The small gray circle symbols show the errors for each test point. The filled diamond symbols show the average error at each photopic adaptation luminance. The error bars are one standard deviation

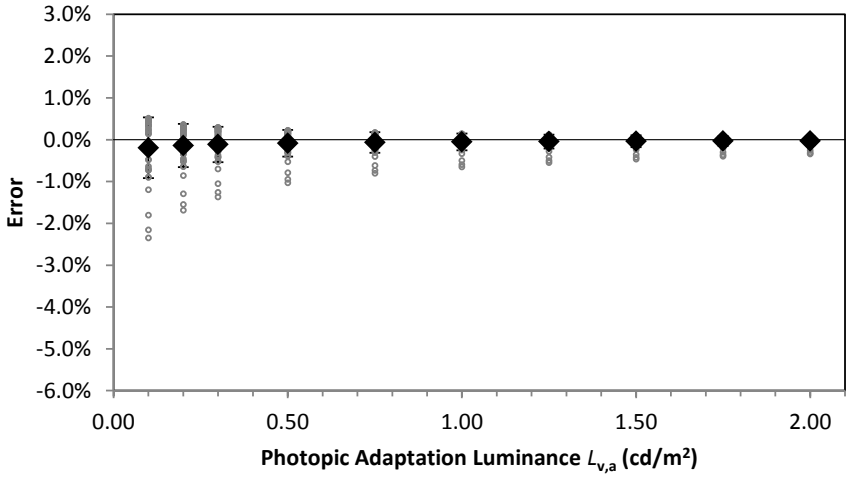

Figure 6.6: Simulated error distribution for the Adaptation SPD method with HPS lighting. All symbols are the same as in Figure 6.5

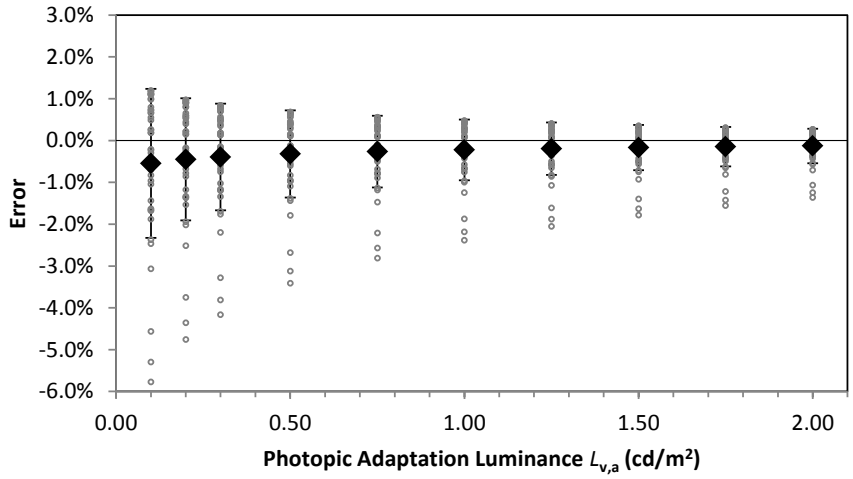

Figure 6.7: Simulated error distribution for the Adaptation SPD method with LED lighting. All symbols are the same as in Figure 6.5

6.4.2 Source SPD method

The errors of the mesopic luminance of the test points for the Source SPD method are shown in Figures 6.8 to 6.10 for MH, HPS, and LED lighting, respectively.

The error distributions shown in Figures 6.8 to 6.10 have similar characteristics to those shown in Figures 6.5 to 6.7. The errors are distributed over a wider range for lower adaptation luminances, as well as for larger absolute differences of the source S/P ratio from one. A unique observation compared with the Adaptation SPD method is that the average error also increases with decreasing the adaptation luminance. This deviation is caused by the difference between the real S/P ratio of the adaptation field and the source S/P ratio, which is used as an approximation of the S/P ratio of the adaptation field in the Source SPD method.

6.5 Discussion

6.5.1 Significance of the error for the simplified measurement methods

The variation of the spectral reflectance of asphalt causes a 3 % to 6 % error distribution for both the Adaptation and the Source SPD methods. However, the average error is less than 1 % for the Adaptation SPD method. On the other hand, the average error for the Source SPD method is nearly 5 % in the worst case.

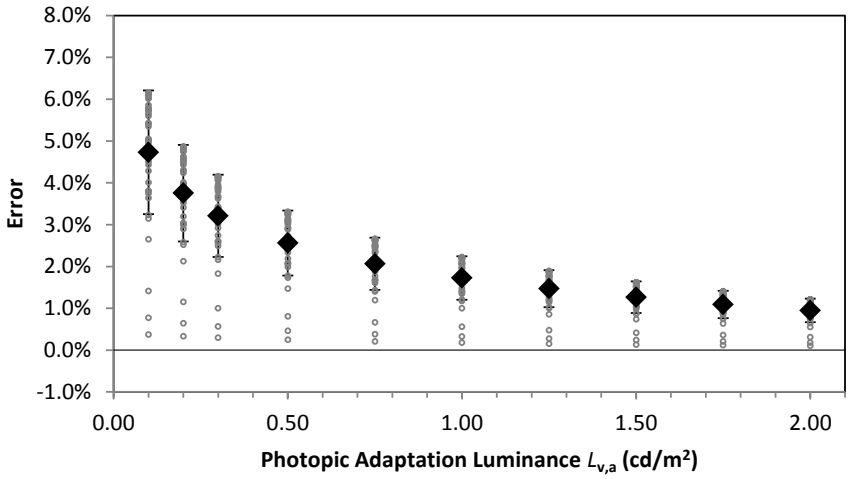

Figure 6.8: Simulated error distribution for the Source SPD method with MH lighting. All symbols are the same as in Figure 6.5

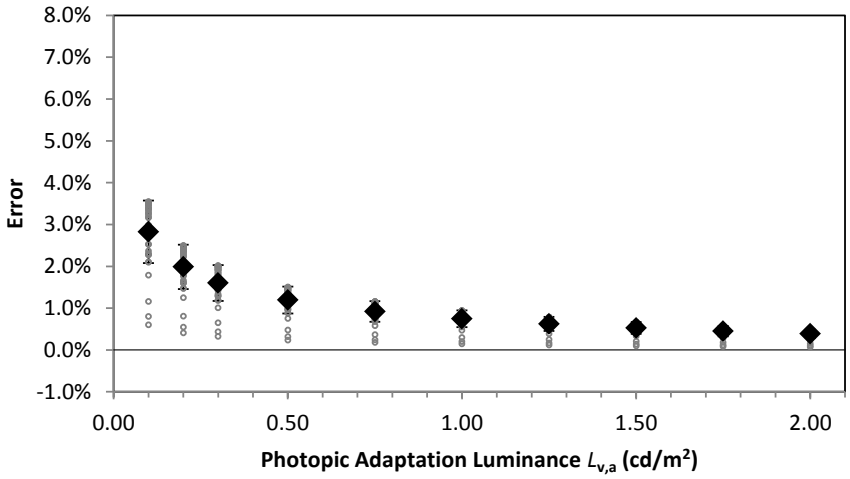

Figure 6.9: Simulated error distribution for the Source SPD method with HPS lighting. All symbols are the same as in Figure 6.5

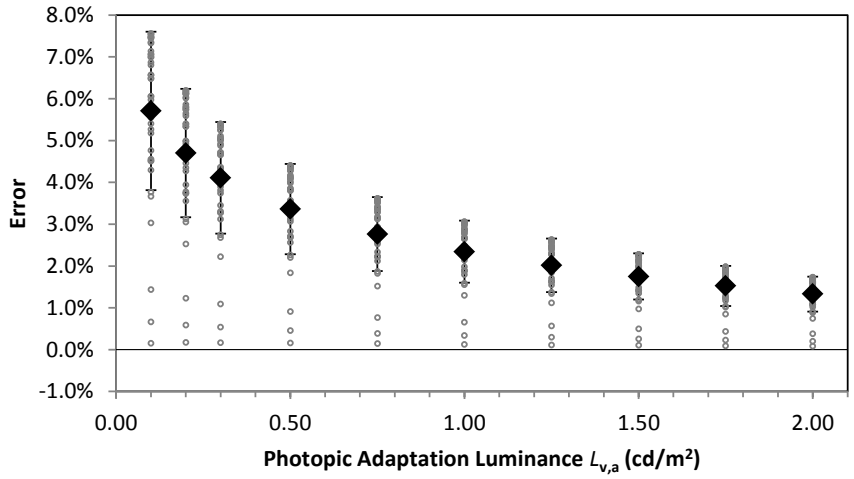

Figure 6.10: Simulated error distribution for the Source SPD method with LED lighting. All symbols are the same as in Figure 6.5

For road lighting, the average luminance or illuminance of the road surface is usually specified and required for installations. Thus, the average error rather than the error distribution is matter. Since the measurement uncertainty only caused by measurement instruments is considered of the order of 5 % , and since there are many other significant uncertainty sources (e.g. the measurement procedure, weather conditions, and electrical power supply conditions) [102], the overall uncertainty of field measurements may reach 10 %. Actually, a measurement uncertainty of 10 % is sometimes acceptable in practice.

Comparing with the field measurement uncertainty, the average error for the Adaptation SPD method can obviously be considered insignificant. The average error for the Source SPD method may or may not be significant depending on the conditions and the overall measurement uncertainty. Thus, a correction method for the Source SPD method will be discussed in the following section.

Note that the error simulation is based on two assumptions. One of them is that the adaptation field is completely filled with a road surface. If the adaptation field and the test objects include not only road surfaces but also other objects such as pedestrians, trees, buildings, signs, etc., the error for the simplified methods may be larger than the simulated values. The diversity of the tested road surface SPDs is limited and the SPDs of the objects other than road surface are expected to have greater variation.

The second assumption is that the adaptation field is composed with 42 isomet-

rics parts, the SPDs of which correspond to the data employed from the Santa Barbara Asphalt Road Spectral Library. The luminance of the parts is also assumed the same each other. Thus, each SPD contributes the simulation results in the same proportion. However, in real lit scenes, the luminance is expected to be non-uniform in the adaptation field. Also, the composition of the SPDs may be different from that of the simulation. The error by the simplified methods may vary depending on these differences.

6.5.2 A correction method for the Source SPD method

Comparing the error simulation results with those for the Adaptation SPD method, the error source is obvious: the deviation of the SPDs of the test points from the source SPD due to the spectral reflectance of the test points. Thus, a correction method using a typical spectral reflectance of test points can be proposed for the Source SPD method. When the typical spectral reflectance of the test point $R_{\mathrm{typ}}(\lambda)$ is known, a correction factor c for the source S/P ratio can be determined as:

$$c = \frac{K'_{\mathrm{m}} \int S(\lambda) R_{\mathrm{typ}}(\lambda) V'(\lambda) d\lambda}{K_{\mathrm{m}} \int S(\lambda) R_{\mathrm{typ}}(\lambda) V(\lambda) d\lambda} \cdot \frac{1}{R_{\mathrm{SP,s}}}. \tag{6.9}$$

Then, Equation 6.5 in the Source SPD method can be replaced with the following equation:

$$L'_{\mathrm{v,a}} \simeq c R_{\mathrm{SP,s}} L_{\mathrm{v,a}}. \tag{6.10}$$

Although the correction factor c varies depending on the combination of the light source and the test point, the values of the correction factors for various light sources are similar for the typical spectral reflectance of road surfaces. This is because the usual road surfaces have broad spectral reflectance, which means non-zero reflectance throughout the visible spectral range. Figure 6.11 shows correction factors for asphalt and concrete in the spectral reflectance library with 125 light sources used for general lighting. This source SPD data set is from NIST CQS (Color Quality Scale) Excel spreadsheet for calculation of a new color rendering metric [103]. It includes conventional light sources such as discharge lamps and fluorescent lamps, existing LED sources, possible LED sources such as RGB-LEDs, etc. As shown in Figure 6.11, each road surface has the similar correction factors for almost all light sources. One exceptional source, the correction factor

of which is around one, is a low pressure sodium lamp because it produces light of predominantly one wavelength. The mean of the correction factors is 0.898 for asphalt and 0.865 for concrete. Each of these values can be employed as the characteristic correction factor for each road surface material. By applying the correction factor for asphalt, the errors of the mesopic luminances of test points for LED, which shows the largest error in the Source SPD method, are reduced as shown in Figure 6.12. The magnitude of error is almost the same as that for the Adaptation SPD method.

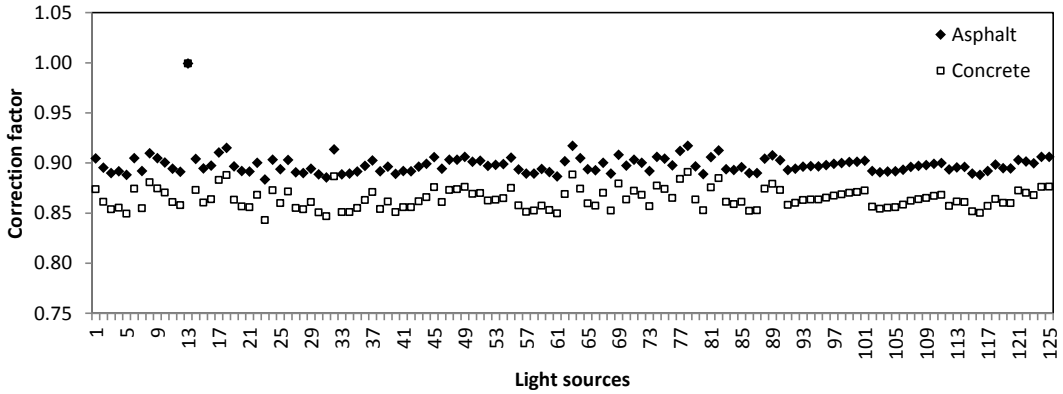

Figure 6.11: Correction factors for various light sources with spectral reflectance data of asphalt and concrete

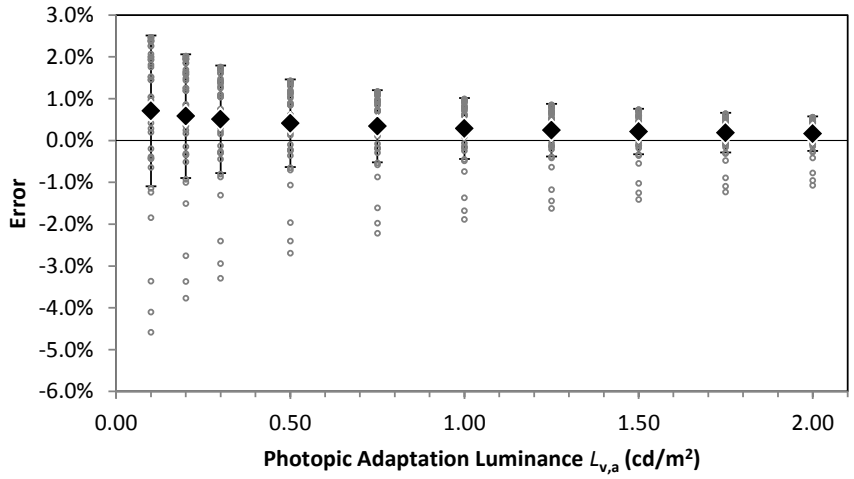

Figure 6.12: Simulated error distribution for the corrected Source SPD method with LED lighting. The source S/P ratio was corrected with the correction factor (= 0.898). All symbols are the same as in Figure 6.5

6.5.3 Robustness to different-color sources in the adaptation field

Since the Source SPD method relies on the source SPD employed in the lighting installation, existence of different-color sources (or objects), such as show windows near the lighting installation, causes an error in the mesopic luminances of test points. To clarify the robustness of the method, error simulations were conducted for a lighting scene where LEDs are employed as main sources and where the test points are also unintentionally lit by HPS.

In this error simulation, the real S/P ratio of each test point was determined as:

$$R_{\mathrm{SP,t},i} = \frac{K'_{\mathrm{m}} \int \{(1-x)S_{\mathrm{LED}}(\lambda) + xS_{\mathrm{HPS}}(\lambda)\} R_i(\lambda) V'(\lambda) d\lambda}{K_{\mathrm{m}} \int \{(1-x)S_{\mathrm{LED}}(\lambda) + xS_{\mathrm{HPS}}(\lambda)\} R_i(\lambda) V(\lambda) d\lambda} \tag{6.11}$$

where $S_{\mathrm{LED}}(\lambda)$ and $S_{\mathrm{HPS}}(\lambda)$ are the SPD of LED and HPS, respectively. The coefficient x is the ratio of the HPS light in the total light illuminating the test point. This ratio is referred to as "HPS ratio" in this section. Seven levels of x, which are 0 to 0.15, were employed for the simulation. It was assumed that all test points to be measured were lit with the same HPS ratio. The real mesopic luminance for each test point was determined by the rigorous method using Equation 6.11 instead of Equation 6.6, while the mesopic luminance of the test points with the Source SPD method was calculated from the S/P ratio of the LED source. The S/P ratio for the Source SPD method was corrected by using the method described in Section 6.5.2.

The simulation results are shown in Figure 6.13. It shows that the error depends on the existence of the different-colored light. A higher HPS ratio causes a larger error in the mesopic luminance of the test points. However, the magnitude of the average error is 4.6 % in the worst case, which can be considered as relatively small. In most cases, the average error is less than 3 %. When the HPS ratio is known, a correction, which is similar with that in Section 6.5.2, can be applied to reduce the error.

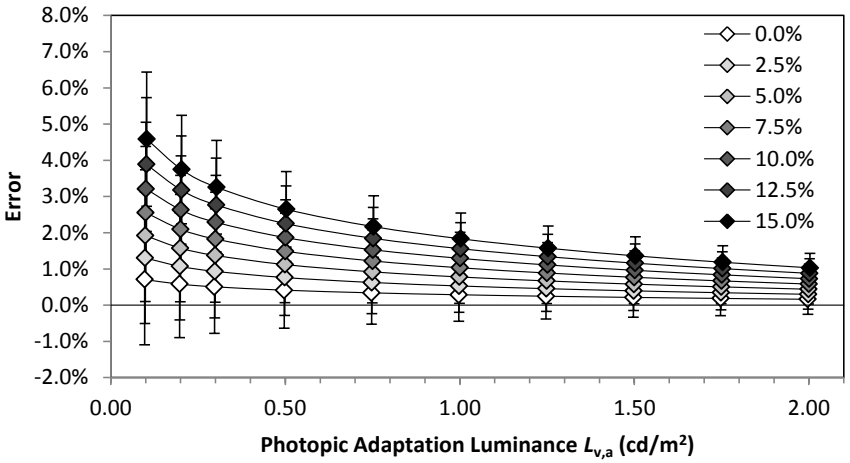

Figure 6.13: Simulated errors in the mesopic luminance calculated with the Source SPD method in some adaptation fields illuminated with LEDs and HPS. Each symbol shows a different HPS ratio (0 % to 15 %) in the adaptation field mainly lit by LEDs. The error bars show one standard deviation of the errors

7 Conclusions

First, this study reviewed the history of mesopic photometry to reveal how the mesopic photometry system recommended in CIE 191 [3] could be utilized for lighting application. An analysis shows roughly 10 % to 40 % of energy consumption, depending on the source SPD and the adaptation luminance, could be reduced for artificial lighting in the mesopic range (e.g. road lighting) by implementing the mesopic photometry system. On the other hand, some limitations of the mesopic photometry system are also recognized. It cannot be used for foveal visual tasks, high-saturated-color lighting, and comparisons of the visual task efficiency in different adaptation levels. Overall, the mesopic photometry system could either reduce energy consumption or improve visual performance for some outdoor lighting applications. However, before they are realized, two remaining issues need to be addressed: defining the adaptation field for real lit scenes, and identifying applications where the mesopic photometry system could be used. I decided to address the former issue in this study.

A big question to define the adaptation field was whether the surrounding luminance, which is luminance distribution outside a peripheral task point, affects the adaptation state significantly or not. To answer this question, this study conducted experiments to measure the surrounding luminance effect on the adaptation state at a peripheral task point, as described in Chapter 3. The results show that the adaptation state on a peripheral task point mainly depends on the local luminance at the task point even at a mesopic light level. The observed surrounding luminance effect was small enough to predict the adaptation state simply from the local luminance when the luminance distribution is relatively uniform. However, the experimental results also suggest that the surrounding luminance effect is larger than the veiling luminance at the fovea. Based on these observations, it is suggested that eye movements and the task area of the lit scene should also be taken into account for adaptation field definitions. This means

that the adaptation field can vary depending on lighting applications because eye movements and the task area are application dependent.

In Chapter 4, the surrounding luminance effect by a high-luminance point source was measured in vision experiments to characterize the effect on the adaptation state of high-luminance sources, such as luminaires and head-lamps of oncoming cars in real lit scenes. The effect was examined with respect to the luminous intensity and the position of the point source. The results show that the surrounding luminance effect can be described as the veiling luminance but with a different model from existing ones. The estimated magnitude of the effect is not so significant for real lighting installation: the negative difference on the mesopic luminance is less than 5 % for road lighting applications in compliance with the CIE road lighting recommendation. Since the surrounding luminance effect is considered as the veiling luminance, the effect also depends on the relative position of the task point and the point source causing the effect. By comparing the experimental results with existing veiling luminance models, it was shown that the surrounding luminance effect decreases more rapidly with increasing visual angle between the task point and the point source than predictions with the existing models. Therefore, a new model, which can more accurately predict the experimental results, has been proposed. The new model is more suitable to predict the surrounding luminance effect from luminaires in road lighting than existing models.

In Chapter 5, a simulation method was developed and applied to luminance distribution data of real lit scenes to give suggestions for adaptation field definitions. The simulation method consolidates adaptation factors, revealed in this study or in existing studies. It is considered to be able to determine the adaptation luminance for typical road lighting scenes at night. The simulation results were compared simple predictors for the adaptation luminance. The comparison suggests that the adaptation luminance can be predicted with the average luminance of the area of measurement (AOM), i.e. the design area of the road surface in a lit scene, where the lighting intends to illuminate. This can reasonably predict the adaptation luminance for motorists' eye movements in all of the luminance distribution examples. For pedestrians' eye movements, it also works for most of the scenes, but underestimates the adaptation luminance for some scenes that have high-luminance sources just around the AOM. It suggests that care is needed in using the average luminance of the AOM as the adaptation luminance when

many extraneous high-luminance sources exist near the AOM in the lit scene.

The rigorous measurement method for the mesopic quantities in compliance with CIE 191 needs special instruments, which are not available widely in practice at present. Thus, in Chapter 6, two simplified mesopic measurement methods, the Adaptation and Source SPD methods, were proposed and the error was simulated with real road surface spectral reflectance data. The Adaptation SPD method can relax the required accuracy of the special instruments, while the Source SPD method allows field measurements only with conventional instruments. When assuming that the adaptation field is filled with a road surface, the error simulation shows that the average error for the Adaptation SPD method is considered insignificant. The average error for the Source SPD is nearly 5 %, which may or may not significant depending on conditions and the overall measurement uncertainty. However, a proposed correction method by using a typical road surface spectral reflectance can reduce the average error for the Source SPD method sufficiently. It was also shown that the proposed method is robust for extraneous sources with different SPD. The error simulation results suggest that the mesopic luminance of the road surfaces can be measured accurately enough with only a conventional luminance meter, when the source S/P ratio and the correction factor for the test points, determined from typical road surface spectral reflectances, are available.

Comprehensively, a conclusion of this study is that the adaptation field for the mesopic photometry system can be defined as the design area of lighting design for typical road lighting. In this case, the adaptation luminance can be measured by using a conventional luminance meter with the Source SPD method proposed in Chapter 6. Unfortunately, for lit scenes with extraneous bright light sources near the design area, the adaptation field definition does not necessarily give sufficient adaptation luminance estimation. For the meantime, a reasonable measure is just refraining from use of the mesopic photometry system for such lit scenes. For the lit scenes with extraneous sources, further research based on various real luminance distribution data is needed. Once such additional data is available, the same methodology in this study can be applied and could give general solutions.

As shown above, I have provided visual evidences and a methodology for adaptation field definitions. Also, I have proposed an adaptation field definition for typical road lighting and a pragmatic field photometric measurement method to

verify lighting installation in the mesopic range. These allow more optimized lighting products and installation for some outdoor lighting application with the mesopic photometry system. Or, those enable choice of the most visually effective light sources at the same energy consumption by quantitative evaluation. This study has paved a way for safer, more reassuring, and more energy-efficient outdoor lighting.

Bibliography

[1] The basis of physical photometry, 2nd edition. CIE 18.2, Commission Internationale de l'Éclairage, Vienna, 1983.

[2] Photometry – the CIE system of physical photometry. ISO 23539:2005 (CIE S010/E:2004), International Organization for Standardization, Geneva, 2005.

[3] Recommended system for visual performance based mesopic photometry. CIE 191, Commission Internationale de l'Éclairage, Vienna, 2010.

[4] Gibson KS and Tyndall EPT. Visibility of radiant energy. *Scientific Paper of the Bureau of Standards*, 19, 1923.

[5] *CIE Compte Rendu, Session 6*, 1924.

[6] Osterberg G. *Topography of the Layer of Rods and Cones in the Human Retina.* Acta ophthalmologica: Supplementum. Nyt Nordisk Forlag, Copenhagen, 1935.

[7] Purkinje JE. *Neue Beiträge zur Kenntniss des Sehens in Subjectiver Hinsicht.* Reimer, Berlin, 1825.

[8] Lighting of roads for motor and pedestrian traffic. CIE 115, Commission Internationale de l'Éclairage, Vienna, 2010.

[9] LEDs and worldwide market for lighting fixtures. S 52, Centre for Industrial Studies, Milano, 2015.

[10] Puolakka M and Halonen L. Implementation of CIE 191 mesopic photometry –ongoing and future actions. In *Proceedings of the CIE 2012*, pages 64–70. Commission Internationale de l'Éclairage, 2012.

[11] Hardis JE. Visibility of radiant energy. In *A century of excellence in measurements, standards, and technology – A chronicle of selected NBS/NIST publications, 1901-2000*. Special Publication 958, National Institute of Standards and Technology, 2012.

[12] Walsh JWT. *Photometry*. Constable & Company, London, 1926.

[13] Eppeldauer GP. Optical radiation measurements based on detector standards. Technical Note 1621, National Institute of Standards and Technology, Gaithersburg, 2009.

[14] *CGPM Compte Rendu, Session 9*, 1948.

[15] *CIE Compte Rendu, Session 12*, 1951.

[16] Crawford BH. The scotopic visibility function. *Proceedings of the Physical Society. Section B*, 62(5):321, 1949.

[17] Abney WW and Festing RE. Colour photometry. *Philosophical Transactions of Royal Society of London*, 177:423–442, 1886.

[18] Blevin WR and Steiner B. Redefinition of the candera and the lumen. *Metrologia*, 11:97–104, 1975.

[19] Jones OC. Proposed changes to the SI system of photometric units. *Lighting Research and Technology*, 10(1):37–40, 1978.

[20] *CGPM Compte Rendu, Session 16*, 1979.

[21] Principles governing photometry. Monographie 83/1, Bureau International Des Poids et Measures, Sévres, 1983.

[22] Wald G. Human vision and the spectrum. *Science*, 101(2635):653–658, 1945.

[23] Mesopic photometry: History, special problems and practical solutions. CIE 81, Commission Internationale de l'Éclairage, Vienna, 1989.

[24] Testing of supplementary systems of photometry. CIE 141, Commission Internationale de l'Éclairage, Vienna, 2001.

[25] Eloholma M, Viikari M, Halonen L, Walkey H, Goodman T, Alferdinck J, Freiding A, Bodrogi P, and Várady G. Mesopic models – from brightness matching to visual performance in night-time driving: a review. *Lighting Research and Technology*, 37(2):155–175, 2005.

[26] Koenig A. Ueber den helligkeitswerthe des spectralfarben bei verschiedener absoluter intensitat. *Abhandlungen stir Physiologischen Optik*, pages 144–213, 1903.

[27] Houston RA. The relative visibility of different colours of the spectrum. *Philosophical Magazine*, 6(25):715–732, 1913.

[28] Hecht S and Williams RE. The visibility of monochromatic radiation and the absorption spectrum of visual purple. *The Journal of General Physiology*, 5:1–33, 1922.

[29] Sloan LL. The effect of intensity of light, state of the adaptation of the eye, and size of photometric field on the visibility curve. *Psychological Monographs*, 38(1):1–87, 1928.

[30] Weaver KS. The visibility of radiation at low intensities. *Journal of the Optical Society of America*, 27(36):36–43, 1937.

[31] Walters HV and Wright WD. The spectral sensitivity of the fovea and extrafovea in the Purkinje range. *Proceedings of the Royal Society of London, Series B*, 131:340–361, 1942.

[32] Kinney JAS. Effect of field size and position on mesopic spectral sensitivity. *Journal of the Optical Society of America*, 54(5):671–677, 1964.

[33] *CIE Compte Rendu, Session 14*, 1960.

[34] *CIE Compte Rendu, Session 15*, 1964.

[35] *CIE Compte Rendu, Session 16*, 1968.

[36] ILV: International lighting vocabulary. CIE S 017, Commission Internationale de l'Éclairage, Vienna, 2011.

[37] Palmer DA. A system of mesopic photometry. *Nature*, 209:276–281, 1966.

[38] Palmer DA. Standard observer for large-field photometry at any level. *Journal of the Optical Society of America*, 58(9):1296–1299, 1968.

[39] CIE 10 degree photopic photometric observer. CIE 165, Commission Internationale de l'Éclairage, Vienna, 2005.

[40] Trezona PW. A system of general photometry designed to avoid assumptions. In *Proceedings of the CIE 21st Session*, pages 30–33. Commission Internationale de l'Éclairage, 1987.

[41] Sagawa K and Takeichi K. Spectral luminous efficiency functions in the mesopic range. *Journal of the Optical Society of America A*, 3(1):71–75, 1986.

[42] Sagawa K and Takeichi K. System of mesopic photometry for evaluating lights in terms of comparative brightness relationships. *Journal of the Optical Society of America A*, 9(8):1240–1246, 1992.

[43] Kokoschka S and Bodmann HW. Ein konsistentes system zur photometrischen stralungsbewertung im gesamten adaptationsbereich. In *Proceedings of the CIE 18th Session*, pages 217–225. Commission Internationale de l'Éclairage, 1975.

[44] Ikeda M, Huang CC, and Ashizawa S. Equivalent lightness of coloured objects at illuminances from the scotopic to the photopic level. *Color Research and Application*, 14(4):198–206, 1989.

[45] Ikeda M and Ashizawa S. Equivalent lightness of colored objects of equal Munsell chroma and of equal Munsell value at various illuminances. *Color Research and Application*, 16(2):72–80, 1991.

[46] CIE supplementary system of photometry. CIE 200, Commission Internationale de l'Éclairage, Vienna, 2011.

[47] He Y, Rea MS, Bierman A, and Bullough JD. Evaluating light source efficacy under mesopic conditions using reaction time. *Journal of the Illuminating Engineering Society*, 26:125–138, 1997.

[48] He Y, Bierman A, and Rea MS. A system of mesopic photometry. *Lighting Research and Technology*, 30(4):175–181, 1998.

[49] Rea MS, Bullough JD, Freyssinier-Nova JP, and Bierman A. X – a system of mesopic photometry based on reaction time measurement. In *Proceedings of the CIE Symposium 2002 on Temporal and Spatial Aspects of Light and Colour Perception and Measurement*, pages 51–58. Commission Internationale de l'Éclairage, 2002.

[50] Rea MS, Bullough JD, Freyssinier-Nova JP, and Bierman A. A proposed unified system of photometry. *Lighting Research and Technology*, 36(2):85–111, 2004.

[51] Performance based model for mesopic photometry. Report 35, Helsinki University of Technology, Lighting Laboratory, Espoo, 2005.

[52] Freiding A, Eloholma M, Ketomäki J, Halonen L, Walkey H, Goodman T, Alferdinck J, Várady G, and Bodrogi P. Mesopic visual efficiency I: detection threshold measurements. *Lighting Research and Technology*, 39(4):319–334, 2007.

[53] Walkey H, Orreveteläinen P, Barbur J, Halonen L, Goodman T, Alferdinck J, Freiding A, and Szalmás A. Mesopic visual efficiency II: reaction time experiments. *Lighting Research and Technology*, 39(4):335–354, 2007.

[54] Várady G, Freiding A, Eloholma M, Halonen L, Walkey H, Goodman T, and Alferdinck J. Mesopic visual efficiency III: discrimination threshold measurements. *Lighting Research and Technology*, 39(4):355–364, 2007.

[55] Goodman T, Forbes A, Walkey H, Eloholma M, Halonen L, Alferdinck J, Freiding A, Bodrogi P, Várady G, and Szalmas A. Mesopic visual efficiency IV: a model with relevance to nighttime driving and other applications. *Lighting Research and Technology*, 39(4), 2007.

[56] The use of terms and units in photometry — implementation of the CIE system for mesopic photometry. CIE TN 004, Commission Internationale de l'Éclairage, Vienna, 2015.

[57] Raynham P and Saksvikrønning T. White light and facial recognition. *The Lighting Journal*, pages 29–33, 2003.

[58] Rea MS, Bullough JD, and Akashi Y. Several views of metal halide and high pressure sodium lighting for outdoor applications. *Lighting Research and Technology*, 41(4):297–314, 2009.

[59] Mesopic vision and public lighting — a literature review and a face recognition experiment. TNOReport TNO-DV 2010 C435, Nederlandse Organisatie voor Toegepast Natuurwetenschappelijk Onderzoek, Soesterberg, 2010.

[60] Fotios S, Yang B, and Cheal C. Effects of outdoor lighting on judgements of emotion and gaze direction. *Lighting Research and Technology*, 47(3):301–315, 2015.

[61] Yang B and Fotios S. Lighting and recognition of emotion conveyed by facial expressions. *Lighting Research and Technology*, 47(8):964–975, 2015.

[62] The effect of spectral power distribution on lighting for urban and pedestrian areas. CIE 206, Commission Internationale de l'Éclairage, Vienna, 2014.

[63] Code of practice for the design of road lighting part 1: Lighting of roads and public amenity areas. BS 5489-1, British Standards Institution, London, 2013.

[64] Evaluation of the impact of spectral power distribution on driver performance. Technical Report FHWA-HRT-15-047, U. S. Department of Transportation, Federal Highway Administration, McLean, 2015.

[65] Roadway lighting. IES RP-8-14, Illuminating Engineering Society of North America, New York, 2014.

[66] Spectral effects of lighting on visual performance at mesopic lighting levels. IES TM-12-12, Illuminating Engineering Society of North America, New York, 2012.

[67] Akashi Y, Rea MS, and Bullough JD. Driver decision making in response to peripheral moving targets under mesopic light levels. *Lighting Research and Technology*, 39:53–67, 2007.

[68] Narisada K. Visual perception in non-uniform fields. *Journal of Light and Visual Environment*, 16(2):81–88, 1992.

[69] Narisada K. Perception under road lighting conditions with complex surroundings. *Journal of Light and Visual Environment*, 19(2):5–14, 1995.

[70] Heynderickx I, Ciocoiu J, and Zhu XY. Estimating eye adaptation for typical luminance values in the field of view while driving in urban streets. In *Proceedings of CIE Centenary Conference*, pages 41–47. Commission Internationale de l'Éclairage, 2013.

[71] Winter J and Völker S. Typical eye fixation areas of car drivers in inner-city environments at night. In *Proceedings of the 12th LUX EUROPA*, pages 30–33. LUX EUROPA, 2013.

[72] Cengiz C, Kotkanen H, Puolakka M, Lappi O, Lehtonen E, Halonen L, and Summala H. Combined eye-tracking and luminance measurements while driving on a rural road: Towards determining mesopic adaptation luminance. *Lighting Research and Technology*, 46(6):676–694, 2014.

[73] Winter J, Fotios S, and Völker S. Gaze direction when driving after dark on main and residential roads: Where is the dominant location? *Lighting Research and Technology*, doi:10.1177/1477153516632867, 2016.

[74] Collection in vision and colour, on the course of the disability glare function and its attribution to components of ocular scatter. CIE 124/2, Commission Internationale de l'Éclairage, Vienna, 1997.

[75] Holladay LL. Action of a light source in the field in lowering visibility. *Journal of the Optical Society of America*, 14:1–15, 1927.

[76] Stiles WS. The effect of glare on the brightness difference threshold. *Proceedings of the Royal Society London B*, 104:322–355, 1929.

[77] Stiles WS. The scattering theory of the effect of glare on the brightness difference threshold. *Proceedings of the Royal Society London B*, 105:131–146, 1929.

[78] Akashi Y and Rea MS. Peripheral detection while driving under a mesopic light level. *Journal of the Illuminating Engineering Society*, 31:85–93, 2002.

[79] An investigation of headlamp glare: Intensity, spectrum and size. DOT HS 809 672, U. S. Department of Transportation, National Highway Traffic Safety Administration, Washington DC, 2003.

[80] Aguirre RC, Colombo EM, and Barraza JF. Effect of glare on reaction time for peripheral vision at mesopic adaptation. *Journal of the Optical Society of America A*, 28(10):2187–2191, 2011.

[81] Crawford BH. Visual adaptation in relation to brief conditioning stimuli. *Proceedings of the Royal Society London B*, 134:283–302, 1947.

[82] CIE Internationale Beleuchtungskommission. *Sekretariatsberichte der Zehnten Tagung, Scheveningen, 1939*. Band I, 1942.

[83] Holladay LL. The fundamentals of glare and visibility. *Journal of the Optical Society of America*, 12:271–319, 1926.

[84] Road lighting calculations. CIE 140, Commission Internationale de l'Éclairage, Vienna, 2000.

[85] Glare evaluation system for use within outdoor sports and area lighting. CIE 112, Commission Internationale de l'Éclairage, Vienna, 1994.

[86] IJspeert JK, de Waard PWT, van den Berg TJTP, and de Jong PTVM. The intraocular straylight function in 129 healthy volunteers; dependence on angle, age and pigmentation. *Vision Research*, 30:699–707, 1990.

[87] Vos JJ. Reflections on glare. *Lighting Research and Technology*, 35(2):163–175, 2003.

[88] Stiles WS and Crawford BH. The effect of a glaring light source on extrafoveal vision. *Proceedings of the Royal Society London B*, 122:255–280, 1937.

[89] CIE equations for disability glare. CIE 146, Commission Internationale de l'Éclairage, Vienna, 2002.

[90] Hubel D. Eye, brain and vision. Retrieved October 18 2015, from `http://hubel.med.harvard.edu/index.html`.

[91] Foulsham T, Walker E, and Kingstone A. The where, what and when of gaze allocation in the lab and the natural environment. *Vision Research*, 51(17):1920–1931, 2011.

[92] Ikegami Y, Inoue Y, and Hara N. Study on evaluation method of visibility by effective luminance for which various visual factors is considered. In *Proceedings of the 2013 CJK Lighting Conference*, pages 181–184. CJK Lighting Conference Committee, 2013.

[93] Terai N, Iwamoto K, and Akashi Y. Influence of veiling luminance caused by a peripheral glare source on extra-foveal vision. In *Light Sources 2016: Proceedings of the 15th International Symposium on the Science and Technology of Lighting*, pages 25–28. Foundation for the Advancement of the Science & Technology of Light Sources, 2016.

[94] Shpak M, Karha P, Porrovecchio G, Sjoberg A, Smid M, and Ikonen E. A two channel photopicscotopic luminance meter as a basis for mesopic photometry. In *Proceedings of the CIE 2012*, pages 433–434. Commission Internationale de l'Éclairage, 2012.

[95] Road lighting Part 4: Methods of measuring lighting performance. EN 13201-4:2003, Comité Européen de Normalisation, Brussels, 2003.

[96] IES guide for photometric measurement of roadway and street lighting. IES LM-50-99, Illuminating Engineering Society of North America, New York, 1999.

[97] Lighting for roads. JIS Z 9111:1988, Japanese Industrial Standards Committee, Tokyo, 1988.

[98] Specifying product performance for mesopic applications. CIE TN 005, Commission Internationale de l'Éclairage, Vienna, 2015.

[99] Report on quality metrics related to mesopic measurements of SSL. Technical Report EMRP-ENG-05-4.3.4, European Metrology Research Programme, Teddington, 2013.

[100] Herold M and Roberts D. Spectral characteristics of asphalt road aging and deterioration: implications for remote-sensing applications. *Applied Optics*, 44:4327–4334, 2005.

[101] Herold M and Schurke J. Santa Barbara asphalt road spectral library. Retrieved March 15 2016, from `http://www.geogr.uni-jena.de/~c5hema/spec/roads/sb_road_data.htm`.

[102] On site measurement of the photometric properties of road and tunnel lighting. CIE 194, Commission Internationale de l'Éclairage, Vienna, 2011.

[103] Davis W and Ohno Y. Color quality scale. *Optical Engineering*, 49(3):033602–033602–16, 2010.

List of Publications

Journal papers

1. Uchida T and Ohno Y. Defining the visual adaptation field for mesopic photometry: Does surrounding luminance affect peripheral adaptation? *Lighting Research and Technology*, 46(5):520–533, 2014.

2. Uchida T and Ohno Y. Defining the visual adaptation field for mesopic photometry: How does a high-luminance source affect peripheral adaptation? *Lighting Research and Technology*, 47(7):845–858, 2015.

3. Uchida T, Ayama M, Akashi Y, Hara N, Kitano T, Kodaira Y, and Sakai K. Adaptation luminance simulation for CIE mesopic photometry system implementation. *Lighting Research and Technology*, 48(1):14–25, 2016.

4. Uchida T and Ohno Y. Defining the visual adaptation field for mesopic photometry: Effect of surrounding source position on peripheral adaptation. *Lighting Research and Technology*, doi: 10.1177/1477153516638555, 2016.

5. Uchida T and Ohno Y. Simplified field measurement methods for the CIE mesopic photometry system. *Lighting Research and Technology*, doi: 10.1177/1477153516643571, 2016.

Proceedings papers

1. Uchida T and Ohno Y. An experimental approach to a definition of the mesopic adaptation field. In *Proceedings of the CIE 2012*, pages 71–76. Commission Internationale de l'Éclairage, 2012.

2. Uchida T and Ohno Y. Effect of high luminance sources to peripheral adaptation state in mesopic range. In *Proceedings of CIE Centenary Conference*, pages 529–536. Commission Internationale de l'Éclairage, 2013.

3. Uchida T and Ohno Y. Angular Characteristics of the surrounding luminance effect on peripheral adaptation state in the mesopic range. In *Proceedings of CIE 2014*, pages 273–280. Commission Internationale de l'Éclairage, 2014.

4. Uchida T. Adaptation luminance simulation for CIE mesopic photometry system implementation. In *Proceedings of 28th CIE Session*, pages 307–316. Commission Internationale de l'Éclairage, 2015.

5. Uchida T and Ohno Y. M/P ratio method for mesopic luminance measurement. In *Proceedings of CIE 2016*, pages 402–409. Commission Internationale de l'Éclairage, 2016.

Presentations

1. Uchida T, Zong Y, Miller CC, and Ohno Y. A Practical Photometer for CIE Performance Based Mesopic Photometry System. *CORM 2011*, Gaithersburg, MD, the United States, May 4-6, 2011.

2. Uchida T. Experimental study of the visual adaptation field in mesopic photometry. *CIE Introductory Tutorial & Workshop on Mesopic Photometry*, Vienna, Austria, January 24-25, 2012.

3. Uchida T and Ohno Y. An Experimental Approach to a Definition of the Mesopic Adaptation Field. *CORM 2012*, Ottawa, Canada, May 29-June 1, 2012.

4. Uchida T and Ohno Y. An Experimental Approach to a Definition of the Mesopic Adaptation Field for CIE 191 (in Japanese). *2012 Annual Conference of IEIJ*, Yamaguchi, Japan, September 6-8, 2012.

5. Uchida T, Ohno Y, and Zong Y. Design of Mesopic Photometers based on CIE 191. *CORM 2013*, Gaithersburg, MD, the United States, May 7-9, 2013.

6. Uchida T and Ohno Y. Surrounding High-Luminance Source Effect on Peripheral Adaptation in Mesopic Range (in Japanese). *2013 Annual Conference of IEIJ*, Nagoya, Japan, September 5-7, 2013.

7. Uchida T, Ohno Y, and Zong Y. Development of Mesopic Photometers based on CIE 191. *CORM 2014*, Gaithersburg, MD, the United States, May 21-23, 2014.

8. Uchida T and Ohno Y. Angular Characteristics of the Surrounding Luminance Effect on Peripheral Adaptation State in Mesopic Range (in Japanese). *2014 Annual Conference of IEIJ*, Saitama, Japan, September 4-6, 2014.

9. Uchida T and Ohno Y. Research on Adaptation Field Definition for CIE Mesopic Photometry System Installation. *CIE/USA Annual Meeting 2014*, Seattle, WA, the United States, October 6, 2014.

10. Uchida T and Ohno Y. A Mesopic Adaptation Luminance Simulation based on Luminance Distributions (in Japanese). *2015 Annual Conference of IEIJ*, Fukui, Japan, August 27-29, 2015.

11. Uchida T and Ohno Y. A Simplified Method for the Mesopic Luminance Measurement (in Japanese). *2016 Annual Conference of IEIJ*, Tokyo, Japan, August 30-31, 2016.

Other article

1. Uchida T. What are Remaining Issues for Implementation of the CIE Mesopic Photometry System? (in Japanese) *Journal of the Illuminating Engineering Institute of Japan*, 97(4):213–217, 2013.